# Study of a high temperature solution growth process for the development of heavily doped 4H-SiC substrates

Yun Ji Shin

▶ **To cite this version:**

Yun Ji Shin. Study of a high temperature solution growth process for the development of heavily doped 4H-SiC substrates. Chemical and Process Engineering. Université Grenoble Alpes, 2016. English. NNT : 2016GREAI058 . tel-01587801

**HAL Id: tel-01587801**

**https://theses.hal.science/tel-01587801v1**

Submitted on 14 Sep 2017

**HAL** is a multi-disciplinary open access archive for the deposit and dissemination of scientific research documents, whether they are published or not. The documents may come from teaching and research institutions in France or abroad, or from public or private research centers.

L'archive ouverte pluridisciplinaire **HAL**, est destinée au dépôt et à la diffusion de documents scientifiques de niveau recherche, publiés ou non, émanant des établissements d'enseignement et de recherche français ou étrangers, des laboratoires publics ou privés.

Communauté
UNIVERSITÉ Grenoble Alpes

# THÈSE

Pour obtenir le grade de

**DOCTEUR DE LA COMMUNAUTÉ UNIVERSITÉ GRENOBLE ALPES**

Spécialité : **Matériaux, Mécanique, Génie civil, Electrochimie**

Arrêté ministériel : 7 août 2006

Présentée par

**Yun Ji SHIN**

Thèse dirigée par **Didier CHAUSSENDE** et
codirigée par **Pierre BROSSELARD**

préparée au sein du **Laboratoire des Matériaux et du Génie Physique**
dans **I-MEP2**

# Étude du procédé de croissance en solution à haute température pour le développement de substrats de 4H-SiC fortement dopes

Thèse soutenue publiquement le **13 Octobre 2016**,
devant le jury composé de :

**Dr. Gabriel FERRO**
Directeur de recherche, CNRS, UCB Lyon 1, Rapporteur
**Prof. Mikael SYVAJARVI**
Professeur, U. Linköping, Rapporteur
**Prof. Dominique PLANSON**
Professeur, INSA Lyon, Examinateur
**Dr. Sandrine JUILLAGUET**
Maître de conférences, U. Montpellier, Examinateur
**Dr. Pierre BROSSELARD**
Docteur, CALY Technologies, Co-directeur de thèse
**Dr. Didier CHAUSSENDE**
Directeur de Recherche, CNRS, Directeur de thèse

Communauté
UNIVERSITÉ Grenoble Alpes

# Acknowledgement

At the end of this, I should take some time to thank all the people without whom this thesis would never have been possible. Although only my name appears on the cover of this dissertation, a great many people have contributed to its production.

First and foremost I would like to express my sincere gratitude to my supervisor, Dr. Didier Chaussende, who always guided me to the right direction when my steps faltered. I am deeply grateful to him for all the discussions that helped me come up with the related topic in all the time and carefully reading and commenting on countless revisions of this thesis till the end. Because of too long list that I should say thanks to him, it seems impossible to express enough appreciation to him for all advices and encouraging during three years. His patience and support helped me overcome many crisis situations and finish this thesis. I am also deeply grateful to my co-supervisor Dr. Pierre Bresselard for his help and advices. He was always kind to me and trying to help my research, although he was very busy with his own business.

I would like to take a moment to thank my thesis committee members. Thank you to Dr. Gabriel Ferro and Prof. Mikael Syväjärvi for being my rapporteurs. Also thank you to Prof. Dominique Planson and Dr. Sandrine Juillaguet for being examiners of my thesis. Thank you for investing time for my thesis and providing interesting and valuable feedback. I feel honored that you have accepted to be on my committee. Also, special thanks to Sandrine for her great help to work on the SIMS measurements in Montpellier when I really needed help with that.

I would like to thank Dr. Seongmin Jeong, Prof. Won-Jae Lee, Dr. Jung Gon Kim and Prof. Won-Jeong Kim for numerous discussion & characterizations and supporting during my PhD that helped me to understand the scientific phenomena on related topic.

I am also grateful to the members of the Cristallogenèse group with whom I have interacted during last three and a half years, Jean-Marc Dedulle, Theirry Ouisse, Odette Chaix, Eirini Sarigiannidou, Roland Madar, Joseph La Manna, Isabelle Gelard, Lucile Parent-Bert, Lulien

Lefebure, Sven Tengeler, Lu Shi, Shiqi Zhang, Demitrios Zevgitis, Yun Li, and Victoria Cherkas for their great support and encourage me. In my daily work, I have been blessed with those friendly and awesome people. Thanks to them I had the opportunity to study the SiC crystal growth and other many things, including scientific and non-scientific, in such wonderful team. Also, I am happy to thank Beatrice Doisneau for amazing helping me to measure the EBSD with a number of my samples during several months.

I give thanks to all my colleagues in the Laboratoire des Matériaux et du Génie Physique for their cheerfulness and all their supports. Thank you to the members of ASCoF in Grenoble, who gave me years of fun during my stay in Grenoble.

My sincere thanks goes to Dr. Nikolaos Tsavdaris and Dr. Kanaparin Ariyawong have offered much advices and insights throughout my work on the crystal growth and numerical simulations by their experience. This work would not have been possible without their help. My special thanks also goes to Hoang-Long Le Tran helped me to understand my research area better by thermodynamic calculations (and also for French translation!!). They have never refused my questions and favors. I would never forget all the discussions and wonderful moments both in and out of the laboratory with them.

I am deeply thankful to my best friend Ionela Iliescu for helping me get through the difficult times, and for all the emotional support, friendship, and joyful memories. I wish to thank my my close friends Hokwon Kim, Jagyeong Lim and Sylvain Meyer for their heartwarming supports. They always gave me a power and the words inspired me. We have done many thing together for fun! The friendship with them is irreplaceable. She made a big contribution to French summary part. A special thanks to Junhee Choi for both supporting and encouraging me during the last moment of my PhD. He stood by me and helped me with love to endure the hard times. I am sure that he is a biggest supporter of my life as I do.

Lastly, I would like to thank my family for their continuous support and encouragement from Korea. I wish to dedicate this thesis to my late father. I love you all. *-Yun Ji Shin*

# General information

This thesis was studied in *Laboratoire des Matériaux et du Génie Physique (LMGP)* of *Grenoble INP*. It has been partially funded by a grant from the Région Rhône-Alpes (ARC2012) and International Collaborative Energy Technology R&D Program (No. 2012T100100744-3). The main aim of this work is to develop the top seeded solution growth (TSSG) process, with a special focus on heavily p-type doped 4H-SiC crystals by using Al based solvent.

This current thesis is divided in 6 chapters:

First 1 introduces the SiC material and its brief history. Then the physical and electrical properties of most important polytypes of SiC and the applications are presented. The last part of this chapter gives the overview on the growth techniques, including physical vapor transport method and TSSG method.

In chapter 2, the description of the experimental setup and optimum condition for the growth of 4H-SiC crystals can be found. Also, further experimental techniques and three elementary step of TSSG process will be discussed.

Chapter 3 is dedicated to the investigation of the interaction between the liquid solvent and the 4H-SiC surface under equilibrium conditions, i.e. without any growth, using a sessile drop method. This chapter reports the morphological evolution at the liquid/solid interface under equilibrium conditions. We will discuss the effect of time, temperature and the adding of Al to pure liquid silicon (Si) in such viewpoint.

Chapter 4 presents the main experimental results through systematic observation on the 4H-SiC crystals during the initial stage of the process. With the numerical modeling, we will show that the

transient 3C-SiC nucleation occurs on the crystal surface due to strong temperature fluctuations during the contact between the seed and the liquid. This phenomenon can be avoided by either pre-heating the seed crystal before contacting or by adding Al to the liquid Si.

Chapter 5 investigates the effect of rotation speed on the growth surface stability. Based on the interaction between the step flow at the growing surface and the local fluid flow directions close to the surface, we observed the strong morphological instabilities, e.g., macro-step formation. We will discuss the experimental evidence about the relationship between growth rate enhancement and such surface instabilities.

In chapter 6, finally, we evaluate the dopant concentration for both nitrogen as a donor and aluminum as an acceptor from a few selected 4H-SiC samples grown by TSSG process. Dopant concentration of both n- and p-type grown crystals and free carrier concentration of n-type samples will be tested by both Raman spectroscopy and SIMS analysis. We will show that TSSG process is promising for the development of heavily doped n-type and p-type 4H-SiC substrates, respectively.

The last chapter will give the general conclusions of this thesis. Some open issues and perspective for future work will also be discussed.

# Contents

# Chapter 1. Introduction

In the recent trend of energy saving and $CO_2$ emission reduction to help reducing the global warming, one of the most important targets is a higher efficiency in utilizing the electric energy. With this aim in view, modern power electronics devices are suitable for drastic reduction of energy losses from electric power generations to end users utilization.

As the most popular electronic materials, silicon (Si) has established itself as the main material in the power electronic devices industry since 1960s, due to a number of reasons, including the mechanical properties and economic reasons. However, in order to enable wide applications in harsh environments, the goal of the electronic devices goes beyond the limits of Si material. In other words, Si based electronics are not fully satisfying such requirements anymore due to the limitation of their physical properties. From that reason, the wide bandgap (WBG) semiconductor materials, such as silicon carbide (SiC), gallium nitride (GaN), and diamond, are recognized as the most promising materials. Among them, SiC is considered with greatest potential due to its outstanding properties (see Table 1.2), technological maturity and commercial availability of wafers. SiC has more remarkable chemical and electrical properties than Si material. For instance, Si based devices often exhibit significant changes in characteristics over 150°C because of physical limitation and thus cannot operate at temperatures close or higher than that temperature. However, SiC has a higher bandgap of 3 eV (4H-SiC) and higher thermal conductivity (4~5 W/cm·K) than Si material. Thus SiC based devices can be employed at elevated temperatures, higher than Si one, and SiC based devices promise better performances for any power electronics applications.

Since 1950s, much progress in terms of quality and dimensions has been made in SiC bulk crystal production. In recent, 6 inch 4H-SiC wafers grown by vapor phase process were introduced

to the market, although its supply is still quantitatively limited. Such continuous efforts have driven rapid development of SiC based electronic devices. However, we still face several important problems, e.g. to grow the heavily doped 4H-SiC substrates with a good crystalline quality. Thus, this present thesis describes and reviews the 4H-SiC bulk crystal growth from liquid phase, named the Top Seeded Solution Growth (TSSG) process, which is a remarkable process to grow SiC crystal with low defect density and to obtain the high doping level for both p- and n-type substrates. The purpose of this thesis includes set-up of high temperature TSSG puller, development of the processing techniques and understanding of the growth kinetics in liquid phase. In particular, the effect of Al is investigated in each aim of the thesis.

## 1.1. A brief history of SiC

The pioneer works on SiC were conducted in the 19$^{th}$ century. It was named as carborundum, coined by an American chemist Edward G. Acheson in 1892. Actually, he made high temperature experiments with the goal of forming artificial diamond from powdered coke (C) and clay (alundum) using an electric furnace. After heating, he finally found blue crystals consisting of hexagonal SiC. Three years later, he issued a patent for his process, still used today for the production of carborundum, the commercial name of SiC powder for the industry of abrasives [1]. This natural version of SiC was named moissanite in honor to Moissan. Intergrown bulky crystals were usually encountered at the end of the Acheson process. A systematic analysis, by optical and X-ray diffraction investigations revealed polymorphic forms with either hexagonal or trigonal symmetry in the ‘Acheson SiC’. When polymorphism of SiC occurs as a result of difference in crystal stacking sequences along only one direction, this is 'polytypism' associated with ‘polytypes’

named after Baumhauer in 1912 [2]. Natural SiC is extremely rare. It has been defined by the American geologist Charles Milton in 1893, and by a French chemist Henri Moissan in 1905 who found crystallites in meteorite [3].

Since 1950s, Si has been offering multiple advantages for power electronics and no other semiconducting materials could compete with Si in terms of low defect density, long minority carrier life-time, and doping level control. The development of SiC crystal growth technologies began in 1955 with Jan Antony Lely in Philips, who produced SiC single crystal from the vapor phase using a sublimation method (also called the Lely method) [4]. At the beginning, the available size of Lely crystals was too small to develop electronic devices. The breakthrough was achieved by Tairov and Tsvetkov in 1978, when they introduced the seeded sublimation method (also called the modified Lely method) [5]. With the development of the seeded sublimation technique, acceptably large and reproducible single-crystalline SiC wafers became available. In 1991, the first 6H-SiC wafers were commercialized by Cree research Inc. [6] and blue light emitting diodes (LEDS) were demonstrated on it in 1997. Although SiC based LEDS were less efficient than other compound semiconductors such as GaN, the explosive growth of the nitride LED market and full-color displays had a positive impact on the development of SiC crystal growth and technology. As an evidence, the production of 6 inch SiC wafer recently became available from vapor phase. Yet, many researchers are still focusing on the development of SiC single crystal growth technique in order to improve the single crystalline quality with low crystallographic defects density and the better performance of the produced electronic devices.

## 1.2. SiC crystallography

### 1.2.1. Polytypism of SiC

SiC is a compound semiconductor composed of Si and C. SiC crystals exist in few tens of reported polymorphic crystalline structures [7], named polytypes. Each SiC polytype has its own distinct set of electrical properties. The polytypes are expressed by the number of Si-C layers in the unit cell together with the symbol of crystal systems (C: cubic, H: hexagonal, and R: rhombohedral). Among them, only a few polytypes are commonly grown in a reproducible form acceptable for use as an electronic semiconductor. The most common polytypes of SiC presently being developed for electronics are 3C-, 4H- and 6H-SiC, but only 4H- and/or 6H-SiC wafers are currently in commercial use.

In general, 3C-SiC is known as a low-temperature polytype, and 4H- and 6H-SiC are high-temperature polytypes [3] owing to the reliable and suitable growth environment for each polytype. These different polytypes are usually characterized by the stacking sequences of the bi-atomic layers of the SiC structure. The building unit in SiC layers consists of one C (Si) atom surrounded by three Si (C) atoms within the bilayer and having a single bond linked to a Si (C) atom in the layer above. They formed a tetrahedral structure as shown in Figure 1.1(a). These tetrahedra are arranged in such a way that all atoms can be described as forming hexagonal compact plane (which are the so called {0001} basal plane). Figure 1.1(b) shows the simplified SiC layer structure in the (0001) plane. Using a simple ball model, the first bilayer is represented as A. The next bilayer then has the option of positioning its on "B" or "C" lattice sites. Doing so, the stacking sequence of the three types of bilayers (A, B or C) determines the polytypes.

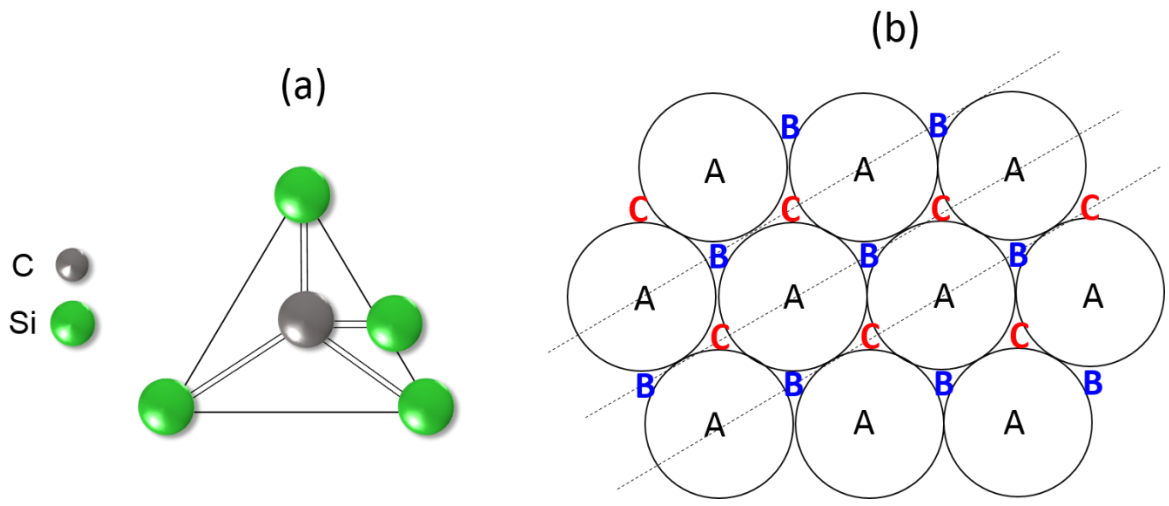


Figure 1.1. Illustration of (a) the SiC unit tetrahedra and (b) projection of the three different positions of the bilayers (hexagonal compact planes).

A projection of the stacking sequences of the main polytypes is shown in Figure 1.2. When SiC bilayers, arbitrarily denoted A, B and C in Figure 1.2, are stacked with the sequence ABCABC..., then the crystallographic structure is the zinc-blende (cubic) structure. This arrangement is known as 3C-SiC or β-SiC. Number '3' refers to the number of layers needed for defining the unit stacking sequence. All the other polytypes are either hexagonal or rhombohedral and are gathered under the generic name α-SiC. The simplest one corresponds to the ABAB... stacking, forming the wurtzite (hexagonal) structure, called 2H-SiC in the Ramsdell notation. All the other α-SiC polytypes can be constructed by a combination of cubic and hexagonal stacking. 4H-SiC consists of an equal number of cubic and hexagonal layers with a stacking sequences of ABCB...., and 6H-SiC is composed of two-third of cubic site and one-third of hexagonal site with a stacking sequence of ABCACB.... 15R-SiC is composed of three-fifth cubic bonds and two-fifth of hexagonal bonds.

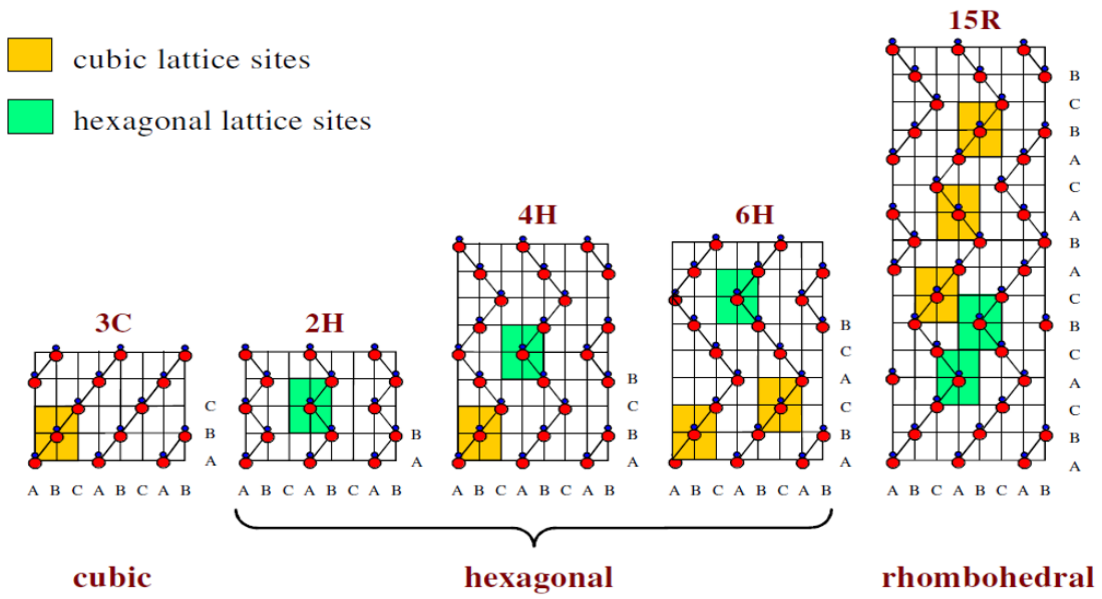


Figure 1.2. The stacking sequences for different SiC polytypes in the [11-20] plane. The cubic lattice site (yellow color box) has the stacking sequence of ABCABC while the stacking sequence of hexagonal lattice sites (green color box) is ABA.

The tendency related to the number of hexagonal site in the unit stacking structure is denoted as hexagonality. In other words, the hexagonality represents the stacking periodicity of each polytype. For example, the hexagonality of 3C-SiC is zero while 2H-SiC has 100% hexagonality. Also, 4H and 6H-SiC have 50% and 33.3% hexagonalities, respectively, and 15R-SiC has almost intermediate value (40%) of them. Due to different stacking sequences, the lattice parameters of both a- and c-axis in each polytype should be changed. All structural characteristics of most important polytypes are summarized in Table 1.1. Since polytypes are built by stacking of bilayers along the c-axis and a lattice parameter of a-axis being almost constant for almost all polytypes, one can expect that they have anisotropy of properties. The degree of anisotropy is measured by the ratio of properties along and perpendicular to the c-axis. However, only 3C-SiC is isotropic.

Table 1.1. Structural characteristics of the most common polytypes of SiC [8]

| Polytype | Space group | a (Å) | c (Å) | Hexagonallity |
|---|---|---|---|---|
| 3C | $T^2_d$-F43m | 4.36 | 4.36 | 0 |
| 2H | $C^4_{6v}$-P6$_3$mc | 3.073 | 5.048 | 100 |
| 4H | $C^4_{6v}$-P6$_3$mc | 3.073 | 10.05 | 50 |
| 6H | $C^4_{6v}$-P6$_3$mc | 3.073 | 15.11 | 33.3 |
| 15R | $C^5_{3v}$-R3m | 3.073 | 37.7 | 40 |

The conditions for obtaining one polytype or the others are not precisely defined. There are however some trends in the abundant literature available on SiC growth from the vapor phase and the liquid phase. The nature of the polytype seems to depend on both the growth rate and the temperature. According to Figure 1.3(a) reported by Knippenberg et al. [3], it may concluded that β-SiC is an unstable modification (metastable) polytype at all temperatures. Also, 2H-SiC is believed to occur at relatively low temperatures between 1300-1600°C. As a general rule, other polytypes, such as 4H, 6H, and 15R, are often observed at the temperature over 2000°C. To be more precise, Inomata et al. [9], reported the probability of polytype occurrences based on several experimental results that 4H-SiC is more stable even at the temperature below 2000°C and 6H-SiC is easily formed at higher temperature condition due to different thermal stabilities. As indicated by dotted line in the Figure 1.3(b), however, there are small differences on the polytype stabilities between 6H and 15R-SiC depending on the growth method.

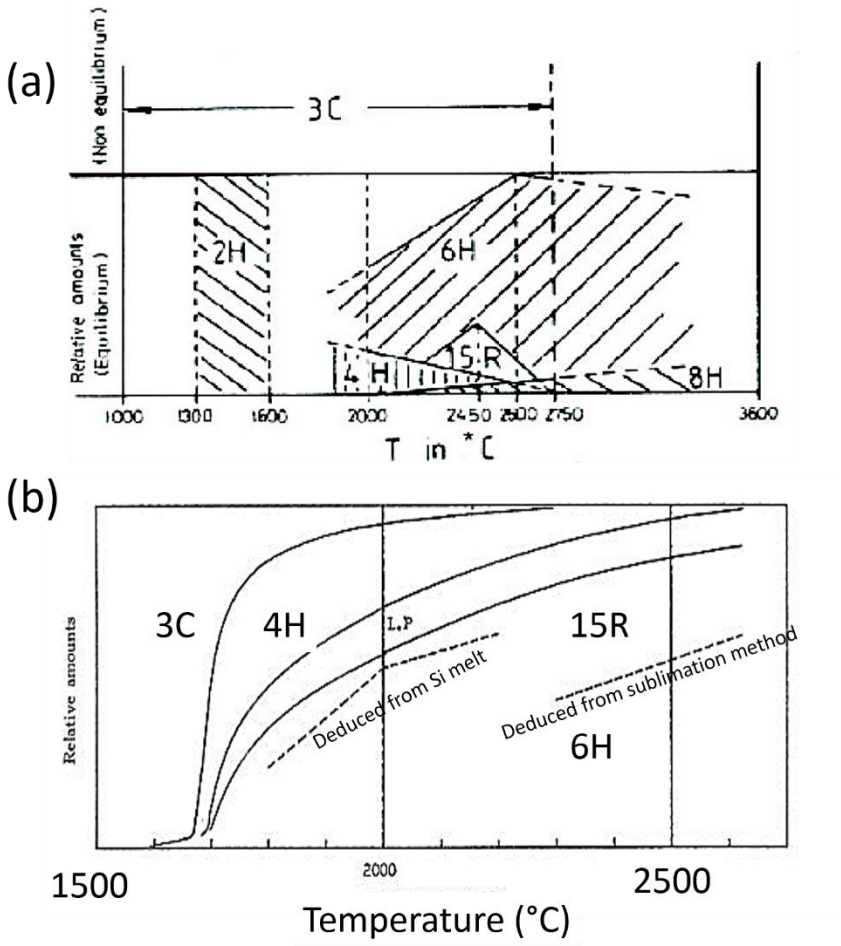


Figure 1.3. Stability diagrams of SiC polytypes as a function of the temperature reported by Knippenberg et al. [3] and Inomata et al. [9]. (a) The relative amount of the different hexagonal structures are separated by stripes. (b) The broken lines between 15R and 6H are deduced from solution growth method (left) and sublimation method (right), respectively.

The polytype of SiC crystal is usually intentionally controlled by the seed crystal. Due to some reasons occurring during the growth process, however, the polytype switching due to the nucleation of foreign polytypes is often observed during the growth process, thus the kinetic and thermodynamic factors for polytype stabilization must be understood and controlled. The main kinetic factor is the polytype replication through spiral growth originating from screw dislocations,

after stable spiral growth has been established in the bulk crystal. Along the steps of spiral, the stacking information is provided, which ensures replication of that polytype in the growing crystal while the spiral core acts as an infinite step source, as long as the spiral growth favorable conditions are maintained. On the other hand, nucleation on the large and flat terrace between steps can naturally take place during the beginning of the growth process. In the solution growth of SiC, the foreign polytype inclusions are quite commonly obtained by 2D nucleation. That is the reason why, the key factors which stabilize a desired polytype is essential to understand and to control the growth conditions for 2D nucleation. It has been suggested by Vodakov et al., that there exists a close relationship between the polytype stability and the C/Si ratio in the growth atmosphere [10]. When the growth atmosphere is C-rich, a polytype with a higher hexagonality becomes stable, e.g. 4H-SiC is more stable than 6H-SiC under such conditions.

Impurity incorporation is also one of the important factors for polytype stabilization. In general, nitrogen (N) doping during the growth is suitable to stabilize the 4H-SiC polytype, while aluminum (Al) doping leads to preferential growth of 6H-SiC polytype. The main reason is that nitrogen atoms occupy the C sites in the lattice, incorporation of nitrogen atoms will cause the growth environment to become slightly C-rich. In the same sense, Sc and Ce are also helpful to stabilize the 4H-SiC by a shift in the growth atmosphere toward C-rich condition [11].

### 1.2.2. Polarity

As described before, the staking sequence of Si-C bilayers along the c-axis determines the polytype. Depending on the terminating atoms of the topmost layer (surface), the {0001} planes have either C or Si terminated layer as shown in Figure 1.4. It will be denoted in the following as (0001) Si-face and (000-1) C-face. The difference in surface energy between both polarities affects

the surface reactivity and behavior in general. For instance, the growth of 4H-SiC is usually favored on the C-face due to its lower surface energy than Si-face [12]. Conversely, 6H-SiC is favored on the Si-face which has higher surface energy [13]. Thus, the polytype of growing crystal is affected by surface polarity. In vapor phase growth process, use of 4H-SiC Si(0001) face under suitable conditions is favorable for 6H-SiC polytype. In contrast, 4H-SiC growth is beneficial on C(000-1) face, irrespective of the seed polytype [14].

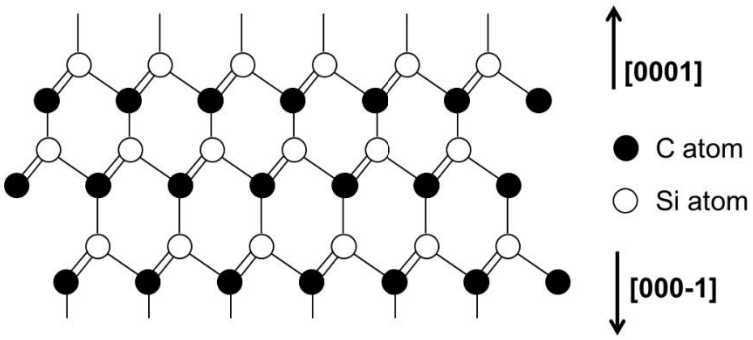


Figure 1.4. Cross-section of the hexagonal structure of SiC. C-face (bottom-side) and Si-face (top-side) can be defined by the type of atom occupying the last layer.

### 1.2.3. Physical and electrical properties

SiC provides multiple advantages for high temperature, high frequency, and high power device applications due to its high thermal conductivity and high critical field for breakdown. The most popular and widely reported polytypes for devices (3C, 4H and 6H-SiC) have 2~3 times larger bandgap energy than Si (1.12 eV). SiC exhibits higher values of thermal conductivity, critical electrical breakdown field, and saturated carrier mobilities compared to the conventional semiconductor material such as Si. Table 1.2 shows the comparison of physical properties of SiC,

GaN, and Si materials [15-17]. Those favorable properties of SiC are desirable for efficient high power device operation. For a given hexagonal polytype, which has anisotropy of properties, the electrical properties are also anisotropic. It means that the different stacking sequences in each SiC polytype exhibits different unique fundamental electrical and optical properties.

Table 1.2. Physical properties of SiC polytypes [15-17].

| | Si | GaN | 3C-SiC | 4H-SiC |
|---|---|---|---|---|
| Bandgap (eV) | 1.12 | 3.39 | 2.39 | 3.26 |
| Intrinsic carrier concentration ($cm^{-3}$) | $10^{10}$ | $10^{10}$ | $\sim10^{-1}$ | $\sim10^{-7}$ |
| Breakdown field ($MV \cdot cm^{-1}$) @$N_D=10^{17}$ $cm^{-3}$ | 0.6 | 3.3 | >1.5 | 3 |
| Electron mobility ($cm^2/V \cdot s$) @$N_D=10^{16}$ $cm^{-3}$ | 1200 | ≤ 1000 | 750 ∥ c-axis | 800 ∥ c-axis<br>800 ⊥ c-axis |
| Hole mobility ($cm^2/V \cdot s$) @$N_D=10^{16}$ $cm^{-3}$ | 420 | ≤ 350 | 40 | 115 |
| Thermal conductivity ($W/cm \cdot K$) | 1.5 | 1.3 | 4~5 | 4~5 |
| Melting point (K) | 1690 | >2500 | ~3100 | ~3100 |

### 1.2.4. Doping control in SiC bulk crystals

For fabrication of vertical-type power devices, low resistivity substrates are required to minimize the series resistance. Also, high resistivity substrates (or vertical device on very high Voltage for 30kV) are desired for fabrication of lateral-type high frequency devices to reduce the

parasitic impedance. In general, N and Al are used as the dopants for n- and p-type substrates, respectively. The dopant incorporation in SiC crystal growth follows the tendencies observed in CVD that nitrogen incorporation is significantly higher on C(000-1) face than on Si(0001) face. In contrast, the opposite trend occur for Al incorporation. Such polarity effect could possibly be explained by surface kinetics. For example, nitrogen incorporates at the C site in the lattice, a nitrogen atom adsorbed onto (000-1) face is bound to three underlying Si atoms, while it is only bond to one Si atom on (0001) face. Thus, desorption of nitrogen atoms absorbed on (000-1) face must be much less than on (0001) face. That could be the reason why nitrogen incorporation is higher on (000-1) and this should also influence the polytype transformation [18, 19]. The case of Al could be explained in a similar manner because Al incorporates on Si-site.

In PVT system, incorporation of Al is much more difficult than nitrogen incorporation because of the depletion of the Al source (gas) during the process. Control of Al source is much easier in liquid, although evaporation rate of Al at the high temperature is strong. Thus, SiC solution growth has attracted the interest for Al doping. Recently, very high dopant density of p-type 4H-SiC substrates are achieved over $10^{20}$ $cm^{-3}$ by both PVT and solution growth processes while typical dopant density of n-type 4H-SiC can hardly reach $10^{20}$ $cm^{-3}$ [19-21].

## 1.3. Electronic applications of SiC

The first use of SiC was an abrasive material since SiC has a hardness of 9.1 on the Mohs scale (Mohs hardness of diamond=10). Now it has become as a very important material for power electronics applications. The SiC homoepitaxial growth technology for lightly-doped SiC epitaxial layers with reasonable quality became available in the early 1990s. Just a year after, 1kV p-n

junction diode using 6H-SiC was firstly demonstrated [22]. Two years later, 1kV Schottky barrier diode (SBD) using 6H-SiC with a low specific on-resistance and operating at 400°C has been demonstrated by Urushidani et al. [23]. In 1995, high voltage 4H-SiC SBD (3kV) was fabricated [24]. One of the typical applications of SiC SBDs was fast diodes employed in a power-factor-correction circuit of switching mode power supplies. Since SiC SBDs maintain a constant reverse recovery time, regardless of the temperature, the operation at high temperature without increased switching losses is possible with SiC SBDs (Figure 1.5). Such performance advantages lead to the downsizing of passive components.

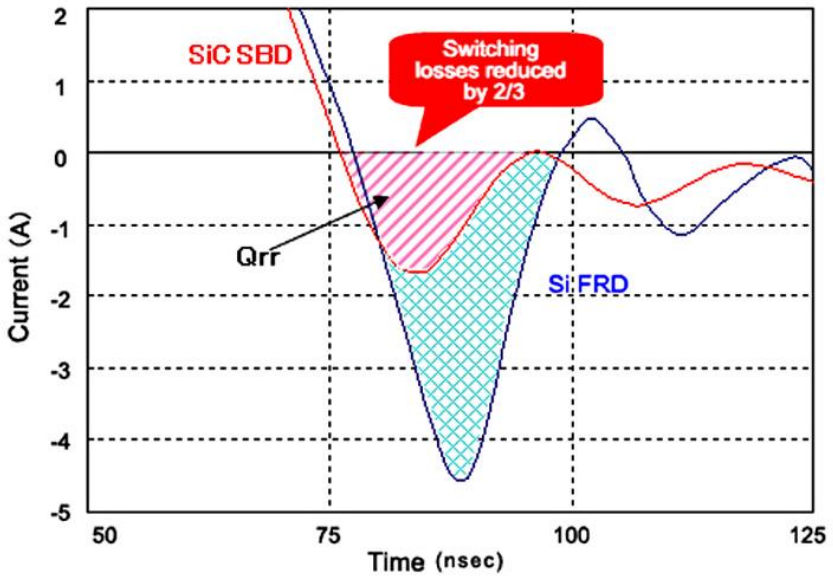


Figure 1.5. Comparison of the switching losses between Si fast recovery diode and SiC Schottky barrier diode reported by Rohm Semiconductor [50].

Another advantage of SiC-based electronics is for the high-voltage and high-current devices, like insulated gate bipolar transistors (IGBTs) and metal-oxide-semiconductor field effect transistors (MOSFETs). SiC power devices have much lower drift-layer resistance than Si devices, e.g., SiC MOSFETs generate no tail current in principle. In 1993, a vertical trench MOSFET of 6H-SiC was demonstrated by Palmour et al., who also extensively developed 4H-SiC trench MOSFETs and BJTs, as important steps toward high-power electronics [25, 26]. Compared to 600V-900V Si MOSFETs, 1200V SiC MOSFETs have smaller chip area (mountable on a compact package) and an ultralow recovery loss of the diodes. Therefore, SiC-MOSFETs are increasingly being used in power supplies for industrial equipments and inverters/converters for high-efficiency power conditioners. Compared to a conventional inverter system with IGBT power module, the use of SiC inverter can reduce the size and weight by 65%. Also, the switching losses are about 65% smaller than the conventional one [27]. Due to the low switching losses of SiC based devices, it can operate at high frequencies (>20 kHz), which is not possible with Si based devices in power levels of over a few tens of kilowatts [28].

## 1.4. SiC single crystal growth

SiC starts to sublimate at the temperature of 1800-2000°C at low pressure. Using the vapor phase, the growth of large diameter SiC single crystals has been demonstrated. Although the SiC growth technique from vapor phase has been significantly advanced, a high quality SiC single crystal with a large diameter, comparable to the Si technology, is still challenging. The main reason is the number of crystallographic defects remaining in SiC crystal such as threading dislocations and stacking faults. However, it is well known that SiC crystal growth from liquid phase leads to

lower dislocation density than other growth methods [29]. This is the main reason why the solution growth is an attractive alternative to the SiC growth from vapor phase.

### 1.4.1. The modified Lely method

Starting from the Lely process at the beginning of 1960s, SiC single crystal growth technology has been significantly improved with the modified Lely method and is still being used as the major growth method for SiC commercial wafers. The typical design of the growth furnace is shown in Figure 1.6. The polycrystalline SiC powder is placed in the graphite crucible as a source and a seed crystal is mounted on a lid of the graphite crucible. At high temperature (usually over 2000°C), a mass transport of the most volatile components (Si, $SiC_2$, $Si_2C$, etc.) from hotter area (SiC powder) to colder area (seed crystal) in the furnace results in the growth of SiC on the seed. Typical values of temperature could be 2300°C for powder source and the seed temperature is usually fixed at about 200°C lower than the source temperature [30]. The mechanism of the growth by vapor phase can be divided into three steps; i) vaporization of the SiC powder source, forming the gaseous species, ii) mass transport of the gaseous species from the powder source to the growth front, governed mainly by diffusion phenomenon, and iii) crystallyzation of the gaseous species onto the seed crystal [31-33]. The main advantages of standard PVT method are the availability of well-developed standard industrial processes and lower costs for both growth machine setup and running. However, the growing crystal quality in PVT method is very sensitive to the thermal and chemical conditions. The main reason is that PVT is a closed system where it is used a black box as a furnace. This is intrinsically a non-stationary process which most of the growth parameters continuously evolve during the process. Thus it is difficult to maintain the thermal stability and chemical distribution during the long time process. Another drawback of PVT is the purity of

grown crystal. The level of purity in the crystal is strongly dependent on the purity of the powder source. Thus it makes rather difficult to obtain high purity crystals and to accurately control the doping concentration in the crystal.

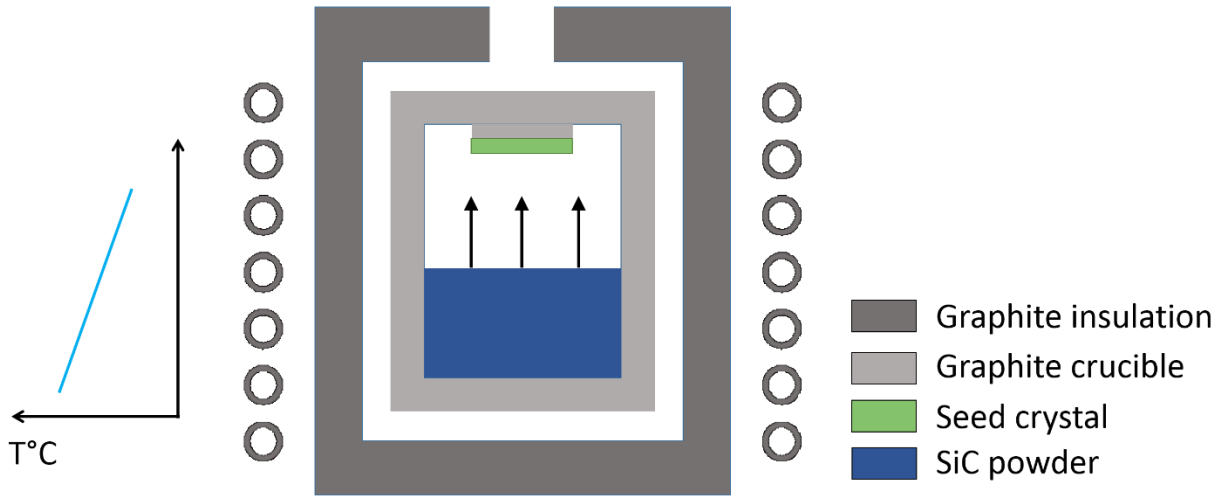


Figure 1.6. Schematic of seeded sublimation method reactor (right) and the temperature profile along the axis of symmetry of the crucible (left).

### 1.4.2. SiC growth from liquid phase

Most single crystalline semiconductors are grown by crystal pulling from the melt such as elemental semiconductors (Si and Ge) or III-V compound semiconductors (GaAs, InP). However, this cannot be applied to SiC. According to the phase diagram presented in Figure 1.7, there exists no stoichiometric SiC liquid phase [34]. In other words, SiC solution growth needs to use non-stoichiometric solutions containing both Si and C [35]. From the calculations, SiC congruent melting occurs only at the pressures exceeding $10^5$ bar at temperature higher than 3200°C [36], which is currently not possible for production of large diameter SiC wafers in the industry. The solubility of C in liquid Si is rather low, about 0.03% at 1400°C and 15% at 2600°C. This is a big

difficulty for SiC solution growth. In order to increase the C solubility in a reasonable temperature and pressure range, various solvent compositions have been studied by several authors (see chapter 2.2). According to their reports, C solubility can be enhanced by the addition of transition elements (Sc, Fe, Cr, Ti, etc.) to the liquid Si.

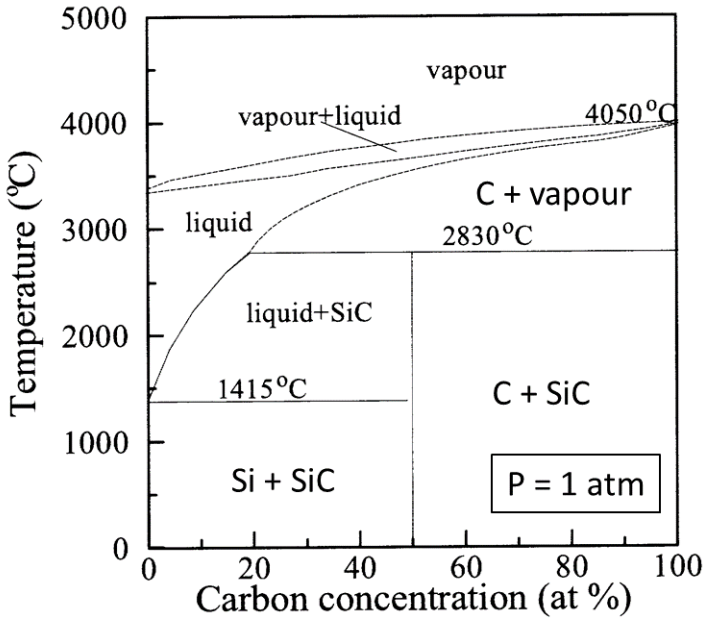


Figure 1.7. Phase diagram of Si-C system.

Several techniques for SiC crystal growth and epitaxial growth from the liquid phase have been demonstrated, such as traveling solvent method, vapor-liquid-solid method, slow cooling technique and top seeded solution growth method [35, 37-39]. Among them, top seeded solution growth (TSSG) method, based on the concept from the Czochralski process, is probably the most successful way for SiC single crystal growth from liquid phase so far. Typical design of TSSG reactor is illustrated in Figure 1.8.

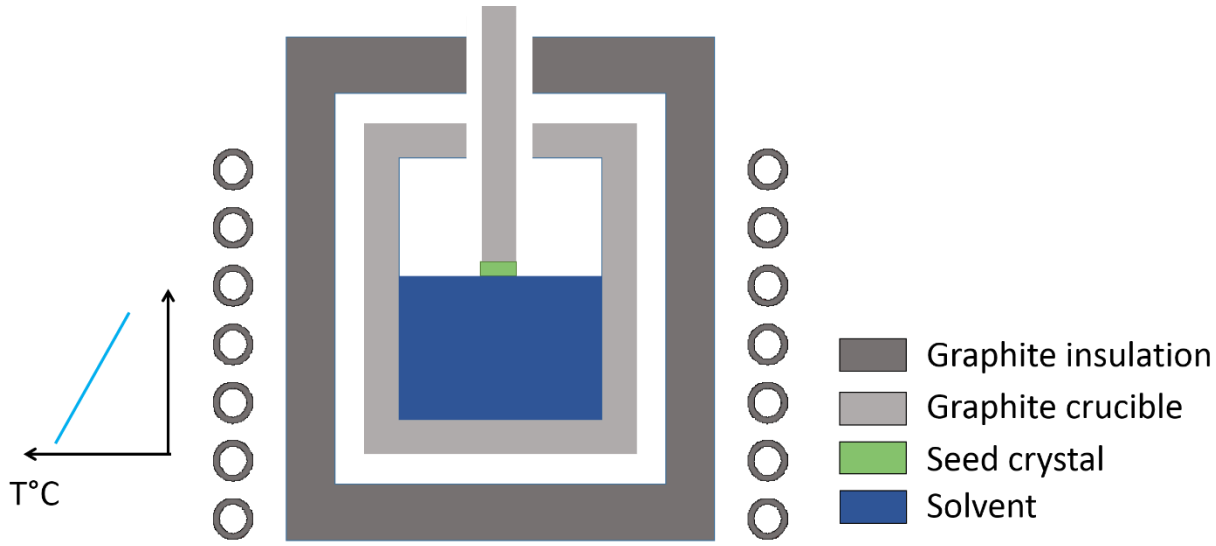


Figure 1.8. Schematic of top seeded solution growth reactor (right) and the temperature profile along the axis of symmetry of the crucible (left).

In TSSG process, the seed crystal is mounted on a graphite rod inserted into the graphite crucible, which is the container of the Si source (melt). Usually, a temperature gradient is applied between the liquid surface (which is usually contacting the seed crystal during the process) and crucible bottom, so that a carbon transport can occur from the dissolution area (higher temperature area; bottom of the crucible) to the growth front (lower temperature area; seed crystal).

In any liquid phase method, the growth occurs due to a local C supersaturation at the liquid-crystal interface. The supersaturation can be created in various ways: 1) by slow cooling of C saturated solution from a high temperature, 2) by slow evaporation of C saturated solution, and 3) by creating of a thermal gradient between a C dissolution area and crystallization area. Indeed, the third technique is the only way to get a stationary state for the growth, allowing the growth of long crystals. The supersaturation distribution close to the growth front (=seed crystal) is related to the

heat and mass transport phenomena. In many experimental approaches, the seed crystal and/or crucible rotation have been applied to enhance the mixing and control the supersaturation distribution in the liquid. For example, accelerated crucible rotation technique (ACRT), implying both accelerated and decelerated movement of the graphite crucible during the process, is usually implemented with the typical maximum rotation speed of 10-20rpm [40, 41]. As a result, this drastically improves the solute concentration homogeneity (and also temperature) in the liquid. It is noted that such rotation mixes the liquid in the same way as a uniformly rotating stirrer in the laminar regime [42].

There are several advantages in SiC solution growth. First, the process occurs under the conditions close to thermal equilibrium resulting in high quality crystals with better polytype controllability [43, 44]. Second, the growing crystal is not exposed to steep temperature gradients, thus the crystal can grow free from thermal constraints. TSSG is performed typically in relatively low temperature environment from 1700°C to 2000°C as compared with PVT. By a proper control of supersaturation at the growth front, it is possible to reduce the defects densities. For example, a core of micropipe, which is a device killer defect originated from super-screw dislocation [45], can be filled during LPE process, and become completely invisible on the growing surface [46, 47]. On the other hand, the temperature below 2000°C is more favorable for 3C-SiC growth, which is rather difficult to achieve at the high temperature condition in PVT system [48]. Because above these temperature ranges, 3C-SiC undergoes a phase transformation to the α-SiC. Recently, Ujihara et al. reported that the dipping solution technique has been successfully applied for 3C-SiC growth via nucleation mechanism on C-face 4H-SiC and Si-face 6H-SiC and it has much lower stacking faults density than that of a 3C-SiC grown by chemical vapor deposition [49].

## 1.5. Purpose and main contribution of the present thesis

The present work focuses on SiC crystal growth by the top seeded solution growth process. There are two main aspects that will be addressed: first, development of the TSSG process for good quality SiC crystal, and second, investigation of the effect of Al on the process and its incorporation into the crystals. We only considered the growth of the 4H-SiC polytype in this work. In the following chapters, we will discuss the different elementary steps of the TSSG process and optimize the conditions to control the growth front stability with reasonable growth rate and a good crystal quality. In addition, we will systematically investigate the morphological stability at the crystal surface under the equilibrium condition without growth and also during the initial stage of the process. At the end of this thesis, we will evaluate the nitrogen and aluminum concentrations in grown crystals and show that TSSG would be a suitable method for heavy doping.

## 1.6. References


[1] Edward Goodrich Acheson, U.S. Patents #492,767 and #615,648. Feb. 28, 1893.

[2] H. Baumhauer, Zeit. Krist. 50, 33, 1912.

[3] W. F. Knippenberg, Philips Res. Repts 18, pp. 161, 1963.

[4] J. A. Lely, Ber. Dtsch. Keram. Ges., 32: pp. 229, 1955.

[5] Yu. M. Tairov, V.F. Tsvetkov, J. Crys. Growth 43(2), pp. 209, 1978.

[6] http://www.cree.com, accessed 27 March 2014.

[7] A.P. Mirgorodsky, Physical Review B, **52**(6), p. 3993, 1995.

[8] N. Tsavdaris, PhD thesis, Université Grenoble Alpes, 2015.

[9] Y. Inomata et al., Yogyo-Kyokai-Shi 77(4), pp.24, 1969.

[10] Y. A. Vodakov et al., Sov. Phys. Solid State, 24, pp. 1377, 1982.

[11] A. Itoh et al., Appl. Phys. Lett. 65, pp.1400, 1994.

[12] K. Kojima, H. Okumura, S. Kuroda, K. Arai, JCG269, vol.2-4, pp.367, 2004.

[13] M. Soueidan and G. Ferro, Adv. Funct. Mater. **16**(7): p. 975-979. 2006.

[14] R. A. Stein et al., Mater. Sci. Eng., B, 11, pp. 69, 1992.

[15] G. L. Harris, *Properties of Silicon Carbide*, EMIS Datareviews Series, no. 13, INSPEC, IEE, UK, 1995.

[16] G. Pensl, H. Morkoc, B. Monemar, and E. Janzen, MSF 264-268, pp.3, 1998.

[17] H. Abderrazak and E. S. Bel Hadj Hmida, *Properties and Applications of Silicon Carbide*, Eds Rosario Gerhardt, ISBN, pp.361-388, 2011.

[18] B. Thomas et al., Mater. Sci. Forum, 527-529, pp. 135, 2006.

[19] T. Kimoto and J. A. Cooper, *Fundamentals of silicon carbide technology*, John wiely & Sons, Singapore, 2014.

[20] K. Eto et al., 858, pp. 77-80, 2016.

[21] K. Kusunoki et al., J. Cryst. Growth, 395, pp. 68-73, 2014.

[22] L. G. Matus, J. A. Powell, and C. S. Salupo, Appl. Phys. Lett., 59, pp.1770, 1991.

[23] T. Urushidani et al., International conference on solid state devices and materials in 1993, proceeding, pp. 813, Chiba, Japan.

[24] T. Kimoto et al., Inst. Phys. Conf. Ser., 141, pp.437, 1995.

[25] J. W. Palmour et al., *Silicon carbided and related materials* 1993, pp.499, 1993.

[26] J. W. Palmour et al., *Compound semicondoctors*, Bristol, pp.377, 1995.

[27] http://www.mitsubishielectric.com/

[28] A. Elasser and T. Paul Chow, proceeding of the IEEE, 90, pp. 969, 2002.

[29] D. Elwell and H. J. Scheel, *Crystal Growth from High-Temperature Solutions*, Academic Press, 2011.

[30] D. Chaussende et al., J. Phys. D: Appl. Phys. 40, pp. 6150, 2007.

[31] J. Drowart, G. de Maria and M. G. Inghram, J. Chem. Phys. 29, pp.1015 (1958)

[32] E. Schonherr, Growth Prop. Appl. Crystallogr. 2, pp.51 (1980)

[33] H. Matsunami, Physica B185, pp.65 (1993)

[34] Tairov et al., *Electrotechnical Materials,* Eds. Koritskii, Yu.V., V.V. Pasynkov, B.M. Tareev. 3, pp. 446, 1988.

[35] D. H. Hofmann and M. H. Müller, Mater. Sci. Eng., B, **61–62**. pp. 29–39, 1999.

[36] R. C. Glass et al., MRS Bulletin, proceeding 22(03), p. 30, 1997.

[37] M. Syväjärvi et al., J. Cryst. Growth, 197, pp. 147-154. 1999.

[38] M. Soueidan et al., J. Cryst. Growth, 293(2): p. 433-437. 2006.

[39] D. Rytz and H. J. Scheel, J. Cryst. Growth 59, pp. 468, 1982.

[40] K. Kusunoki et al., Mater. Sci. Forum, 457-460, pp.123-126, 2004.

[41] K. Kamei et al., J. Cryst. Growth, 311, pp. 855–858, 2009.

[42] H. J. Scheel and E. O. Schulz-Dubois, J. Crys. Growth 8, pp. 304, 1971.

[43] R. Yakimova and E. Janzen, Diamond Relat. Mater. 9, pp. 432, 2000.

[44] K. Kusunoki et al., Mater. Sci. Forum 615-617, pp. 137, 2009.

[45] F. C. Frank, Acta Cryst. vol.4, pp.497, 1950

[46] M. N. Khan et al., J. Crys. Growth 254, pp. 137, 2003.

[47] O. Filip et al., J. Crys. Growth 271, pp. 142, 2004.

[48] W.E. Nelsonet al., J. Appl. Phys. 37, pp.333, 1966.

[49] T. Ujihara et al., J. Crys. Growth 310, pp.1438, 2008.

[50] Rohm Semiconductor, *Silicon Carbide Schottky Barrier Diodes* (CNA110004_wp).

# Chapter 2. Implementation of the top seeded solution growth process

Solution growth is the most suitable process when the compound to crystallize incongruently melts like SiC material. However, there are some technical difficulties faced by the SiC crystal growers. In this chapter, we will introduce several technical points, important for the TSSG method implementation. The geometry of our TSSG process will be presented. Then, we will discuss several options that have been studied for improving the technical issues which may occur during the process and which can be improved, namely i) optimization of solvent composition, ii) rotation of seed crystal, and iii) control of the meniscus.

## 2.1. The TSSG process setup

A modified Czochralski (Cz) puller, named "HULK", has been setup for SiC top seeded solution growth (TSSG). Figure 2.1 shows a schematic diagram of the puller. It consists of three main parts (see Figure 2.1 (1)-(3)):

(1) The supervision and control/command unit. It is composed of power supply and distribution, measurement signal collection and control (T, P, positions …) and the computer based monitoring interface.

(2) The heating unit. It is composed of an induction coil, a capacitor box and a power generator

(3) The reactor, strictly speaking, which is composed of the growth chamber, gas lines (only Ar 99.9% has been used in this work), and vacuum system, based on a primary pump. Two rotation/translation units are located at the top and the bottom of the chamber. Above the

chamber, an optical pyrometer focuses on the crucible through a quartz window to measure the temperature.

The puller is also equipped with safety elements able to stop experiments in case of trouble. The main elements aim at detecting:

- The absence or a too low flow rate of water cooling in the generator and the chamber
- Overheating of the steel chamber (with 4 thermocouples)
- Overpressure with a gauge and a safety valve.
- End of movements with mechanical switches.

The reactor has not been initially designed to work at high temperature; the water cooling of the chamber is usually weak. We thus placed a 6 mm thick graphite felt covering the inner walls of the chamber. This insulation ensures a safe working of the reactor up to 2000°C. There are four useful glass windows with a maximum diameter of 30 mm at top flange of the chamber. Among them, one is used for the temperature measurement and three windows are employed for the direct observation of the crucible with naked eyes during experiments. Heating is achieved by induction with a 40kW power generator operating at a frequency of 15 kHz (HUTTINGER TRUHEAT MF3040). The details of the graphite crucible are given in section 2.1.1. The reactor is equipped with the two rotation/translation units, completed by position transducers at the top and bottom. They drives both the crystal movements through the pulling rod and the crucible through the support rod, both rods being in stainless steel. The whole puller is monitored by a customized automation system developed by STIGMA Company (Grenoble).

The two-colors optical pyrometer (IRCON) placed at the top of the reactor can detect the temperature from 1000°C to 3000°C, using the blackbody radiation phenomena. The pyrometer

focuses on graphite (usually graphite lid or inner crucible wall). Due to the geometrical limit of the chamber design (see Figure 2.2), there is thus a difference, not measured but reproducible, between the measured temperature and the actual temperature at the solvent surface (crystallization region). This temperature difference has been estimated by numerical simulation and is about 30°C, when the solvent temperature is set at 1700°C or more.

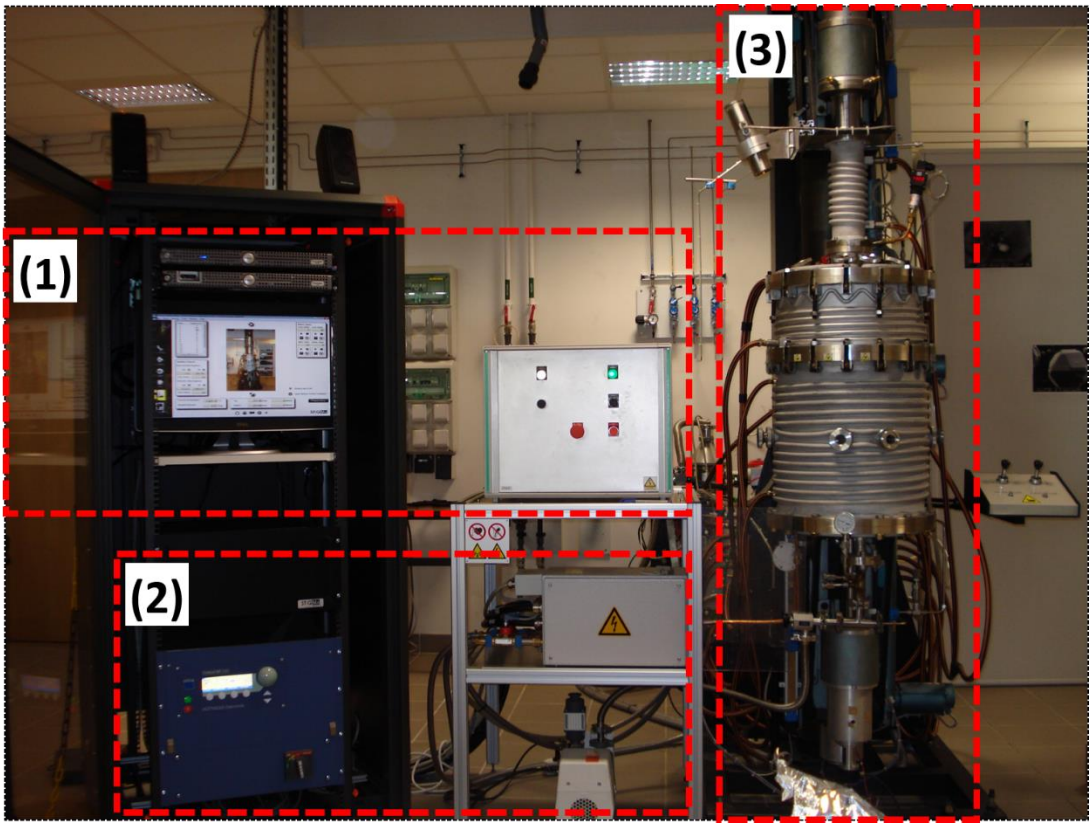


Figure 2.1. Picture of the TSSG puller implemented at LMGP for the growth of SiC, with the three functional units. (1) The supervision and control/command unit. (2) The heating unit. (3) The reactor.

### 2.1.1. The crucible kit

The crucible kit is composed of crucibles strictly speaking, and insulators located inside the chamber. The solution growth process is implemented at high temperature; thus the crucible material must be chemically and physically stable for long time operation at high temperature. There are some required characteristics for the building materials of the crucible: 1) it must withstand high temperature and thermal shocks, 2) it should have a high corrosion resistance with respect to Si based solvents, 3) it must have sufficient electrical and thermal conductivities, and 4) it should have a reasonable price, in the sense that the material itself should be cheap but also easily machinable. Therefore, the most suitable crucible materials for SiC growth is graphite as it fulfils all the criteria listed above. Moreover, the graphite crucible is the most convenient carbon source for SiC synthesis from the liquid-phase.

Figure 2.2 shows the details of the reactor geometry. The graphite crucible is composed of two parts, both having different purposes. First, the furnace which is composed of outer crucible and a lid, acts as a 'susceptor' in this system. The external diameter of the furnace is about 100 mm and is thermally insulated by graphite felt. This susceptor is directly heated by the electromagnetic field applied by induction coil. Indeed, due to the skin effect of induction heating, most of the power density (Joule losses) is deposited in this susceptor. The temperature is measured by optical pyrometer on the inner walls of the graphite lid, with a tilt angle between 45-55°, as shown in Figure 2.2. Second, the inner crucible, which acts both as a solvent container and as carbon source for SiC growth. The external diameter of inner crucible is about 70 mm with a height of 70 mm. As shown in Figure 2.2, the inner crucible has a special groove shape at the top area in order to reduce solvent losses by capillarity during the experiment. This crucible is mainly heated indirectly by radiation from the susceptor.

During the experiments, it is possible to observe directly the surface of the solvent with a mirror, placed vertically above the crucible. Thus, the contact position between seed crystal and the solvent can be detected or confirmed by naked eyes.

As a rule and all over this work, the temperature is higher at the bottom of the small crucible (dissolution area) and lower at the surface of the liquid, where the seed is in contact with the solvent (crystallization area).

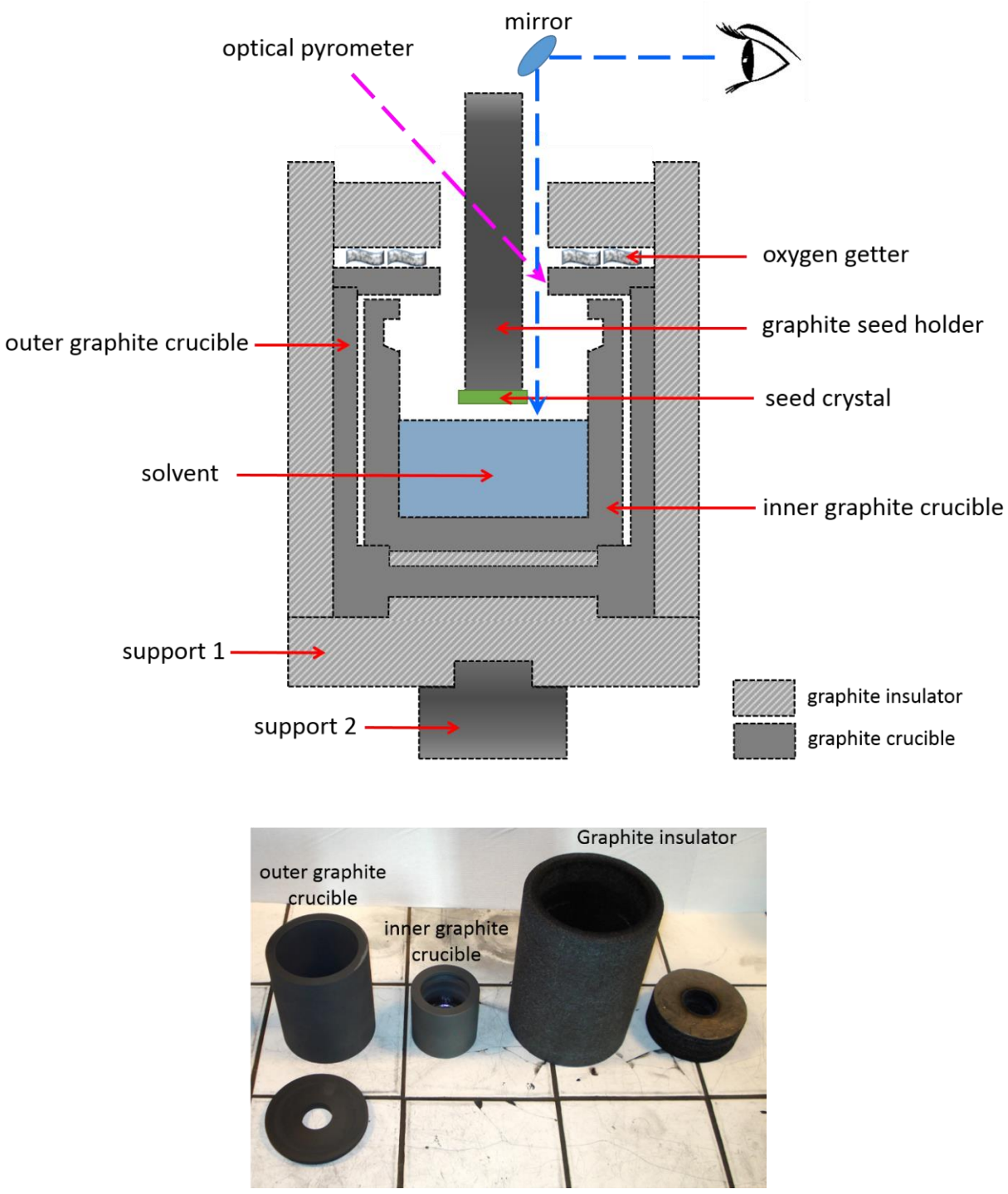


Figure 2.2. Drawing of the TSSG furnace geometry (up) and a camera picture of the different pieces of the crucible kit, composed of graphite crucibles and insulation parts (down).

**-Oxygen getter**

For all the experiments, we used several pieces of titanium-zirconium (Ti-Zr) alloy as oxygen getter material, placed between the graphite lid and the top insulation (see Figure 2.2). The native oxide layers on raw silicon and metal can generate oxide particles floating on the solvent surface. These particles are heterogeneous nuclei for the crystallization of SiC. They can also adsorb at the seed surface and disturb the growth. Then the crystal quality will be decreased due to the inhomogeneous contact between seed crystal and solvent. From the thermodynamic point of view, Zr is a very effective deoxidizing metal. In addition, Ti exhibits a wide solubility range against both oxygen and nitrogen; it is one of the best and simplest getter materials. Theoretically, the equilibrium pressures of oxygen with oxide of Ti and Zr are $1.37 \times 10^{-24}$ and $4.25 \times 10^{-25}$ (Pa) at 1436K, respectively. These values are lower than that of Si ($6.04 \times 10^{-19}$ Pa at 1463K) [1]. Their oxidation kinetics increases with temperature and actively absorbs gases [2, 3]. Experimentally, we observed the significant differences with and without the Ti-Zr getter. With it, the liquid surface can be perfectly clean (free of particle) as seen by direct observation with naked eyes. However, there is a temperature limitation around 1520°C where Ti-Zr alloy starts to melt according to the Ti-Zr phase diagram as shown in Figure 2.3. Even if it is placed far from the hot zone, this alloy is not suitable for using at high temperature, such as above 1800°C. However, even if it melts, the getter has previously cleaned the liquid surface upon heating up.

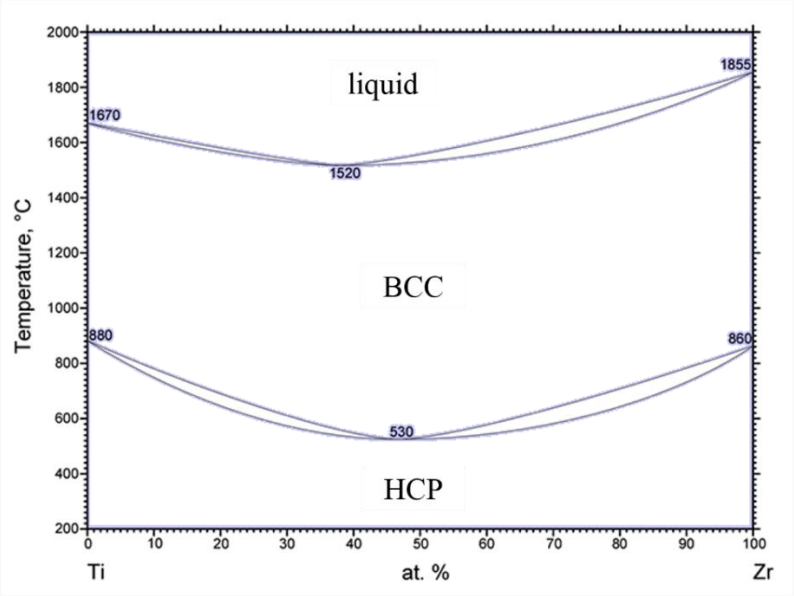


Figure 2.3. Ti-Zr phase diagram [4]. (BCC: body-centered cubic, HCP: hexagonal close-packed)

### 2.1.2. The seed holder

In our top-seeded configuration, the crystallization begins when the seed crystal is vertically dipped into the solvent. The seed holder is made of the same high purity graphite material as the crucible. Several sizes of seed holder are shown in Figure 2.4. They have been adapted to the different diameters of seed crystals.

A special mounting technique has been applied to avoid that the seed crystal falls into the solvent during the process. A graphite based glue (Aremco, Graphi-Bond 551-RN) was used to attach the seed crystal on the graphite holder. Before mounting, small amount of ethanol was added to the dense graphite glue and mixed until it becomes soft. After that it is spread on the graphite holder, then the seed crystal is stuck on it. To dry the glue, the graphite holder was kept in the oven at 150 °C for at least 5 hrs.

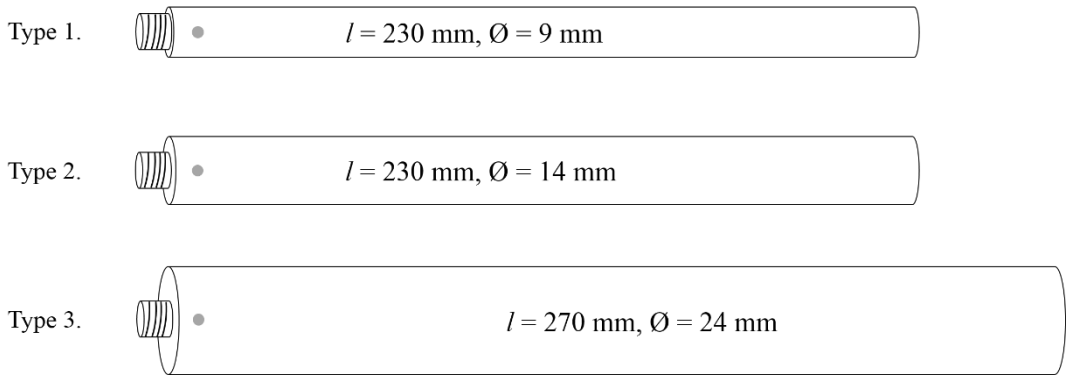


Figure 2.4. Illustration of the different sizes of the graphite seed holder used. Diameters and lengths are adapted to both the size of the seed crystal and/or the targeted dipping position during the growth process.

Figure 2.5 shows the morphology and shape of the crystals grown with respect to the difference between seed and seed holder diameters. It is obvious that supersaturation distribution close to the seed surface is related to the heat flux flowing from the solvent through the seed crystal and then through the graphite rod as long as the seed crystal is in contact with solvent. If the heat flux perpendicular to the crystal surface is homogeneous along the entire crystal diameter (see Figures 2.5(b) and (c)), then the quality of crystal can be homogeneous. In the best conditions, the grown crystal can exhibit the natural hexagonal habits according to the SiC crystal structure. However, if the heat flux distribution is not homogeneous, the related supersaturation distribution will get inhomogeneous and polycrystalline growth could develop at the edge of the crystal. Such latter case is illustrated by Figure 2.5(a). This means that the diameter of the seed holder must be adapted to avoid polycrystal formation. There are actually two main technical sources of polycrystal formation:

- Not adapted diameter of the seed holder. Empirically, if the diameter of seed crystal is over 30% bigger than the one of the seed holder, then it is almost not possible to stabilize the growth front at the edge of the crystal due to the parasitic crystallization started from periphery of the seed (Figure 2.5(a)).
- Contact between liquid and graphite of the seed holder. If the diameter of the seed holder is larger than the one of the seed, or if the seed is dipped too deep in the liquid, then the liquid is in direct contact with the graphite rod. This will give rise to parasitic crystallization. In other words, graphite provides an unexpected host of nucleation sites to compete with the seed crystal when it comes into contact with the solvent. If these unwanted nucleation sites are close to the seed crystal, it will be very difficult to keep the single crystallinity of the growing crystal during long time growth because of the competition between single and polycrystal growth. However, this technical matter can be improved by the meniscus technique. Further details on meniscus will be given in section 2.2.

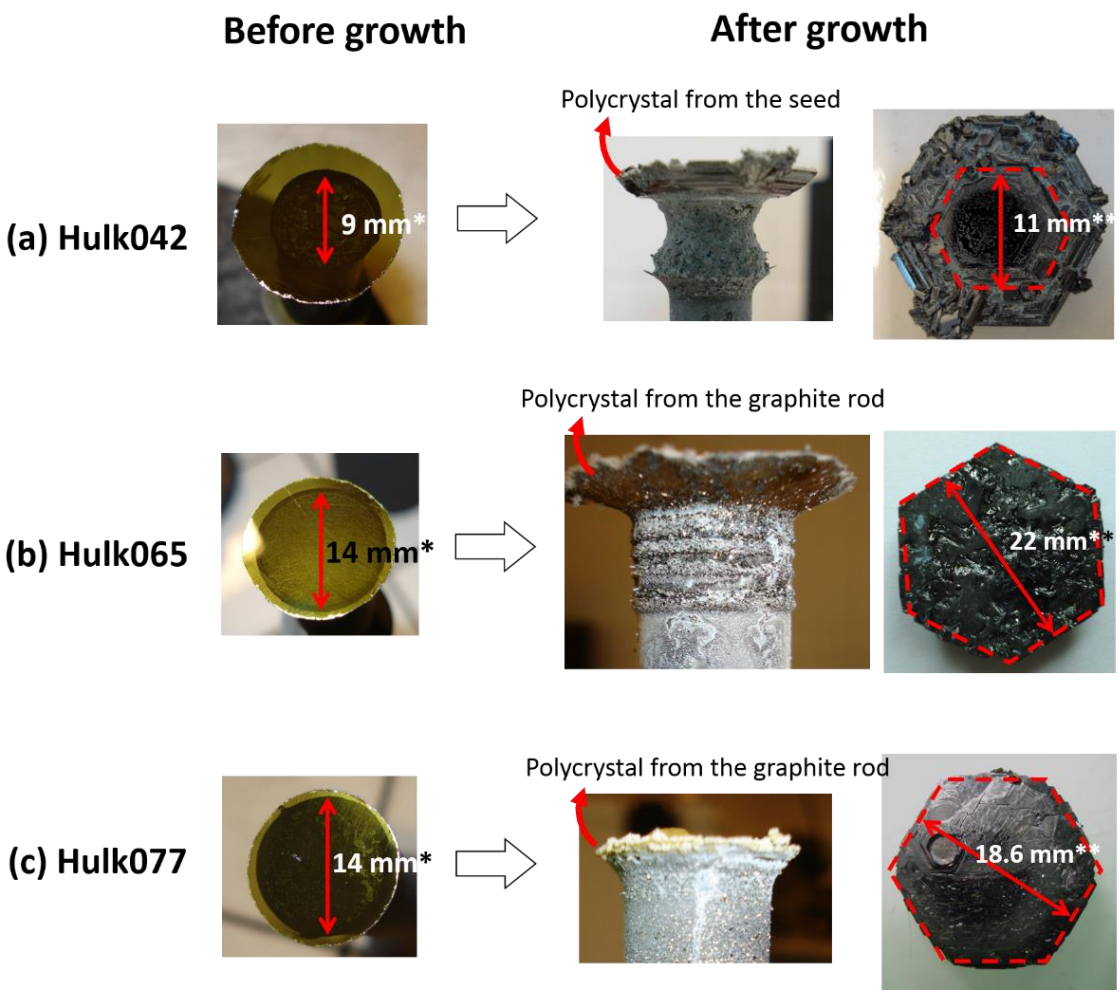


Figure 2.5. Various diameters of the seed crystal and graphite seed holders were used for qualitative comparison. The experiments were carried out under the same conditions (Si-Cr based solvent, 4H-SiC C-face seed crystals, 1mm height of meniscus, 1850-1900°C). On the hexagonal faceted region (inside red dash-line area), polytype of grown layers was 4H-SiC but not outside of this region. (*diameter of seed holder, **diameter of hexagonal faceted region)

## 2.2. Process development

In the TSSG process of SiC, there are three main steps to consider as shown in Figure 2.6, 1) reaction/dissolution of carbon at the graphite/solvent interface, 2) transport of solute from the

dissolution area to the growth front, 3) crystallization of SiC on the seed. These three critical steps must be tackled as each of them is directly or indirectly linked to the final crystal quality. Thus, it is important to discuss about the development of SiC growth process from a technical point of view.

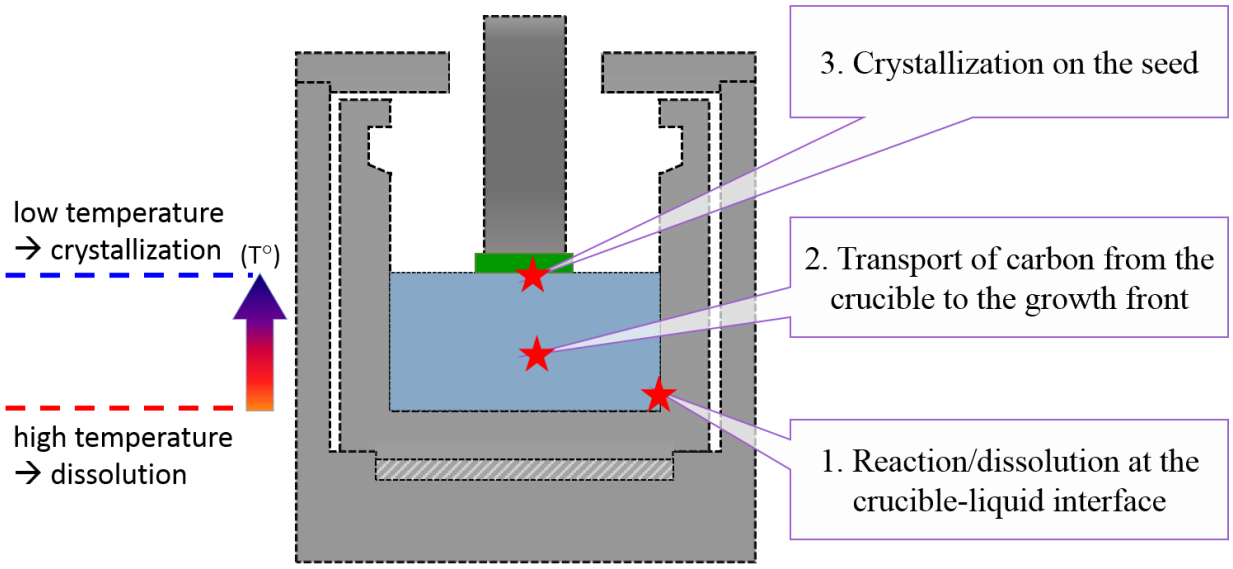


Figure 2.6. The three main steps in the SiC TSSG process: i) reaction/dissolution at the graphite-liquid interface, 2) transport of carbon from the crucible to the seed, 3) crystallization on the seed.

### 2.2.1. Dissolution of carbon at the graphite/liquid interface

The difference between Czochralski (Cz) method and TSSG method is the use of 'melt' and 'solution'. Cz method is usually applied for congruent melt, i.e. melt having the same composition then the solid to crystallize such as silicon and sapphire. TSSG method is often applied for compounds exhibiting non-congruent melting, i.e. the liquid composition is different from that of the solid. In this latter case, the use of solution growth (also called flux growth) is appropriate. The

compound is thus crystallized from its dissolved elements (solute) into a solvent. According to the binary Si-C phase diagram, Si can be used as a solvent for SiC growth. However, the problem is the low solubility of carbon in liquid silicon, resulting in a very low growth rate.

As mentioned, there is no stoichiometric liquid-phase of SiC in the Si-C phase diagram. There is however a liquid in equilibrium with SiC. Durand and Duby summarized several previous studies on the assessment of carbon solubility determined by weight loss or chemical analysis [6]. As shown in Figure 2.7, the solubility of carbon in liquid Si is about 0.03 at% at 1678 K. In the low temperature range, Dalaker and Tangstad reported one of the best fit graph of carbon concentration compared to the previously reported ones as shown in Figure 2.8 [5]. In this graph, the carbon concentration in molten Si at 1678 K is even lower than Durand's report [6]. It is worth noting that with such a low carbon concentration in the liquid, the resulting growth rate is in the μm/hr range at low temperature. Thus it is necessary to increase the carbon solubility.

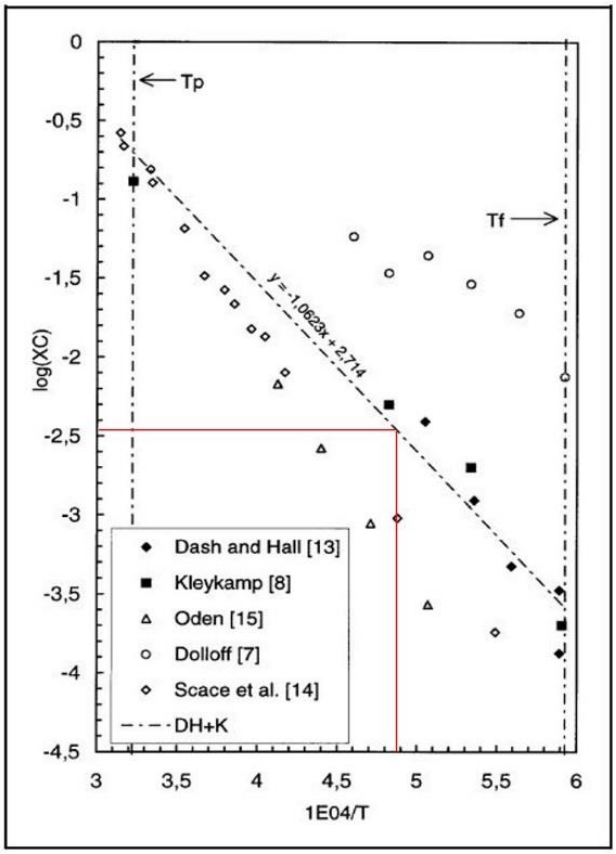


Figure 2.7. Evolution of carbon solubility in liquid Si gathered in ref. [6] in the temperature range from TF = 1414 °C = 1687 K (melting point of Si) to Tp = 3103 K (approximate temperature of the SiC non congruent melting).

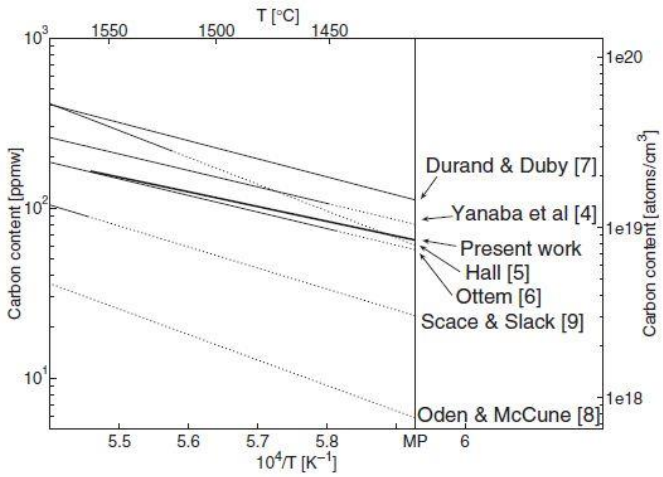


Figure 2.8. Carbon concentration as a function of temperature with previously reported results summarized in Ref [5].

Several studies have reported that adding transition metals (Fe, Ti, Cr, Co, Sc, etc.) to silicon could improve the carbon solubility. Since the solubility of carbon in the solvent directly influences the growth rate, improvement of the growth rate without increasing the temperature can be achieved. From the theoretical point of view, Ivantsov et al. [27] reported that the C solubility in the transition metal alloy increases even at low temperature while the number of *d*-electrons of the added elements decrease. For example, Co ($3d^7 4s^2$) has lower C solubility than Sc ($3d^1 4s^2$) at 1600°C. Earlier, Pellegrini et al. [28] tested several transition elements with different solvent compositions. They demonstrated that it is possible to achieve more than 1 mol% of dissolved carbon in the alloy using Zr, Ti and Cr at 1800°C, but no effect by adding Nb. These results are in disagreement with Ivantsov's assumption. Although Ti ($3d^2 4s^2$) and Cr ($3d^5 4s^1$) have smaller number of *d*-electrons than Co, they could barely achieve 1at% of carbon solubility at 1800°C. Thus we can infer that there is no real general rule and the carbon solubility must be experimentally assessed.

- **Literature study of the transition metal alloys**

In the past decades, many studies on the Si based Si-$M_1$ or Si-$M_1$-$M_2$ systems have been carried out with the aim to increase the carbon solubility in the Si based liquid where M is a specific transition metal such as Fe, Ti, Cr, etc. From Si-transition metal solvents, a maximum of 10 at% of carbon solubility could be obtained. The results from the literature are summarized in Table 2.1 and the details are as follows.

1) Si-Ti solvent: Kusunoki et al. presented several results on SiC solution growth using Ti-Si solvent and developed the system over the past decades. Although values of carbon solubility in

the Si-Ti solvent are not given, they have achieved a growth rate of 60 μm/h at 1650°C using 23at% of Ti in 2004 [7], and successfully demonstrated the growth rate of up to 200 μm/h by using the accelerated crucible rotation technique (ACRT). They also demonstrated a good structural quality of the grown crystals [8, 9]. Most recently, 3 inch diameter 4H-SiC with low defect density was demonstrated using this same solvent composition [10].

2) Si-Fe (Co) solvent: Yashiro et al. investigated the enhancement of growth rate using Si-Co and Si-Fe alloys based on the CALPHAD method and experiments in a low temperature liquid phase epitaxy (LPE) configuration [11]. The growth rates were improved by a factor of 3 (6 μm/h) when adding Co30mol% and by 6 (12 μm/h) when adding Fe50 mol%. The growth rate in pure silicon with similar operating conditions was 2 μm/h. Yoshikawa et al. further studied the phase equilibria in the Fe-Si-C diagram. They showed that a Fe36mol%-Si alloy would dissolve 0.5mol% of carbon in the temperature range of 1523-1723K. It is noted that C solubility in the Si-Fe solvent (adding Fe in the range of 36 ~ 70 mol%) is estimated to be $8.1 \times 10^{-3} \sim 2.1 \times 10^{-4}$ mol% at 1723K, respectively. In this high Fe concentration range, the solubility of carbon in Si-Fe solvent decreases while increasing the amount of Fe. The solubility of C in pure Si solvent is about $7.1 \times 10^{-5}$ mol% at the same temperature. The concentration of carbon increases with the amount of Fe in the low Fe concentration range. Thus Fe36mol%-Si is an optimal solvent composition for the low temperature growth of SiC as it exhibits the highest carbon dissolution.

3) Si-Cr solvent: If the combined growth condition with Si-Ti solvent and ACRT has broken new ground in the field of SiC solution growth with a high growth rate, then chromium would be the most effective transition element for reaching the highest growth rate. Recently, Mitani et al., reported the remarkable achievement on the growth rate, exceeding 760 μm/h in a Si-Cr40at% based solvent at 2323K [12, 13].

4) Si-Sc solvent: M. Syväjärvi et al. has reported on the sandwich configuration for liquid-phase epitaxial growth of SiC using Si-Sc solvent where the growth rate exceeding 300 μm/h could be achieved at 1750°C by adding 28at% of Sc and under high temperature gradient (~50°C/cm) [14, 15].

Table 2.1. Literature overview of the SiC solution growth under various solvent condition.

| Authors | Solvent | T (°C) | growth rate (μm/h) | Conditions |
|---|---|---|---|---|
| K. Kusunoki [7-10] | Si-Ti 23at% | 1650 | 60 | without ACRT technique |
| | Si-Ti 23at% | 1700 | 200 | with ACRT technique |
| N. Yashiro [11] | Si-Co 60mol%<br>Si-Fe 45mol%<br>Si-Ti 30mol% | 1100-1500 | 6<br>12<br>8 | Growth by slow cooling from 1500 to 1100 with 0.5°C/min |
| M. Syväjärvi [14, 15] | Si-Sc 28at% | 1700-1850 | 300 | sandwich method with high temperature gradient of ~50°C/cm |
| T. Mitani [12, 13] | Si-Cr 40at% | 2050 | 760 | |

To summarize, there has been many studies about solvent assessments for SiC solution growth or liquid phase epitaxy. Considering real bulk growth, Ti-Si and Cr-Si alloys are the most convincing ones. The highest growth rate and the longest crystals reported so far were obtained in a chromium based alloy at high temperature, typically higher than 2000°C. For technical reasons, we restricted this work to temperatures lower than 2000°C. We investigated also several possible solvents. In our system, the average growth rate with pure Si was about 15 μm/hr (at 1700°C). The maximum growth rate with Si-Cr based solvent was 470 μm/h at 1900°C. However, it was very

difficult to keep a good crystal quality (i.e. single crystal) with such a high growth rate. The optimum growth rate with homogeneous quality of grown crystal was obtained around 120 µm/hr.

We have seen that graphite is the obvious crucible material used as container for liquid Si at high temperature. When the temperature rises above the melting point of silicon (1414°C), the chemical reaction between $C_{graphite}$ and Si begins at the interface between crucible and solvent, because the graphite is not in equilibrium with liquid Si. Actually, the reaction starts at the solid state, before melting of the alloy. This will be neglected in the following. The dissolution of carbon is thus not a single step process, because it is also associated to a reaction forming a SiC interlayer at the graphite/liquid interface.

### 2.2.2. Transport of carbon: control of the convections

In the TSSG configuration, it has been shown that the growth of SiC was strongly dependent on the carbon transport from the dissolution zone to the crystallization zone, both in terms of growth rate and growth front stability. It is thus essential to understand and control the hydrodynamics of the liquid. The basic study of fluid dynamics in the liquid has already been reported by Mercier et al. [16, 17] and theoretically refined by numerical simulation by Ariyawong [18].

Under the condition of very low solute concentration in the Si solvent at temperature below 2000°C, there are four main convections to be considered (figure 2.9) which are 1) buoyancy convection, 2) Marangoni convection, 3) forced convection, and 4) electromagnetic convection. In order to evaluate the weight of each convection, several dimensionless numbers are available, such as Rayleigh number, Marangoni number, and Reynolds number. These numbers can be used

to characterize the stability of the flow and define the predominant convection. This has been extensively detailed in the PhD theses of Mercier and Ariyawong [18, 21]. The main conclusions are gathered following:

1) Buoyancy convection, which appears naturally is caused by the differences in the temperature or solute concentration in the liquid. The solubility of carbon in Si solvent is rather small (< 1 at%) below 2000°C, thus the effect of solute concentration to the convection can be neglected. Likewise, buoyancy convection will only refer to temperature variation in this study. The hottest zone (or heating zone) of the crucible influences the direction of this convection. For example, when the crucible wall is intensively heated, the buoyancy convection results in the upward flow of fluid along the crucible wall while it flows downward at the center of the crucible as shown in Figure 2.9(a). However, such convective patterns can be reversed when the temperature of crucible bottom is higher than the crucible wall [19]. The intensity of buoyancy convection can be evaluated by the Rayleigh number (Ra) calculated from the Grashof number (Gr) and the Prandtl number (Pr). The Grashof number is the ratio of the buoyancy to the viscous force and the Prandtl number is the ratio of momentum diffusivity to the thermal diffusivity. As a consequence, the Rayleigh number is defined as

$$Ra = Gr \cdot Pr = \frac{g\beta\Delta T L^3}{\nu k}$$

where g is the gravity ($m/s^2$), $\beta$ is the thermal expansion coefficient (1/m), $\nu$ is the dynamic viscosity (Pa·s), $k$ is thermal conductivity ($W/(m \cdot K)$) and $L$ is the characteristic length scale (m). Two Rayleigh numbers ($Ra_{c1}$, $Ra_{c2}$) can be used as a criteria to predict convection instability. The transition from no flow to steady state occurs at $Ra_{c1}$=1708. The transition from steady flow to the unsteady and time dependent flow occur at $Ra_{c2}$=40000. Those are used as

the reference criteria for the flow regime. In order to justify what is the flow regime in our system, it needs to compute Ra for our system and compare to those two critical values. From the Ra number, buoyancy convection can be controlled by the height of the liquid and the temperature gradient. According to the calculation adapted to our system, Ra is computed to be 6.58E-5 [18].

2) Marangoni convection, or thermo-capillary convection appears due to the variation of the surface tension along the liquid-gas interface. If the temperature at the interface between crucible and solvent is higher than near the seed crystal (or middle of the solvent) and if the surface tension is dependent on the temperature, then Marangoni convection will occur and generate a fluid flow from the crucible wall toward the seed crystal as shown in Figure 2.9(b). Marangoni convection depends on the temperature distribution due to the radial thermal gradient. If a flat interface is assumed, the temperature gradient will generate a velocity gradient at the interface which can be written as

$$\eta \frac{\partial u}{\partial z} = \chi \frac{\partial T}{\partial r}$$

where $\chi$ is the Marangoni coefficient which is the temperature derivation of the surface tension ($-2.5\times10^{-4}$ $Nm^{-1}K^{-1}$), $u$ is the radial fluid velocity and $\eta$ is the dynamic velocity. The intensity of Marangoni convection can be defined by the Reynolds number, $Re = 1.2Re_M^{2/3}$ and $Re_M$ is the Reynolds-Marangoni number as

$$Re_M = \frac{-\chi \Delta T L}{\rho v^2}$$

where $\chi$ is the Marangoni coefficient (N/(m·K)), $\rho$ is the density of the solvent ($kg/m^3$) and $v$ is the kinematic viscosity ($m^2/s$). Marangoni convection is affected by the characteristic length

(free surface of the solvent) and thermal gradient along the liquid surface. $Re_M$ in our system is computed to be 2.22E+3.

3) Forced convection is usually generated by the external forces such as the seed crystal rotation or crucible rotation. In our experiments, only the crystal rotates. This creates convection loops with opposite directions compared to buoyancy (Figure 2.9(c)). Due to the rotation of the crystal, azimuthal components of the forced convection are activated. The fluid velocity is thus defined by

$$v_\phi = \Omega_{seed} r$$

where $\Omega_{\text{seed}}$ is the rotation speed of seed crystal and $r$ is the radial coordinate. Thus, forced convection can be enhanced by increasing the rotation speed and the seed crystal diameter. In addition, Reynolds number related with rotation is defined as a ratio of inertial force to viscosity ($v$)

$$Re = \frac{v_{stir} L}{v}$$

For a flow in a cylinder of diameter $d$, the laminar flow occurs when $Re_d < 2000$ while the turbulent flow occurs when $Re_d > 4000$ [20]. In between those two critical values, a transition flow where both laminar and turbulent flows can occur. In our system, for example, the computed Reynold number at 20 rpm seed rotation $Re_{\Omega seed} = 2000$ [18].

4) Electromagnetic (EM) convection, or EM stirring, is caused by the magnetic field of the induction heating system. The effect of EM force on the fluid velocity can be estimated from the screen parameter and Alfven velocity,

$$R_w = \mu_0 2\pi f \sigma_{liquid} L^2$$

$$U_A = \frac{B_{max}}{\sqrt{\mu_0 \rho}}$$

where $\mu_0$ is the magnetic permeability of the vacuum, $\sigma_{liquid}$ is the electrical conductivity of liquid, $f$ is the frequency and $B_{max}$ is the maximum magnetic field strength. From the equation, the average velocity in the bulk liquid is obtained by the relation $U = 0.6 U_A R_w^{-1/4}$. Alfven velocity adapted in our system is computed to be $R_w$=2280 [18]. The non-homogeneously distributed EM force concentrated near the crucible wall due to the skin effect, results in a complex flow pattern as shown in Figure 2.9(d). The effect of the frequency has been studied by Ariyawong. He showed that the flow pattern is completely dominated by EM convection at low frequencies (5 to 15 kHz). In our case, the frequency is 15 kHz. The EM convection is thus very important on the fluid movements and mass transport [18].

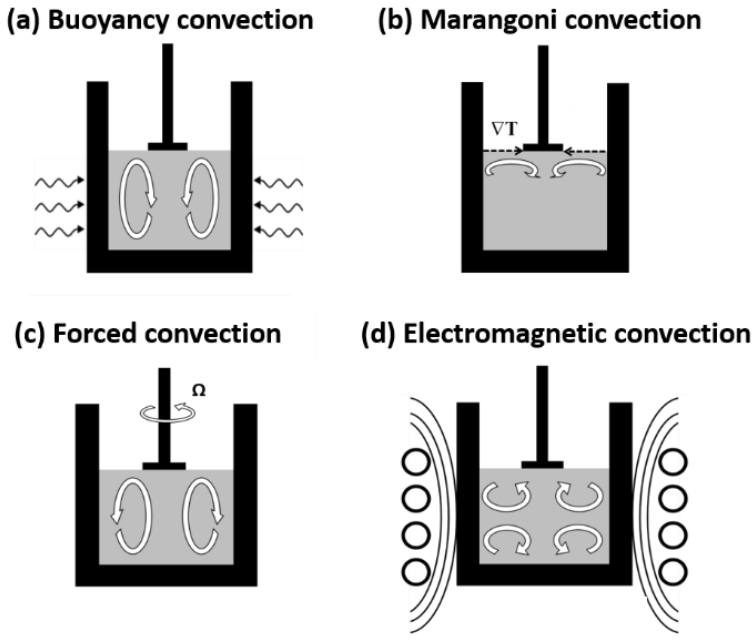


Figure 2 9. Four convection mechanisms occurring in the solution growth process of SiC [18, 21].

### 2.2.3. Crystallization and growth front stability

To date, there are many reported values of growth rates. It has already been detailed in section 2.2.1. But the literature is very poor concerning thorough description of SiC growth kinetics and the related instability issue. This is actually a current important topic for the community as all research group are facing this issue. Figure 2.10 gives an illustration of the growth front instability issue, which results in poor quality of the grown crystal.

The corresponding experimental conditions are summarized in Table 2.2. Here we can see the effect of two applied parameters (temperature and rotation speed of seed crystal) and one response parameter (growth rate). It clearly appears that the growth rate can be increased by increasing temperature and/or rotation speed. However, if the growth rate is over a critical value (above 15 µm/hr and below 70µm/hr in the figure, it seems difficult to keep a stable growth front. Destabilization is associated to inclusions of solvent and formation of cavities in the crystal, as can be seen from the cross-sections. For even longer times, this could give rise to a complete transition from single to polycrystal growth. Nevertheless, below this critical growth rate, it is possible to obtain homogeneous and stable step flow morphology, allowing the growth of a uniform layer without visible defects or inclusions (Hulk036).

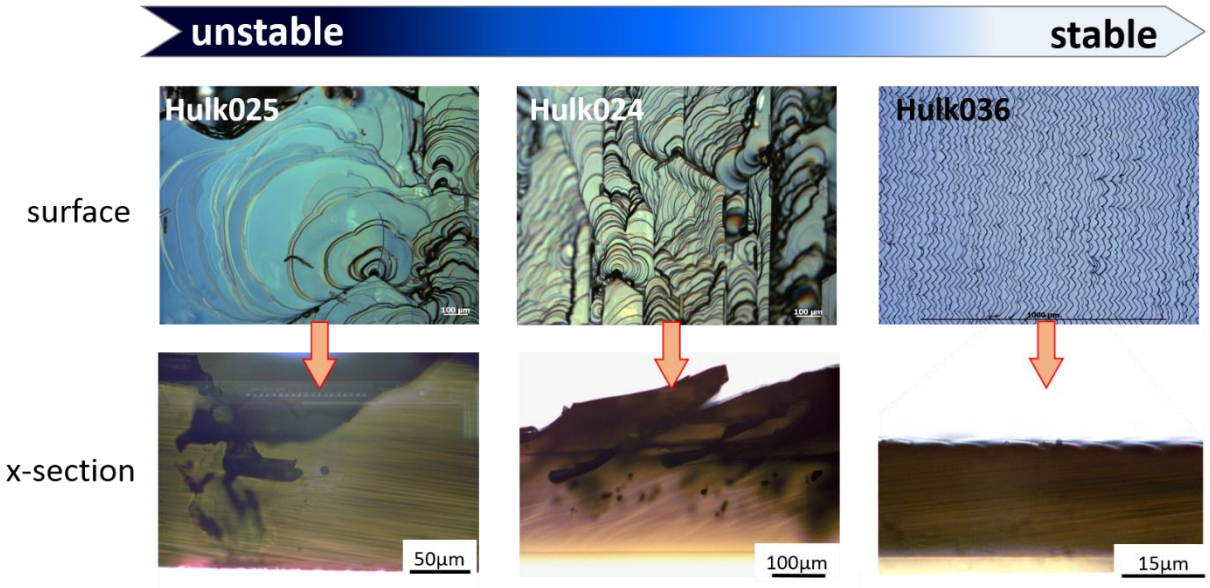


Figure 2.10. Illustration of growth front stability from observation of morphologies both of the surfaces (up) and the cross-sections (down) of thick layers, obtained under different growth conditions. Pictures are collected with optical microscopy.

Table 2.2. Experimental conditions corresponding to Figure 2.10. All experiments were carried out on 4H-SiC 4° off-angle substrates with pure Si solvent. The growth duration was 2~3 hrs.

| | T (°C ) | $\Omega_{seed}$ (rpm) | $R_{g\_max}$ (µm/hr) |
|---|---|---|---|
| Hulk025 | 1850 | 70 | ~90 |
| Hulk024 | 1850 | 30 | ~70 |
| Hulk036 | 1700 | 30 | ~15 |

We can classify the origin of instabilities into two main categories.

- Process related instabilities. By process, it is meant all what is related to transport of heat and mass, and more specifically about inhomogeneity and fluctuation in their distribution.

For example, it could be inhomogeneous temperature and solute distribution at the interface, fluctuations in the convection pattern, turbulence …

- Growth related instabilities. This includes evolution or change of the surface growth mechanism (competition between different growth modes), local congestion of extended defects, improper growth rate, polytype transition ...

## 2.3. Technical details

The optimization of the solvent composition is required in order to obtain a reasonable quality of grown crystal with less defects (i.e., micropipe or solvent inclusion). Such an optimization should improve the process reproducibility and process stability over long time experiment. Firstly, pure Si was used as solvent in order to optimize the growth conditions without defect formation. After that the optimized condition has been developed.

### 2.3.1. Growth procedure

In this study, 4H-SiC polytype substrate was used as a seed crystal for all experiments. The mis-orientation of the substrate was varied in the range of less than 0.5 to 4° toward [11-20] direction and both Si and C-face polarities were used. The experiments were performed with the procedure described in Figure 2.11, according to the following steps: 1) outgassing, 2) temperature ramp-up and thermal equilibrium with liquid homogenization, 3) crystallization and 4) reactor cooling down. Before starting the process, the pressure in the reactor was always controlled to be lower than $1x10^{-2}$ bar without any leakage.

At the first step, the temperature is raised from room temperature up to 1100°C with a heating rate of 43°C/min while outgassing the reactor. When the temperature becomes stable at 1100°C, the reactor is filled with 1 atm of argon and the temperature is increased until the desired growth temperature is reached, with the typical temperature ramp-up rate of 15.5°C/min. After reaching the growth temperature in step 2, the furnace is kept at the growth temperature for at least 20 min in order to reach the thermal equilibrium in the crucible and for stabilizing the solute concentration of the solvent. After that, the seed crystal is moved down to the solvent surface until the contact is established, then the crystallization stage begins (step 3). If the seed rotation is applied, the rotation of seed is started before contacting the solvent, i.e., before the third step. The final step of the process is the temperature cooling down after removal of the crystal from the liquid.

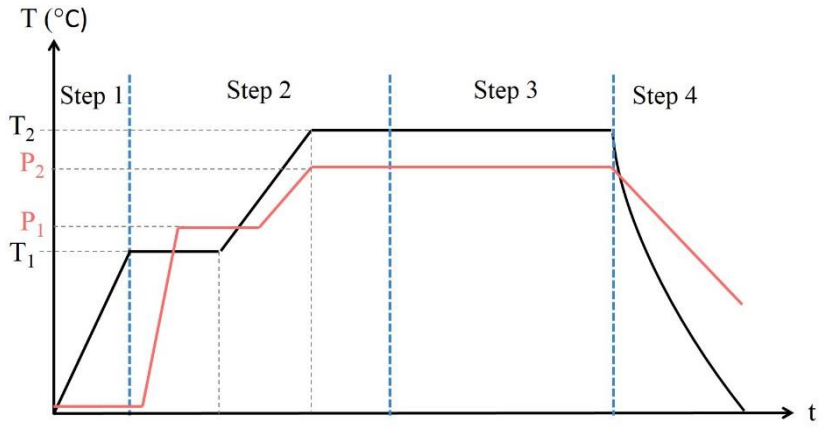


Figure 2.11. Basic experimental procedure for TSSG method. The black line and red line correspond to the temperature and pressure profiles, respectively. $T_1$ is the initial temperature of 1100°C (fixed for all experiments), $T_2$ is the growth temperature. Typically, $P_1$ is about ~0.01bar and $P_2$ is fixed at 1.05bar of argon.

### 2.3.2. Solvent

Electronic grade Si pieces were used as Si source. Medium purity (typically 99.8%) metals have been used for additives (Fe, Cr, etc.) in this study. Addition of Al has been performed for doping by using Al pellets. Theoretically, Al should not have significant effect on carbon solubility in the conditions used (temperature and composition). Carbon was supplied by dissolution from the graphite crucible to the Si liquid at the high temperature. Since growth in pure Si benefits from a much larger background with more data available (both in the literature and at the laboratory), it will be systematically used as reference system to the different developments and studies in this work. All the other solvents will be compared to pure silicon.

### 2.3.3. Rotation technique

Rotation is an additional technique to increase the growth rate by enhancing the carbon transport to the growth front since the growth rate is proportional to the carbon concentration gradient normal to the growth interface. Practically, rotation rate is effective to control the stagnant boundary layer thickness in front of the crystal surface. Also, it allows to drastically improve the uniformity by improving the axisymmetry of the process.

The influence of crystal or crucible rotation to the fluid motion has been considered in several studies [22, 23]. There is a difference in the flow patterns between the rotation of crystal and crucible depending on the rotation direction and speed. The configuration of the possible fluid patterns observed in liquids is summarized in Figure 2.12. Among them, we mainly considered the fluid flow pattern of (5) for all experiments in this study since the crucible was not rotated. Due to the centrifugal forces caused by rotation of the seed crystal, forced convection increases the fluid

velocity in azimuthal direction resulting in the whirlpool like flow pattern. Large rotation rate of the seed with fixed crucible ensures to have a solute flows from the bottom of the crucible to the seed, moving along the symmetry axis and arriving normal to the crystal surface.

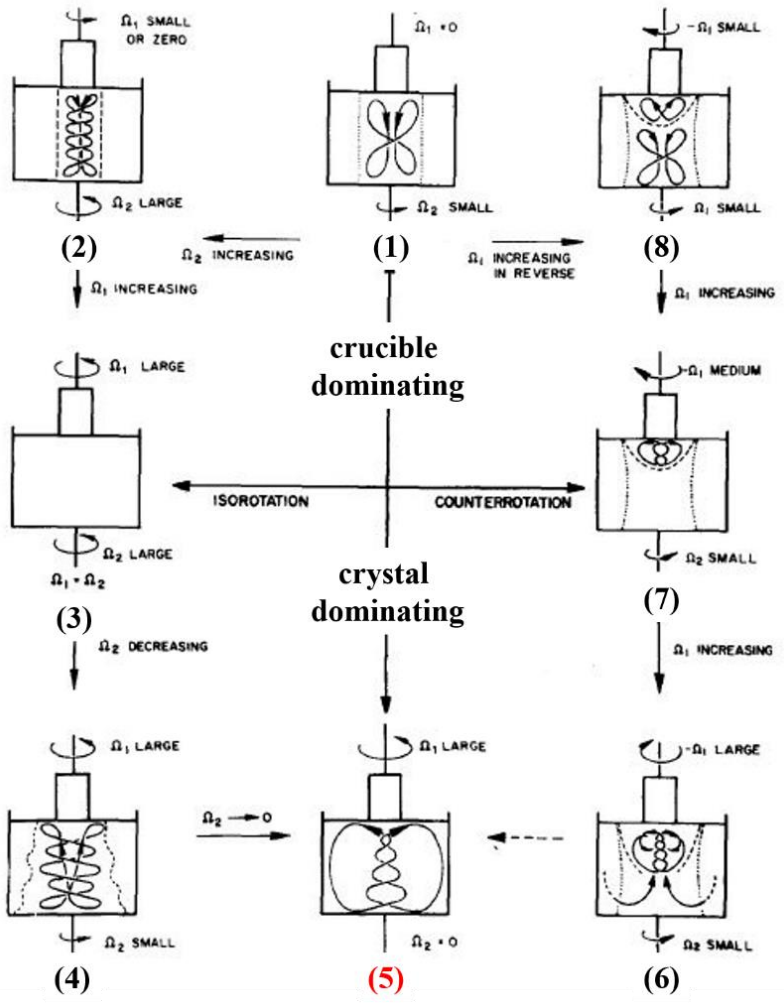


Figure 2.12. The variation of convection patterns depending on the rotation directions and magnitudes of crystal and crucible [22].

- **Crystal rotation**

Figure 2.13 shows the plot of the average growth rate obtained from our experiments using various rotation speeds of the crystal while other growth parameters are kept unchanged. The results are compared with the numerical simulation of the TSSG process under similar process conditions, which has already been discussed in Ariyawong's PhD thesis [18]. The growth rate only slightly changes if the rotation speed is below 30 rpm ($R_g$ = 15 µm/h). However, the growth rate is increased for a rotation speed above 30 rpm. The experimental results and calculation results are in good agreement, but there is a deviation above 100 rpm. It is possibly caused by the excessively high velocity of the fluid flow due to high rotation speed, so this calculation performed in the two-dimensional axisymmetric model may not be able to describe the actual flow occurring in a real three-dimensional regime. Nevertheless, the "pump" effect of the solute by increasing the rotation speed is clearly evidenced in the TSSG growth of SiC.

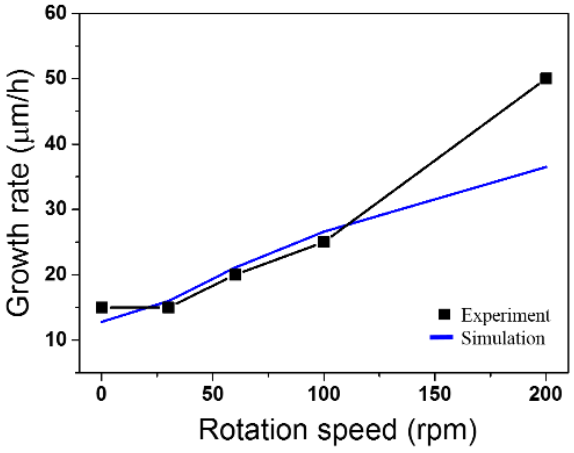


Figure 2.13. Average growth rates plotted as a function of the rotation speed and compared with numerical simulation results [18]. The simulation results are given at the crystal center at 1700°C.

- **Accelerated crucible rotation (ACRT)**

ACRT has been proposed as a technique able to introduce mechanical stirring in crystal growth from convective solution. Consider a crucible with a stationary state, then uniformly accelerate the crucible to rotation along its vertical axis, the solvent close to the crucible wall follows the crucible motion while the solvent at the rotating axis remains at rest due to inertia at the beginning of the rotation. When the solvent at the rotating axis begins to move, the differences of solute concentration and temperature in the solvent will disappear due to the convective flow and heat conduction by alternating accelerated and decelerated crucible rotation [23].

Recently, many studies have focused on the effect of forced convection by ACRT in terms of growth rate enhancement without defect generation. Kusunoki et al, have achieved a high growth rate, of about 150 µm/h without inclusion in the crystal by using this technique [8]. ACRT allows first to improve the solute homogeneity in the bulk of the liquid and second to increase the solute concentration gradient close to the crystal surface. Danno et al. have reported a rather high growth rate of about 330µm/h under optimized growth condition (Si-Cr solvent and high temperature) using the ACRT [24]. Due to technical limitation of our crystal growth puller, we have not used ACRT in the present work.

### 2.3.4. Meniscus

The meniscus is obtained by forming a convex or concave curved surface of the liquid close to the surface of the solid material. This phenomenon is commonly explained by capillary action of the liquid. In the simplest case, when the external forces are absent (under weightlessness condition), the liquid takes ball shape due to the surface tension. This state corresponds to a stable

equilibrium of the liquid since ball shape has the minimum surface energy. Capillary action is the physical phenomenon of the liquid due to adhesive and cohesive forces. Capillary action is commonly observed by the curvature of the liquid surface that is adjacent to another phase such as gas or solid where the meniscus forms. Figure 2.14 shows the general description of the meniscus formation in the TSSG geometry. When the crystal is in contact with the liquid surface, a capillary bridge (or a meniscus bridge) forms at the interface, which defines the wetted area on the crystal surface. The shape of a meniscus bridge between crystal and liquid surface changes as the solid is slowly moving away from the liquid.

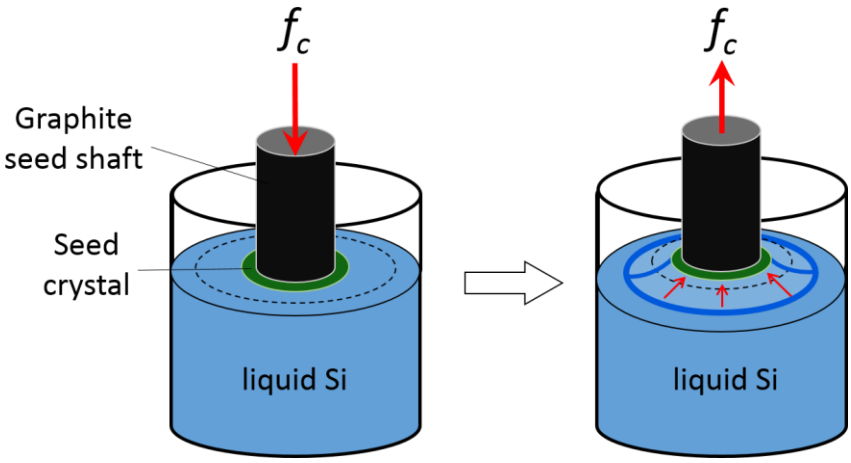


Figure 2.14. Schematic illustration of the meniscus formation in TSSG process. $f_c$ is the external force controlled by the translation unit and the red arrow marks the movement of the seed holder.

Surface curvature of the liquid gives rise to a capillary pressure which is related to an average surface curvature $Q$ via Laplace's equation

$$p_c = p_{liquid} - p_{gas} = 2\gamma_{lg}Q$$

where $p_c$ is the capillary pressure difference across the fluid interface, $p_{liquid}$ and $p_{gas}$ are the pressure in the liquid and gas phases respectively, $\gamma_{lg}$ is the interfacial tension between liquid and gas. Typically, the pressure would be higher in the phase to which the concavity of the interface is presented. If the pressure between two phases are equal, then $Q$=0, and also $p_c$=0. From the equation, average surface curvature is defined by $Q = \frac{1}{2}\left(\frac{1}{R} + \frac{1}{R'}\right)$, where R and R′ are the principal radii of curvature related to the pressures between the inside and outside of the liquid. It is noted that the surface tension at the liquid-gas interface and its curvature (and it would be the curvature of meniscus surface) can be defined by assigning R and R'.

Interaction of surface tension at the interfaces between liquid-gas $\gamma_{lg}$ and solid-gas $\gamma_{sg}$ are responsible for the meniscus as shown in Figure 2.15. Theoretically, the contact angle of the liquid quantifies the wettability of the solid surface by the liquid via Young's equation. However, the interfacial energy between liquid and solid $\gamma_{ls}$ can be neglected in this study since the seed crystal is completely wetted for the homogeneity of the growth interface (contact angle $\theta = 0$). For this reason, the angle of meniscus curvature may be substituted for the contact angle. The meniscus angle depends on the solvent composition and the crystal it is in contact with. The meniscus angle can be determined by the balance of the forces according to the Young's equation

$$\gamma_{sg} = \gamma_{lg} cos\theta$$

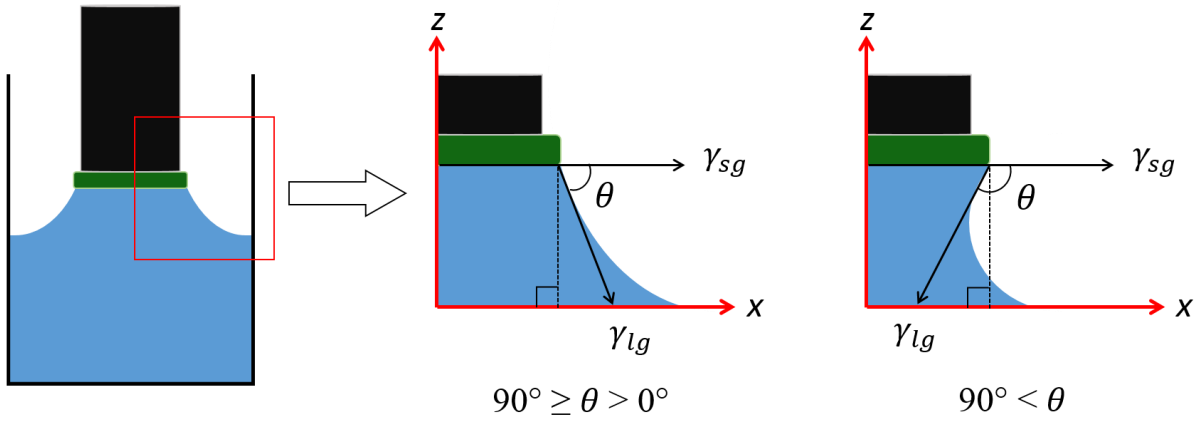


Figure 2.15. Illustration of the convex (middle) and concave (right) shapes of the meniscus dependent meniscus angle between seed and liquid.

For instance, if the crystal surface is wetted by the solvent and the meniscus angle $\theta$ approaches $90° \geq \theta > 0°$ (see Figure 2.15), indicating that wetting of the surface is very favorable, the interaction between liquid and solid should be strong [26]. In such case, the diameter of growing crystal would be larger than the original diameter of seed crystal. This phenomenon was clearly observed in the cases of Hulk042, Hulk037 and Hulk045 as shown in Figure 2.16. On the other hand, if the cohesive force of the liquid is higher than the interaction strength between liquid and solid as for the nonwettable liquid, meaning that the wettability of the solid surface is very low, then the meniscus angle $\theta > 90°$ can be expected (see Figure 2.15). Such high contact angle means that wetting of the surface is unfavorable, thus the fluid will minimize contact with the crystal surface and form a compact liquid surface. In this case, grown crystal diameter is smaller than the original diameter, as shown in Figure 2.16 (Hulk046).

| Meniscus height | Meniscus angle | |
|---|---|---|
| 1 mm (Hulk042) | 39° | 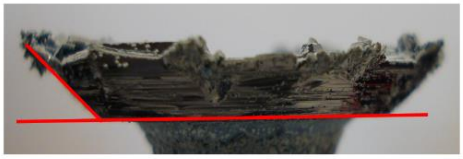 |
| 2 mm (Hulk037) | 50° | 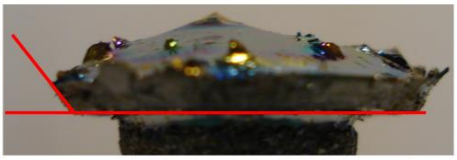 |
| 3.6 mm (Hulk045) | 70° |  |
| 4.3 mm (Hulk046) | 120° |  |

Figure 2.16. Different shapes of the meniscus bridge depending on the meniscus heights with Si-Cr solvent. The angle of meniscus was decreased while the meniscus height was increased

Technically, we cannot measure directly the contact angle between the solid and the liquid. The two information we can get are

- The meniscus height: it is simply measured by the position of the seed. The reference height is first measured when the seed touches the liquid surface. Then the seed is pulled out from the liquid surface and placed at the desired height. The position is accurately measured by a vertical position transducer. The contact between liquid and crystal is identified by direct observation.

- The shape of the crystal: we suppose that this shape is reminiscent of the liquid/gas interface shape, i.e. of the meniscus shape.

With these two measurable data, we tried to describe the meniscus for different solvents (Si100at%, Si-Cr and Si-Fe) in a temperature varying between 1700 and 1850°C. The maximum height of the meniscus was significantly changed by changing solvent compositions, due to the different capillary forces of each element. Results are summarized in Figure 2.16; they qualitatively agree well with the results reported by Daikoku et al [25]. With Si-Cr solvent, the maximum height of the meniscus with the angle of almost 90° was about 4 mm. Also, 1~2 mm height of the meniscus was most suitable to enlarge the crystal without polycrystal surrounding the grown crystal, whatever the solvent composition. Using an appropriate meniscus, SiC single crystal was successfully grown at a growth rate of over 300 µm/h with a diameter enlargement of about 41% compared to original seed size.

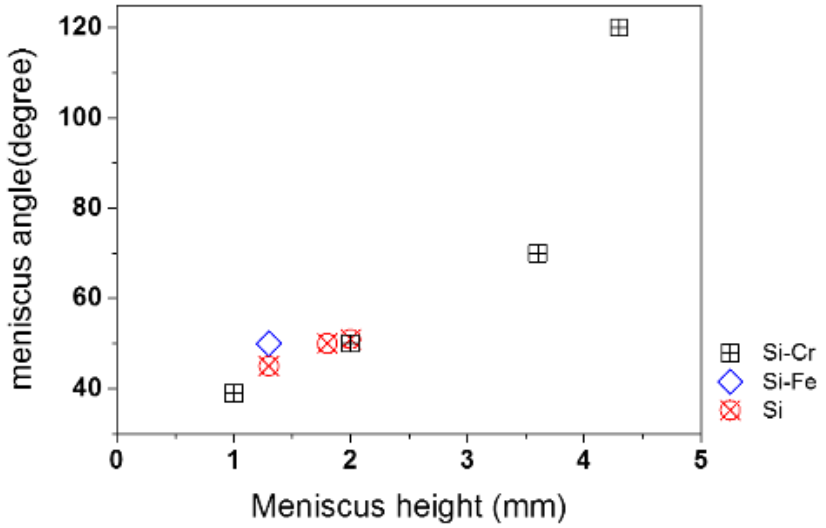


Figure 2.17. Variation of the contact angle depending on the meniscus height.

## 2.4. Conclusions of chapter 2

The important technical issues of the SiC top seeded solution growth process were discussed in this chapter. The crystal growth puller has been described. We also introduced the three elementary process steps i) dissolution of carbon, ii) transport of carbon from the source to the seed and iii) crystallization of SiC on the seed.

Based on this short technical presentation, we have exposed the different parameters and phenomena that have been scanned in this work in order to improve the growth process.

- To increase the growth rate, Si-Cr based solvent was mainly used and compared with pure Si solvent. The average growth rate with pure Si solvent was about 15µm/hr (at 1700°C). The maximum growth rate with Si-Cr based solvent was 470µm/hr at 1900°C. The typical growth rate with homogeneous quality of grown crystal was chosen to be ~120µm/hr.
- The enlargement of crystal was demonstrated by using the meniscus technique. With a 1 mm height of the meniscus, it was also possible to avoid parasitic crystallization of polycrystal around the seed.
- The effect of the rotation rate on the growth rate was studied with various rotation speed from 0 to 200rpm. The growth rate was almost constant below 30 rpm, however, it increased with a rotation speed above 30 rpm. As a consequence, the growth rate at the highest rotation speed of the crystal was about 50µm/h with pure Si solvent, i.e. more than 3-tims that without rotation. Such experimental results show a good agreement with numerical calculation results.

Combining all those improvements, we have successfully grown a 4H-SiC crystal, at a growth rate of over 300 µm/h and enlarged the diameter by about 41% compared to the original seed size.

## 2.5. References


[1] Y. H. Kim et al., J. Alloys Compd., 248(1-2) pp. 251-258, 1997.

[2] E. Gemelli and N. H. A. Camargo, Revista Matéria, 12(3), pp. 525-531, 2007.

[3] G. Bakradze PhD thesis, University of Stuttgart, 2011.

[4] http://resource.npl.co.uk/mtdata/databases.htm

[5] H. Dalaker and M. Tangstad, Mater. Trans., JIM, 50(5), pp. 1152-1156, 2009.

[6] F. Durand and J.C. Duby, J. Phase Equilib., 20(1), pp. 61-63, 1999.

[7] K. Kusunoki et al., Mater. Sci. Forum, 457-460, pp.123-126, 2004.

[8] K. Kusunoki et al., Mater. Sci. Forum, 527-529, pp. 119-122, 2006.

[9] K. Kamei et al., J. Cryst. Growth, 311, pp. 855–858, 2009.

[10] K. Kusunoki et al., J. Cryst. Growth, 395, pp. 68-73, 2014.

[11] N. Yashiro et al., Mat. Sci. Forum, 527-529, pp. 115-118. 2006.

[12] T. Mitani et al., J. Cryst. Growth, 401, pp. 681–685, 2014.

[13] T. Mitani et al., J. Cryst. Growth, 423, pp. 45-49, 2015.

[14] M. Syväjärvi et al., Mater. Sci. Eng., B, 46, pp. 329-332, 1997.

[15] M. Syväjärvi et al., J. Cryst. Growth, 197, pp. 147-154. 1999.

[16] F. Mercier et al., J. Cryst. Growth, 312, pp. 155–163, 2010.

[17] F. Mercier et al., Jpn. J. Appl. Phys., 50, pp. 035603. 2011.

[18] K. Ariyawong PhD thesis, Université Grenoble Alpes, 2015.

[19] V. Nikolov et al., Mat. Res. Bull. 17, pp. 1491-1498, 1982

[20] J. P. Holman, Heat Transfer, (McGraw-Hill Series in Mechanical Engineering), New York, pp. 215-218, 2002.

[21] F. Mercier PhD thesis, Institut Polytechnique de Grenoble, 2009.

[22] J. R. Carruthers and K. Nassau, J. Appl. Phys., 39, pp. 5205, 1968.

[23] H. J. Scheel, J. Cryst. Growth, 13–14, pp. 560-565, 1972.

[24] K. Danno et al., Mat. Sci. Forum, 645-648, pp. 13, 2010.

[25] H. Daikoku et al., Mat. Sci. Forum, 645-648, pp. 13-16, 2012.

[26] N. Eustathopoulos et al., in Wettability at high temperatures. Oxford, Pergamon, 1999.

[27] V. Ivantsov et al., Mat. Sci. Forum, 264-268, pp. 73, 1998.

[28] P. W. Pellegrini and J. M. Feldman, J. Crys. Growth, 27, pp. 320-324, 1974.

# Chapter 3. Investigation of the interaction between the liquid solvent and the 4H-SiC surface under equilibrium conditions

One of the main objective of this work is to achieve high Al doping (p+ type) of 4H-SiC crystals. It is thus important to study the effect of Al addition to the liquid on the growth front. As the Si-face is more suited to reduce nitrogen level in the crystal, we focused on Si-face, as should ensure the lowest N incorporation together with the highest Al-incorporation. This chapter aims at describing further the nature of the effect of Al on the growth interface. Using a sessile drop method, investigation of the surface reconstruction of a Si-face, 4°misoriented (0001) 4H-SiC surface in contact with pure silicon or Al-Si alloys has been carried out in the 1600-1800°C temperature range. In pure silicon and at 1600°C, the surface evolves with a three stage process: i) a slight dissolution stage forming steps, ii) a fast step-bunching leading to parallel macro-steps and iii) a slower step leading equilibrium morphology, composed of (0001), (10-1n) and (01-1n) facets. Increasing the temperature to 1800°C or adding a few percents of Al drastically enhance the second stage, but apparently reduce the third one.

## 3.1. Introduction

High temperature solution growth has been recently reconsidered as a promising approach for the growth of 4H-SiC single crystals [1]. The possibility of large diameters [2], high growth rates [3], and the achievement of high quality crystals [4] have been separately demonstrated; their combination could make it a serious competitor to the current industrial sublimation growth process. However, the growth front stability is a strong remaining issue. The occurrence of macro-

steps on the surface usually gives rise to instabilities, which in turn result in solvent trapping into the crystal. Such effect is obviously accompanied by a wealth of extended defects and generally leads to a dramatic deterioration of the crystal quality. A few percents of Al, added to the solvent (usually a Si based alloy) have been reported to stabilize the growth front by reducing the development of macro-steps on the (0001) C-face [5]. Although spectacularly demonstrated, its exact role is still unclear because of the intricate mixture of phenomena taking place in the growth process [6]. All the previous studies have tried to link the surface morphology with the process parameters [7], i.e. under growth conditions but none of them could have brought fundamental data about the intrinsic properties of the liquid-SiC interface without any growth. Focused on the vicinal (0001) Si-face, because added Al on Si-face is much more pronounced for step bunching [10], this chapter aims at bringing new insights first on the SiC surface morphology when put in contact with liquid Si at high temperature and second, on the effect of Al on the liquid-SiC interface properties.

## 3.2. Experimental details

A sessile drop method has been implemented in an inductively heated graphite furnace (Figure 3.1). Due to the small size of the sample (typically a square SiC substrate of 15x15 $mm^2$, with a droplet of 6-7 mm in diameter) compared to the whole graphite crucible (susceptor of 200 mm height), the sample can be considered as almost isothermal. Two temperature measurements, performed with dichromatic optical pyrometers, are collected just above and below the sample. The coil position is adjusted so as to set similar values for both temperatures, within the precision of the measurements (<1% of the measure). In the following, all the temperatures given are the bottom values.

The sequence of operations is the following and is described in Figure 3.2:

1. Electronic grade silicon (piece of wafer) and if relevant high purity Al pieces are prepared, together with a (0001) Si-face 4H-SiC substrates misoriented of 4° towards the <11-20> direction. Both SiC substrates and alloy pieces are first deoxidized in HF solution.
2. They are placed on a graphite piece, with the pieces of Si (Al) just put on the SiC surface.
3. The graphite crucible is then assembled. The circular area at the center is dedicated to the top temperature measurement. A small lateral hole in the graphite cover allows first a direct observation of the sample and second an access for a graphite tool in order to remove the liquid alloy before cooling down.
4. The crucible is wrapped in graphite insulation and loaded in the chamber.
5. After one night of pumping under primary vacuum, the crucible is first heated up to 1100°C under vacuum in order to outgas the different graphite pieces. At 1100°C, the chamber is filled with 0.9 bar of high purity argon. Samples are then heated up at 16°C/min and kept for different times, temperatures and Al-Si alloy compositions.
6. At the end of the temperature plateau, the liquid is absorbed (with graphite felt or a piece of Ta or Nb, which is perfectly wet by liquid silicon). The absorption of the liquid is very fast, less than 1 second. This ensures that no modification of the surface morphology can occur due to parasitic crystallization upon cooling down the saturated droplet. The crucible is then naturally cooled down and opened.

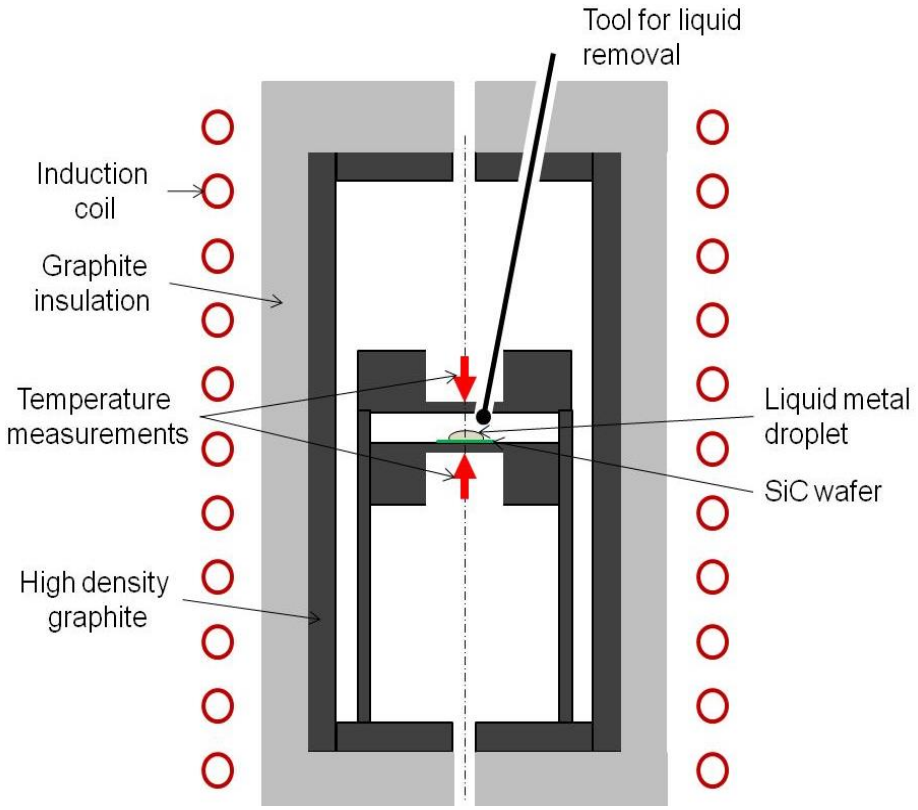


Figure 3.1. Experimental set-up implemented for studying the interaction between a liquid droplet and the SiC substrate. Red arrows are the two temperature measurements. A special tool allows removing the liquid at high temperature, before cooling down.

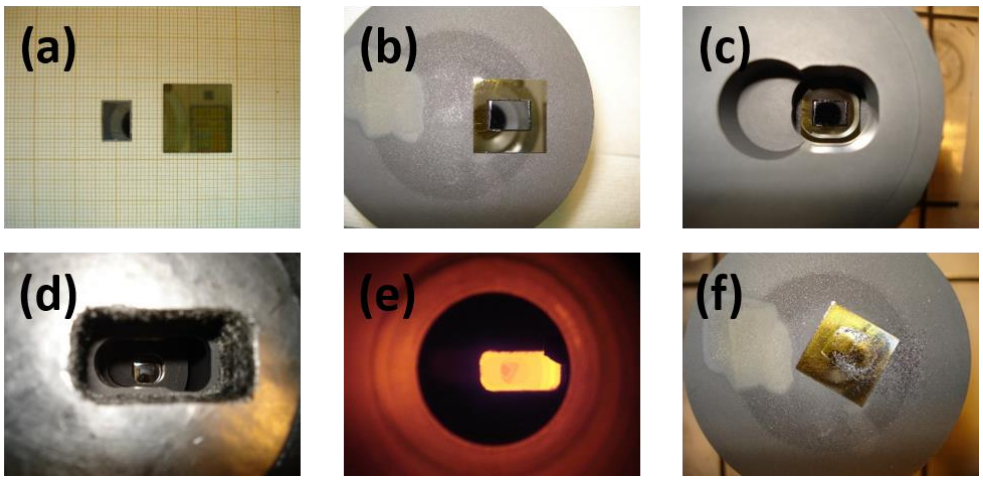


Figure 3.2. Experimental sequence. The details are given in the main text.

After cooling down, the samples are etched in HF : $HNO_3$ aqueous solution to remove the residual metal, if any. The surfaces are then observed by Nomarski differential interference contrast (NDIC) optical microscopy, scanning electron microscopy (SEM) and atomic force microscopy (AFM).

Statistics of step widths are evaluated from a sample of 300 to 400 steps collected from several representative NDIC pictures of the different samples. In order to get quantitative description of the surfaces, we performed some statistics from the NDIC pictures. The procedure is briefly described in Figure 3.3. From the raw NDIC picture (a), some parameters are processed such as brightness, contrast and threshold in order to remove the grey background and to clearly see step edges (b). Then, profiles extracted from section of the pictures, taken perpendicular to the step edges are plotted and processed (c). This allows to give a distribution of terrace widths. Special care has been taken to work on areas as representative as possible and to avoid any singularities on the sample morphologies.

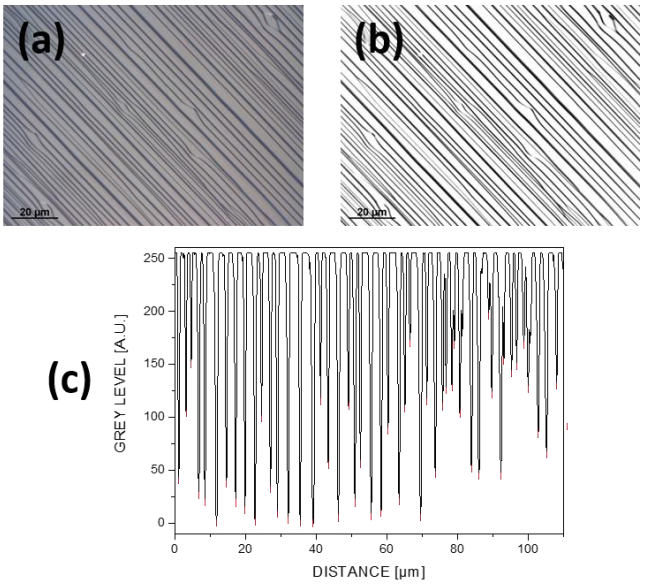


Figure 3.3. Raw NDIC optical microscopy picture of the SiC surface after cleaning (a), an adjustment of brightness and contrast (b), and the extraction of a profile from a section perpendicular to the step edges (c).

## 3.3. Results and discussion

Whatever the conditions, SiC crystal surface in contact with a silicon-based liquid alloy is subjected to a reconstruction in order to minimize the liquid-SiC interfacial energy. Starting from an "epi-ready" surface preparation (chemical-mechanical polishing), the vicinal surface created by the 4° off-cut angle from the c-axis evolves by bunching the bilayer steps together and forming a steps and terraces structure. Of course, the initial substrate surface is atomically flat; nothing can be detected with NDIC optical microscopy.

### 3.3.1. Importance of liquid removal

The following figure (Figure 3.4) shows an experiment where the Si droplet has been only partially removed at the end of the run. The step width distribution is centered around 2.1 µm when the surface is cooled down without a liquid on top. Assuming that there is no step evolution at the vapor-solid interface during cooling down, this surface morphology corresponds to the liquid-SiC interface "frozen" in its high temperature state. The surface is rather different when it cools down with a droplet on top. Of course, as the surfaces were submitted to exactly the same conditions before cooling down, it can be stated that both areas exhibited the morphology of Figure 3.4(a) at the end of the temperature plateau, just before cooling down. Thus, the evolution of morphology that appears in Figure 3.4(b) is only due to cooling under the droplet. It results in much smaller step widths, whose distribution is centered on 1.0 µm, i.e. about half of Figure 3.4(a). During cooling down, the liquid is no longer equilibrated with SiC and the liquid composition shifts towards the pure Si side (following the SiC liquidus) accompanied with SiC precipitation on the substrate. This surface is thus not an "equilibrium" morphology but a growth morphology. A

decrease of the step width while increasing the supersaturation is perfectly consistent with the standard BCF theory of crystal growth in the case of step flow growth mode.

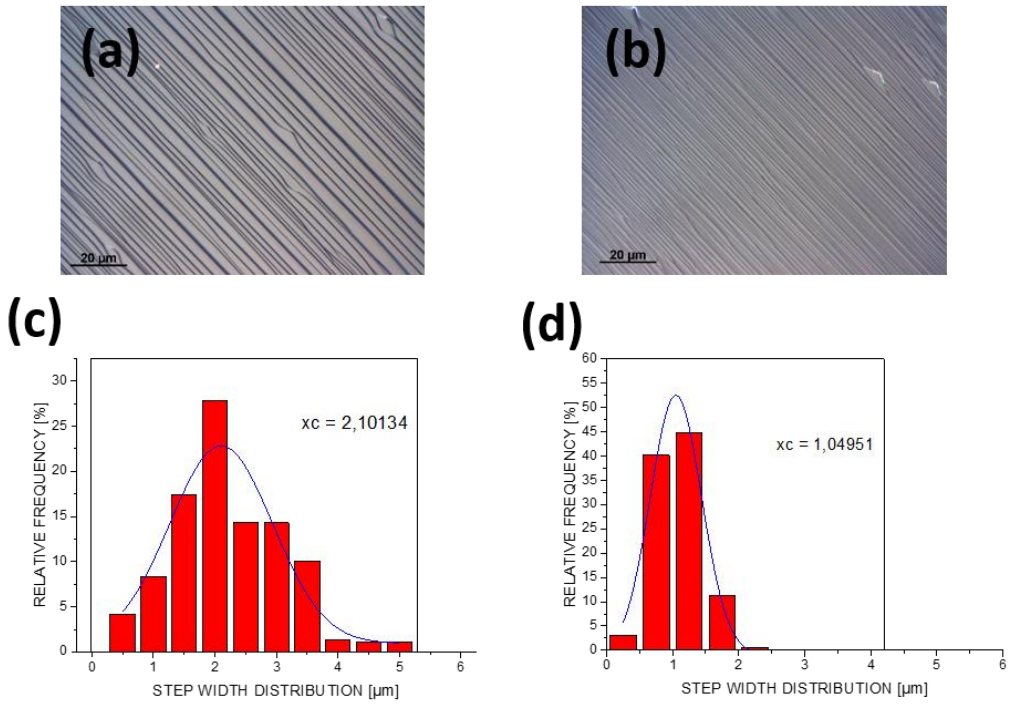


Figure 3.4. Raw NDIC optical microscopy pictures of the SiC surface cooled without droplet on top (a) and with a droplet on top (b). Corresponding step statistics calculated from the NDIC pictures of the SiC surface cooled without droplet on top (d) and with a droplet on top (e). The experimental conditions were : T=1600°C, pure Si, time = 180 min.

### 3.3.2. Effect of time

In pure silicon and for a short time at 1600°C (Figure 3.5(a) and Figure 3.6(a)), the distribution of terrace width is narrow and centered on 1.1 µm. The same experiment kept for a longer time (Figure 3.5(b) and Figure 3.6(b)) exhibits a slightly broader distribution around a maximum at 2.1 µm. As it is just an evolution with time of the previous sample, we can speculate that the macro-

steps mainly gather two by two. It is worth noting that AFM observation of the terrace surface for this two cases did not reveal any steps, even at the nanometer scale; the minimum possible step height in SiC being 0.25 nm which corresponds to one Si-C bilayer.

### 3.3.3. Effect of temperature

The situation is rather different if the sample is heated at much higher temperature -1800°C- for a short time (Figure 3.5(c) and Figure 3.6(c)). Even if the maximum is located around 1.9 µm, the terrace width distribution is much broader with some steps having a width bigger than 10 µm. On large terraces, a few smaller steps can be observed in Figure 3.5(c). These steps are of 1 or 2 nm height, which corresponds to one or two times the c lattice parameter of 4H-SiC. Again, no single Si-C bilayer could be evidenced.

### 3.3.4. Effect of Al addition

Adding a few percents of Al into liquid silicon for a short experiment at 1600°C produces a strong effect on the SiC surface morphology (Figure 3.5(d) and Figure 3.6(d)). Similar to the effect of temperature, the Al strongly spread the step width distribution up to 12 µm for the largest steps. In this case, the highest frequency is centered on 4.1 µm. Again, 1 nm height steps can be observed on larger terraces, typically one per terrace.

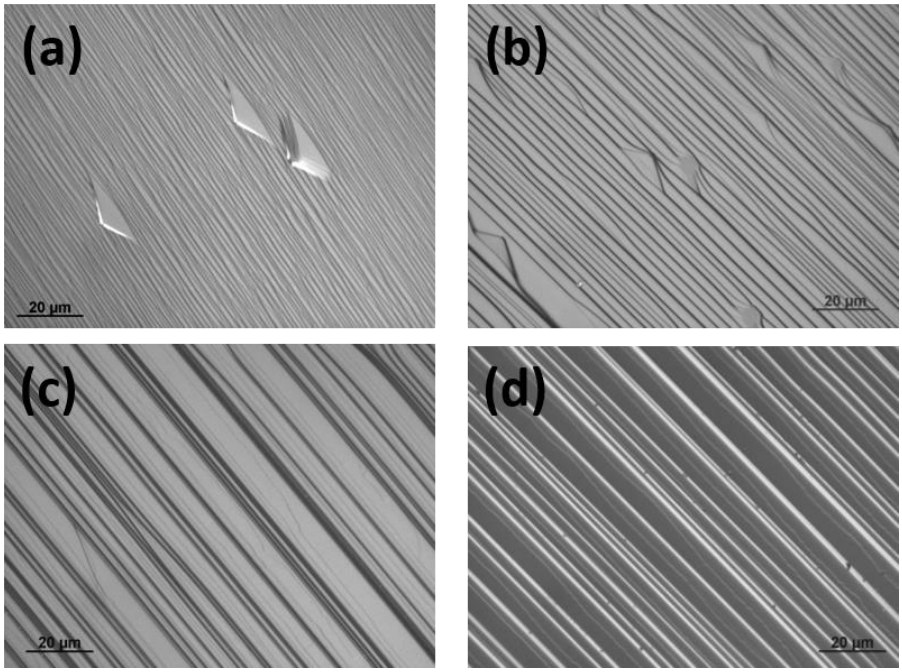


Figure 3.5. NDIC pictures of the 4°off (0001) 4H-SiC surfaces after having been in contact with (a) liquid Si during 30 minutes at 1600°C, (b) liquid Si during 180 minutes at 1600°C, (c) liquid Si during 30 minutes at 1800°C and (d) liquid Al-Si (5 at% Al) during 30 minutes at 1600°C.

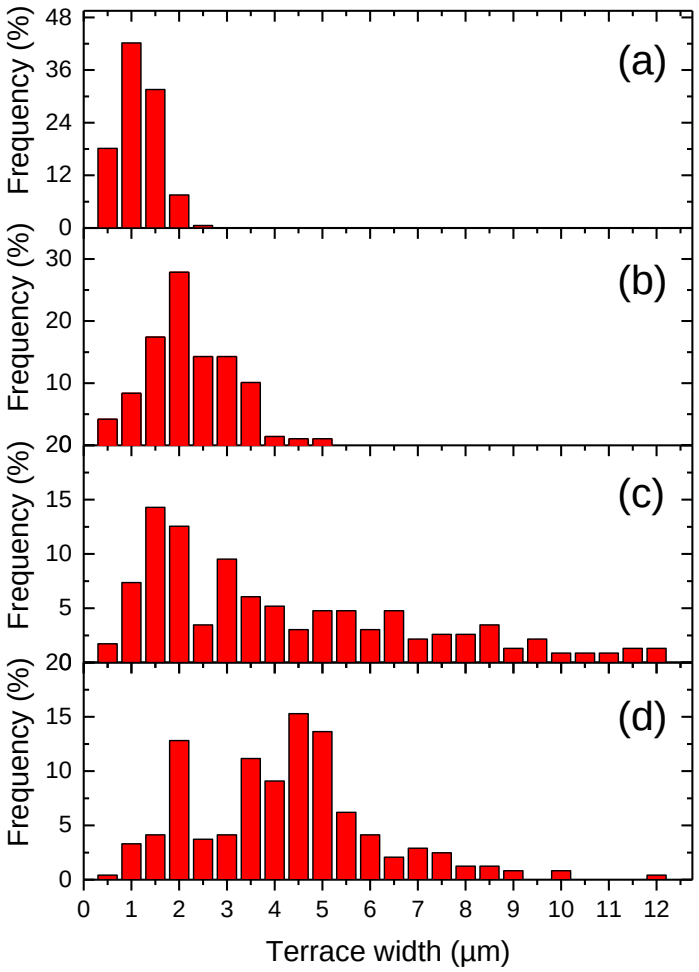


Figure 3.6. Distribution of terrace widths analysed from NDIC pictures of the 4°off (0001) 4H-SiC surfaces after having been in contact with (a) liquid Si during 30 minutes at 1600°C, (b) liquid Si during 180 minutes at 1600°C, (c) liquid Si during 30 minutes at 1800°C and (d) liquid Al-Si (5 at%Al) during 30 minutes at 1600°C.

A common feature to all the surface morphologies presented in Figure 3.5 is that all the steps are almost parallel. The step edges are not perfectly straight if the step height is small (for instance in Figure 3.5(a)) but are getting straighter with increasing step height (Figure 3.5(b-d)). From that respect, Figure 3.5(c) and d are very interesting as macro-steps (big step height) are perfectly straight but the small steps (of 1 nm step height) located on large terraces are not so. Locally, a

few triangles can be observed but such disturbances do not dominate the main pattern of parallel macro-steps.

### 3.3.5. Further morphological evolution and discussion

Keeping the experimental conditions of Figure 3.5(a) and (b) (1600°C, pure silicon) for much longer time, here 6 hours, leads to a totally different morphology (see Figure 3.7). The step edges, initially perpendicular to the <11-20> direction, progressively disappear to form a zig-zag structure with the two step edges perpendicular to the <01-10> and <10-10> directions. They are actually not simple step edges and the SEM picture of Figure 3.7 clearly show the development of facets with the generic (10-1n) and (01-1n) orientations. At the tip formed by these two facets, some initial steps (perpendicular to the <11-20> direction) are still locally visible, split in several smaller steps and presenting a rough ledge.

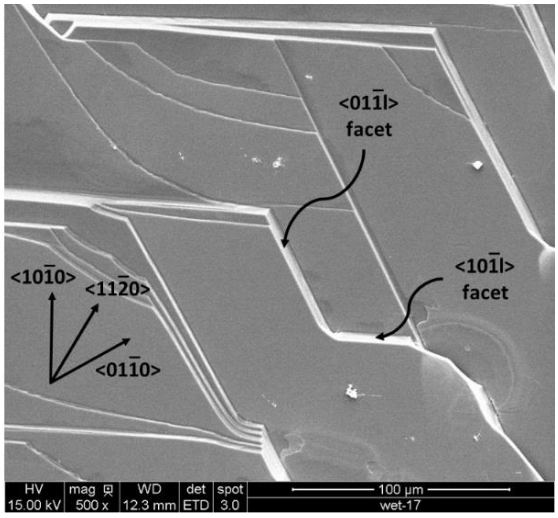


Figure 3.7. SEM picture of the 4°off (0001) 4H-SiC surface after having been in contact with liquid Si during 360 minutes at 1600°C.

4°off vicinal (0001) surface of 4H-SiC (Si-face) thus presents an evolution in three stages to develop “equilibrium” morphology (see Figure 3.8). As the liquid is not in thermodynamic equilibrium with SiC, the first stage starts with a slight dissolution of the SiC surface in order to saturate the droplet with dissolved carbon. This initiates the movement of steps at the surface. This dissolution period is most probably very fast, as reported by Dalaker et al.[8] who demonstrated that equilibrium was established within a couple of minutes at most. Then the second stage consists of bunching of the small steps to generate straight macro-steps keeping the same orientation. This leads to a metastable pattern of bunched macro-steps that can be kept for a long time (up to 3 hrs in our case, in pure Si at 1600°C). The third and last step, which seems to be slower, drives the surface morphology to a more stable state, composed of (0001), (10-1n) and (01-1n) facets. This transition time between stages two and three is most probably not fixed. We speculate that if there is no fluctuation allowing to initiate the third stage, this bunched parallel macro-steps could be maintained even longer. This global evolution could be described as analogous to the well-known Ostwald step rule mechanism in the sense that a metastable state first occur because it is faster than the equilibrium state.

By waiting very long reaction time, i.e. 6 hrs at 1600°C the surface is subject to strong faceting, and exhibits a morphology that can be assimilated to an “equilibrium” one. However, there are a few singularities that are unexplained to date. For instance, the re-entrant edges appear not to be stable and a local dissolution occurs creating a kind of hole.

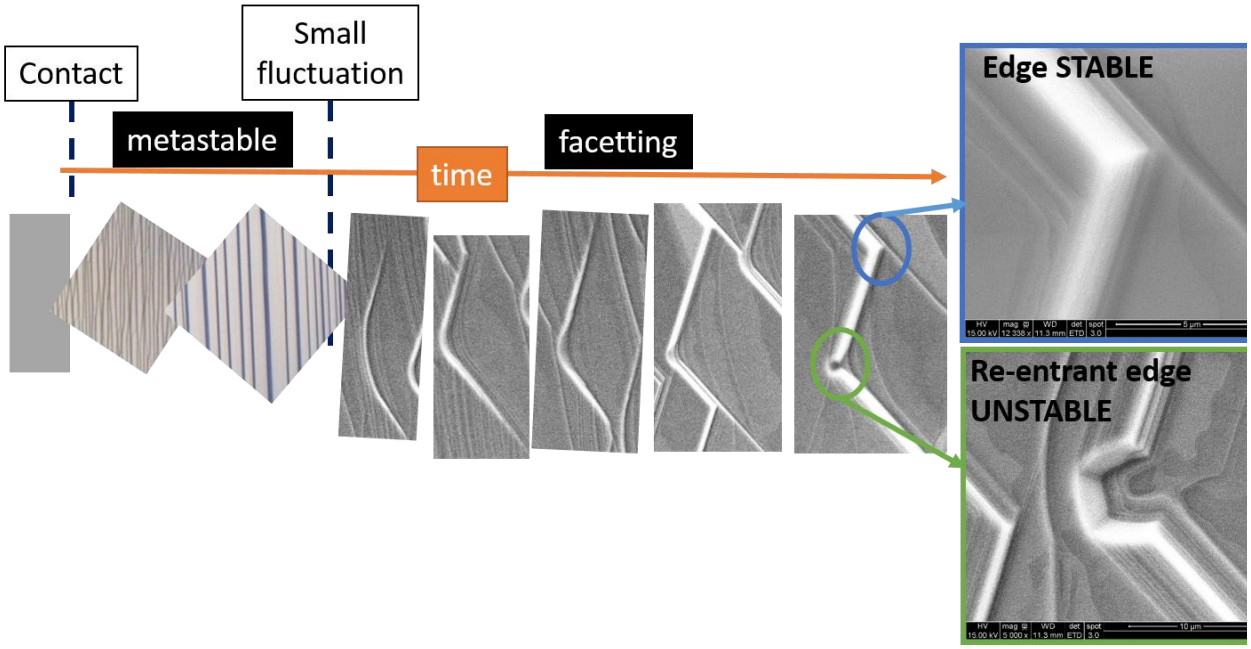


Figure 3.8. Description of the surface evolution scenario when the 4H-SiC surface is put in contact with liquid silicon at 1600°C.

Increasing the temperature to 1800°C or adding a few percents of Al drastically enhance the kinetics of the second stage, explaining that after 30 minutes, the step bunching is much more pronounced than in the case of pure silicon at 1600°C. However, they both strongly reduce the third stage, whose driving force is directly the minimization of the interfacial energy. Macroscopically, all looks like they both decrease the driving force for third stage. This reconstruction of the interface is based on local dissolution-crystallization of SiC. At a microscopic scale, the mechanism is not identified, especially about the role of interfacial tension anisotropy. Komatsu et al [9] have shown that Al or Tin (Sn) would increase the interfacial energy in $Si_{0.6}Cr_{0.4}$. Our results suggest indirectly that both temperature and Al addition decrease the interfacial energy, as we suppose that it constitutes the driving force for the evolution between stages 2 and 3. In that sense, Al would act as a surfactant at the liquid silicon/Si-face of 4H-SiC interface. The two results

are not necessarily in contradiction as Komatsu et al. worked in Si-Cr solvent at much higher temperature and on the C-face.

## 3.4. Conclusions of chapter 3

A sessile drop method has been implemented under perfectly isothermal conditions to study the surface reconstruction of a Si-face, 4°off (0001) 4H-SiC surface in contact with pure silicon or Al-Si alloys at high temperature. The effects of time, temperature and nature of liquid solvent have been investigated. In pure silicon and at 1600°C, the surface evolves with three consecutive stages: i) a fast creation of steps due to an initial slight dissolution of the substrate surface, ii) step-bunching leading to parallel macro-steps (which seems to be a metastable state) and iii) a slower step leading to equilibrium morphology, composed of (0001), (10-1n) and (01-1n) facets. Increasing the temperature to 1800°C or adding a few percents of Al drastically enhance the second stage, but apparently reduce the third one. From the observation of the first stage, it is clear that Al increases the kinetics of step movements on the surface. Further investigations are necessary to identify the exact mechanism of the observed trends. Wetting angle measurements would be highly beneficial to investigate the effect of temperature and additives on the liquid-SiC interfacial energy.

## 3.5. References

[1] D. Chaussende et al., J. Phys. D: Appl. Phys. 2007. **40**(20): p. 6150-6158.

[2] K. Kusunoki et al., J. Cryst. Growth, 2014. **395**: p. 68-73.

[3] M. Kado et al., Mat. Sci. forum, 2013. **740-742**: p. 73-76.

[4] Y. Yamamoto et al., Mat. Sci. forum, 2014. **401**: p. 681-685.

[5] T. Mitani et al., J. Cryst. Growth, 2014. **401**: p. 681-685.

[6] F. Mercier et al., J. Cryst. Growth, 2010. **312**(2): p. 155-163.

[7] C. Zhu et al., J. Cryst. Des., 2013. **13**(8): p. 3691-3696.

[8] H. Dalaker and M.Tangstad, Mater. Trans., JIM, 2009. **50**(5): p. 1152-1156.

[9] N. Komatsu et al., poster presented in ICSCRM2015, Sicily, 2015.

[10] S. Harada et al., Mater. Sci. Forum, 2014, 778-780: p. 67-70.

# Chapter 4. Transient phenomena during the seeding stage of 4H-SiC solution growth

In this chapter, we address the seeding stage of the SiC growth process by systematical observation, which is critical for getting the high crystalline quality. Combining the results with numerical modelling, we have demonstrated that under improper seeding conditions, strong temperature fluctuations close to the seed surface could give rise to transient phenomena such as the parasitic nucleation of 3C-SiC even at high temperature. This could be suppressed by either pre-heating of the seed crystal before contact, or adding Al to the solvent. Also, we will show that Al-Si solvent can reduce the surface roughness. As a consequence, it presents a smoothening effect on the C-face.

## 4.1. Introduction

Power electronics is subjected to profound changes following the development of high performance Silicon Carbide (SiC) power devices. This is directly linked to the recent achievement of large size, high quality SiC material with well controlled properties [1]. With the aim of always improving further the performances, basic research on material synthesis for both bulk substrates and active epilayers is still very dynamic. In this context, TSSG process has recently regained much interest for SiC crystal growth because of its potential for reaching outstanding crystalline quality. The first validation of this approach was the demonstration of a very efficient dislocation conversion mechanism [2] which, when applied to epitaxial growth, paved the way of very low dislocation density [3]. However, the SiC solution growth process is still in its infancy. Further

development will be attainable only after tackling many scientific and technological issues related to the process. Among them, the "seeding stage" which usually gathers in-situ surface preparation and the early stages of growth is of the first importance as it impacts all the subsequent growth. During physical vapor transport (PVT), it has been shown both experimentally and analytically that the in-situ surface reconstruction was very important to set-up a stable step-flow growth mechanism from the beginning [4, 5]. The higher nitrogen incorporation during this early stage of growth was also pointed as the source of extended defects in the crystal [6]. However, considered as a "technological" issue, the seeding stage is not extensively studied despite its critical importance. In this chapter, we address the seeding stage of 4H-SiC solution growth. More specifically, we have systematically observed the surface morphologies obtained on different seed substrate terminations. We also set an additional constraint to this work: we want to avoid in-situ etching (dissolution) of the seed crystal at the beginning, in order to be able to start the growth even from a very thin epilayer. With such constraints, we will show that improper seeding conditions could give rise to transient nucleation of 3C-SiC, even at high temperature. Pre-heating of the seed and adding Al will be demonstrated as obvious but efficient solutions to solve this problem.

## 4.2. Experimental details

A standard SiC TSSG process has been implemented, using inductively heated graphite crucible insulated with graphite felts. The general principle and a full description of the crucible design has already been explained in chapter 2. In each experiment, both Si (0001) and C (000-1) faces and with both nominally on-axis and 4° off-cut towards <11-20> direction 4H-SiC substrates were

used as seed crystals. These four crystals were mounted on the same graphite seed holder using graphite glue and kept in contact with the solvent for 10 minutes. Before contact, the solvent was kept at process temperature for 30 min in order to get saturated with carbon. This has been implemented to reduce, or ideally avoid melt back of the seed during the first stages after contacting the liquid surface. The process temperature varied from 1700°C to 1900°C. Experimental parameters with the corresponding typical growth rates for each growth temperatures are summarized in Table 4.1. Since the added Al does not significantly change the carbon solubility in the liquid Si [21], we consider that increasing the temperature to 1900°C slightly enhances the carbon solubility in the liquid. At the end of the experiments, residual solvent solidified on the crystals was removed by acidic etching in HF + $HNO_3$ (1:1) solution.

Table 4.1. The experimental details of 4H-SiC TSSG process.

| Series. | Solvent | Seed crystal | Temperature (°C) | Process duration | Growth rate |
|---|---|---|---|---|---|
| 1 | pure Si | 4H-SiC on/4°-off Si/C-faces | 1700<br>1800<br>1900 | contact for 10 min | 1700°C: ~10 µm/h<br>1800°C: ~11 µm/h<br>1900°C: ~13 µm/h |
| 2 | Si-10at%Al | | | | |
| 3 | pure Si | | 1800 | seed pre-heating for 30 min + contact for 10 min | |

- **Seed crystal pre-heating process**

In addition to the standard growth experiment (series 1 and 2 in Table 4.1), we pre-heated the seed crystals (series 3) with the aim to reduce the effect of thermal fluctuations that occur at the beginning of the dipping stage. The detail will be described in the section 4.3.

- **Grown surface characterization**

The growth surface morphologies were systematically observed by NDIC optical microscopy, SEM and AFM. Polytypes in grown layers were routinely identified by Raman spectroscopy. After that, electron backscattered diffraction (EBSD) analysis was applied to map quantitatively the polytype distribution over the grown surfaces.

EBSD mapping technique can provide statistical data on the nature and the orientation of the different phases, here of the polytypes during the SiC crystal growth [8, 9]. In the SEM, polytype determination through EBSD mapping is based on the diffraction pattern (Kikuchi band) generated by the backscattered electrons. The intersections of Kikuchi bands correspond to crystal zone-axis. A complete description of the EBSD technique may be found in a published comprehensive report in ref. [10]. A TSL-Edax (DigiView III camera) installed on a Zeiss Ultra55 SEM with the orientation imaging microscopy (OIM$^{TM}$6) software was used for the EBSD imaging and data treatment. For getting an accurate EBSD pattern from the as grown very rough surfaces, these surfaces were slightly polished with colloidal silica under alkaline conditions. The results of EBSD mapping were treated by neighbor phase correlation (NPC) clean program using OIMTM6 analysis. NPC clean method processed data points with minimum confidence index (CI). The phase (orientation) of such points can be changed into the phase (orientation) which match the majority of the surrounding neighbors. If there is no majority, then such points can be changed randomly according to one of the phase (orientation) of neighbors.

## 4.3. Experimental results and discussions

- **General grown surface morphologies**

Typical morphologies of as grown SiC crystal surfaces, after long term experiments are shown in Figure 4.1. These samples were grown on 4H-SiC on-axis and 4°-off, both Si/C-faces substrates using pure Si solvent at 1700°C. The growth duration was varied from 2 to 3 hrs. The surface morphology on the on-axis substrates were very rough due to faceted 2D islands while the step bunched structure was observed on the off-axis substrates. From Raman spectroscopy, mainly 4H-SiC polytype has been observed for all cases.

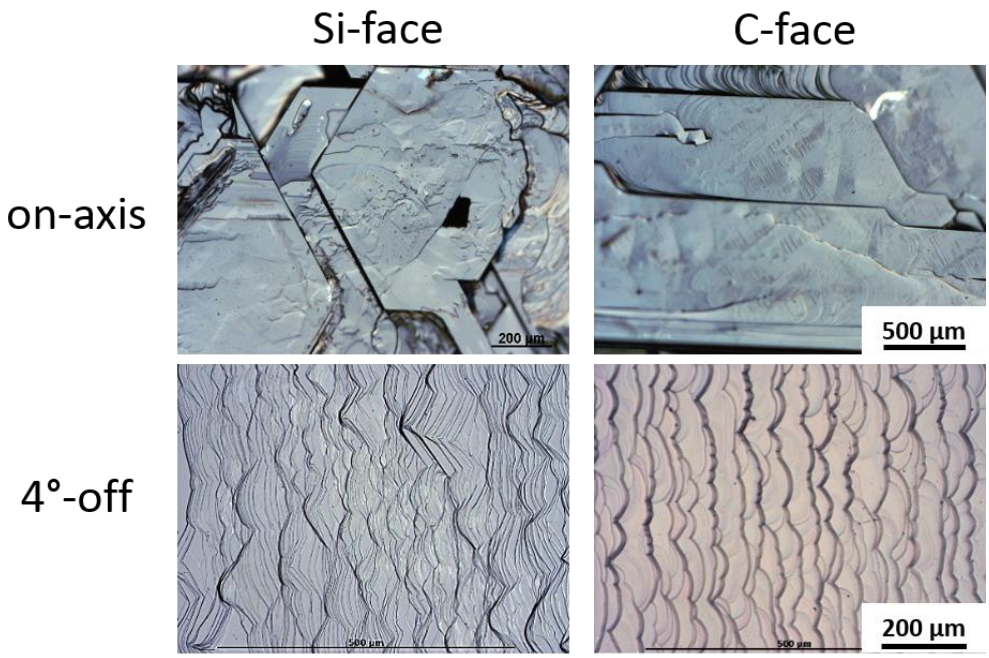


Figure 4.1. NDIC optical microscopy pictures, taken from typical grown surface morphologies after long term experiment on the Si-/C-faces on/off-axis substrate at 1700°C.

### 4.3.1. Growth on the on-axis substrates

- **Surface morphologies in pure Si**

Figure 4.2 shows the NDIC optical microscopy pictures of the as-grown morphologies for on-axis surfaces of the first series. The corresponding EBSD maps are gathered in Figure 4.3. On the Si-face and at all temperatures, the grown surface morphology is characterized by a domain structure, which is rather different compared to the usual growth surface in pure Si solvent presented in Figure 4.1. The density of domain boundaries increases while increasing the growth temperature (Figure 4.2a-c). From EBSD maps, the grown layers mainly consist of the 3C-SiC polytype, with the usual two 3C variants (called twinned domains) that can easily form on the c-plane of 4H-SiC substrates [11]. The proportion of each variant is roughly similar. It can be stated that the boundaries observed with the optical microscopy correspond to twin boundaries (TBs), also referred to as double positioning boundaries (DPBs), which demarcate the interface between two twinned 3C-SiC domains. At 1700°C and 1800°C, the crystal surface is totally covered with 3C-SiC. At 1900°C, a few 4H-SiC domains are present but are clearly in the minority. On the C-face, surface morphologies are rather different compared to the Si-face. Figure 4.2d and Figure 4.2e show quite rough surface, consisting of a mixture of circular and triangular features. The related EBSD maps show that the grown layers are entirely composed of 3C-SiC (see Figure 4.3d and e), again with the two 3C variants. A drastic change of the surface morphology occurs at 1900°C (Figure 4.2f). There is no more visible domain boundary and the surface is covered by steps of various heights, characteristic of a layer-by-layer growth mechanism. Most of the steps seem to originate from the crystal edge. In this case, the grown layer is of 4H-SiC polytype with only a few small domains of 3C-SiC scattered over the large terrace on the grown surface (Figure

4.3f). The polytypes of the grown layers have been confirmed by Raman spectroscopy and the results match with EBSD analyses (see Figure 4.13).

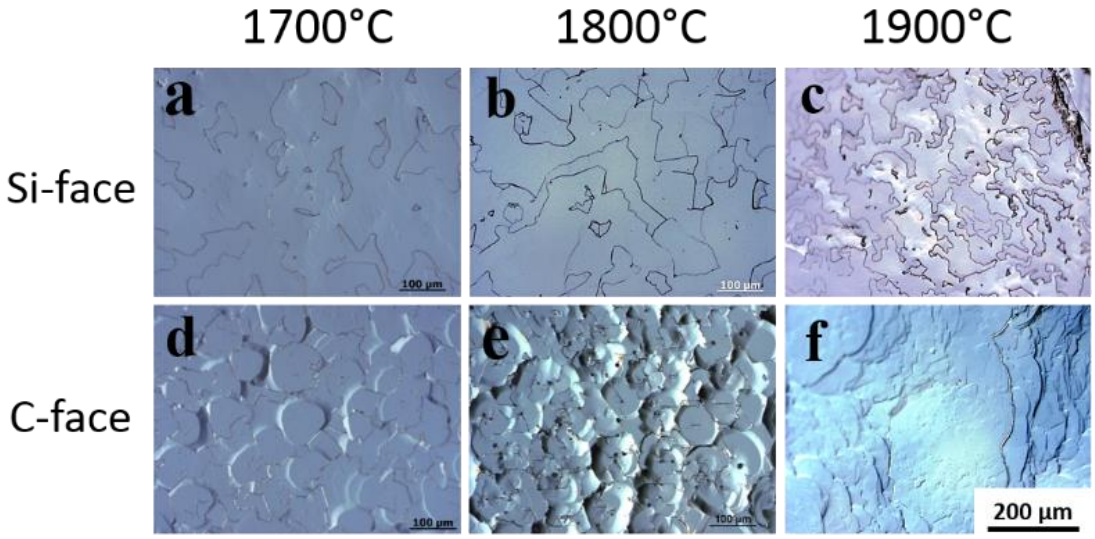


Figure 4.2. As grown surface morphologies observed by NDIC optical microscopy, for the on-axis samples of the first series (Si- and C-faces; pure Si solvent, three different temperatures, 1700, 1800, 1900°C; growth time of 10 min).

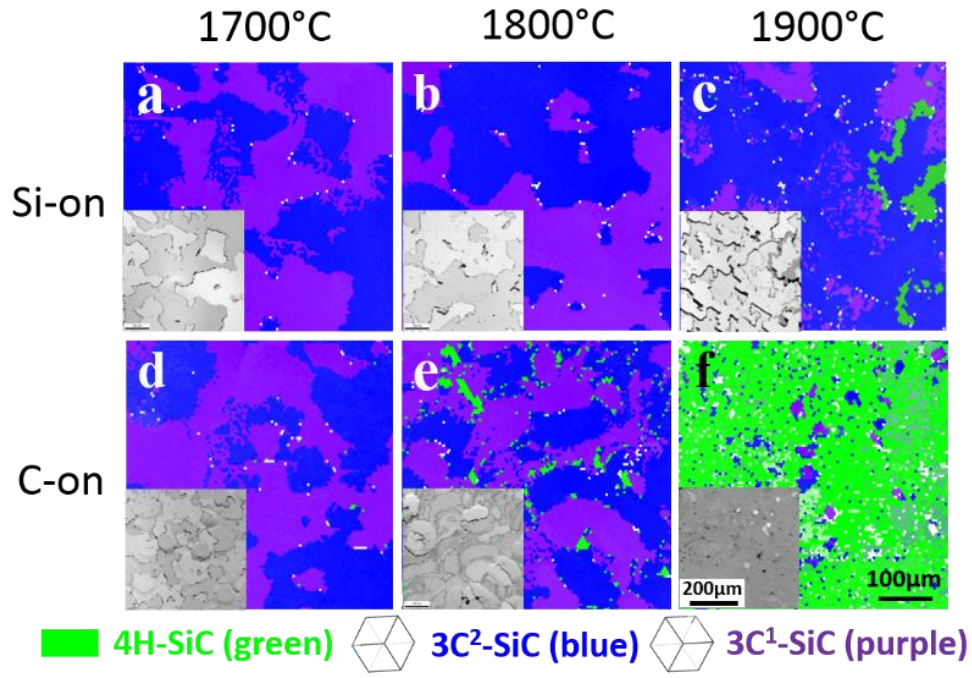


Figure 4.3. EBSD maps for the on-axis samples of the first series in Table 4.1. Blue and purple areas correspond to two different orientations of 3C-SiC. Green areas correspond to 4H-SiC polytype. Inserts are the SEM images at the same location as EBSD maps (mapping scale: squares of 500 x 500 $\mu m^2$)

- **Surface morphologies in Al-Si**

In this case, layers are growth on on-axis substrates under the condition of second series in Table 4.1, all the other parameters being similar to the first series except the solvent composition, which is Si based solvent with Al content of 10at%. Whatever the process temperatures and for both substrate polarities, there is no twin boundary that can be observed, as shown in Figure 4.4. The corresponding EBSD maps are gathered in Figure 4.5. These morphologies are actually sharing a common feature with Figure 4.2f: the surface is composed of steps of various heights with some large terraces. It is always difficult to compare the steps on the on-axis surfaces as the

step patterns are closely related to the step sources, i.e. to the way the steps are generated at the surface. Depending on the observation area, it is possible to show totally different features and then to draw totally different conclusions. Thus, we will discuss in this study the main characteristics without pointing further details. In this way, all the steps propagate in a single direction and the density of steps is very high as can be seen in Figure 4.4a, d, and e. These morphologies are thus issued from a huge, single source of steps. In the Figure 4.4b, c, and f, several directions of step propagation can be evidenced. These morphologies come from the contribution of distinct sources of steps, spatially separated. Those sources of steps have been identified as spirals for most of the cases. EBSD maps reveal the absence of 3C-SiC polytype at 1700°C for both polarities (Figure 4.5a and d). A few small 3C-SiC domains can be seen at 1800°C and 1900°C, with a 3C-SiC coverage increasing from the C-face to the Si-face. To help visualization, we indicate the location of the spiral growth centers on the SEM inserts in Figure 4.5, when clearly identifiable. The correlation is straightforward; there is no 3C-SiC polytype where we can evidence spiral growth centers. From Raman spectroscopy, mainly 4H-SiC polytype has been observed but 6H-SiC polytype has also been occasionally identified in the grown layer (see Figure 4.13).

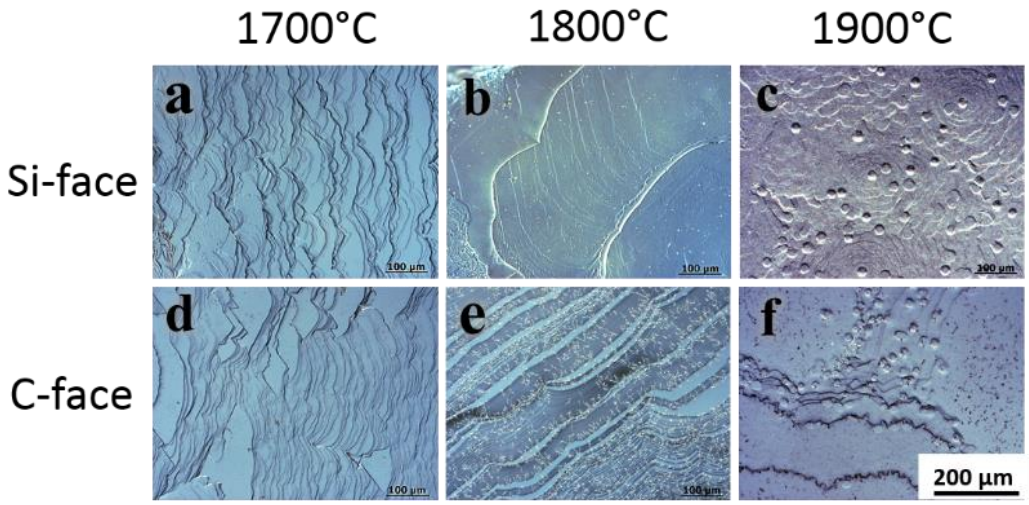


Figure 4.4. As grown surface morphologies observed by NDIC optical microscopy, for the on-axis samples of the second series in Table 1.

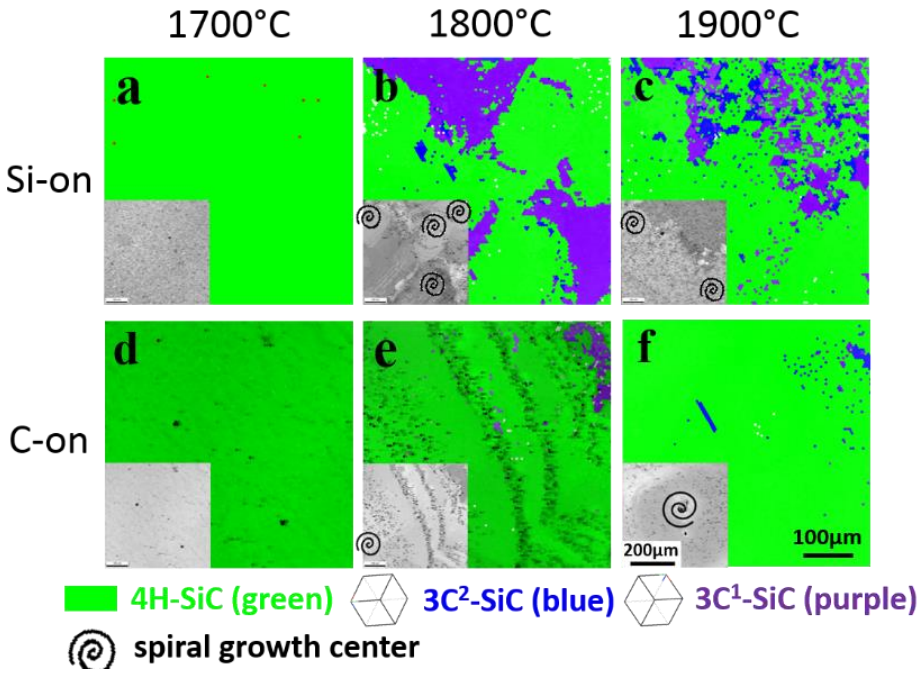


Figure 4.5. EBSD maps for the on-axis samples of the second series in Table 1. Blue and purple areas correspond to two different orientations of 3C-SiC. Green areas correspond to 4H-SiC polytype. Inserts are the SEM images at the same location as EBSD maps (mapping scale: squares of 500 x 500 $\mu m^2$).

### 4.3.2. Growth on 4° off-axis substrates

Due to the off-cut angle of the vicinal surface, step structures usually appear creating a vicinal surface. If the vicinal surface is unstable, the formation of big steps by bunching of small steps can give rise to high roughness during long time growth process. Figure 4.6 and Figure 4.7 show the NDIC pictures of as grown morphologies for 4° off-axis surfaces of series 1 and 2, respectively. For all these cases, the layers were grown by the so-called step-flow growth mechanism. Obviously, all the steps propagate towards the [11-20] crystallographic direction. In these cases, it was not possible to identify the polytype using EBSD mapping because the strong roughness combined with the 4° off-angle made totally inaccurate the indexation of the diffraction patterns. The systematic Raman spectroscopy analysis has thus been conducted instead of EBSD analysis as shown in Figure 4.14, confirming that the grown layers are exclusively of 4H-SiC polytype without any 3C-SiC or 6H-SiC polytypes.

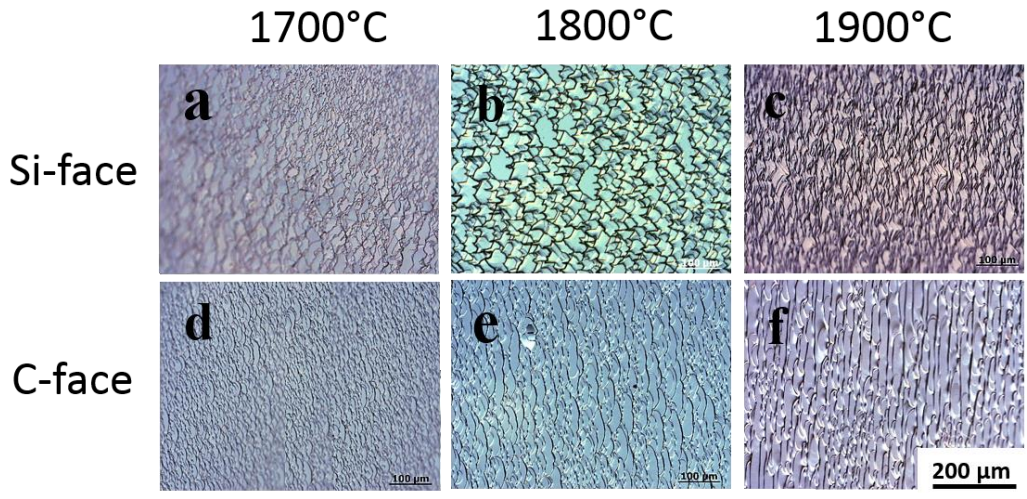


Figure 4.6. As grown surface morphologies observed by NDIC optical microscopy, for the off-axis samples of the first series in Table 1.

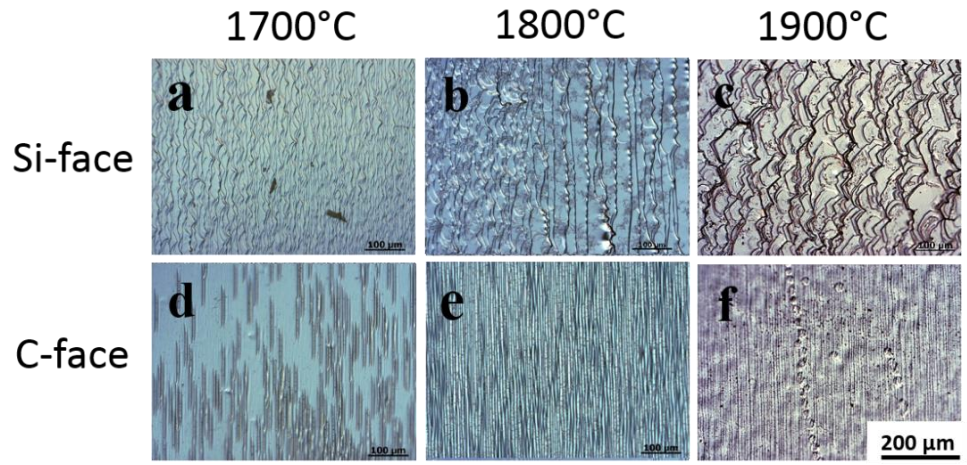


Figure 4.7. As grown surface morphologies observed by NDIC optical microscopy, for the off-axis of the second series in Table 4.1.

- **step heights**

The large steps, usually called macro-steps come from the bunching of the smaller ones during layer-by-layer growth of SiC single crystals. Figure 4.8 presents the evolution of the step heights as a function of the temperature for 4° off-axis samples with both pure Si and Al-Si solvents. The heights of the steps have been measured by AFM. Here we only focused on small steps, i.e. those constituting the step flow. Big macro-steps are not considered in the statistics. Values given in Figure 4.8 correspond to average of a set of measurements at different locations up to a threshold of 100 nm height.

The height of steps is globally decreased in Al-Si solvent and without forming any macro-steps even at high temperature (Figure 4.7f). Especially, the effect of the temperature is stronger on the Si-face with pure Si solvent than the other cases. The steps are smaller on the C-face than on the Si-face for given experimental conditions. Also, the addition of Al to Si solvent reduces the mean step height at every growth temperature.

Considering now the evolution of the surface morphologies on the steps, it is obvious that Al-Si solvent can drastically reduce the surface roughness on the Si-face. From the comparison between Figure 4.6c and 4.7c, adding Al to the Si solvent is effective to the formation of zigzag-shaped and faceted macro-steps. On the C-face, the situation is rather different: the step heights at all temperatures have very small difference in pure Si, however, the surface roughness is the smallest in Al-Si solvent. These effects of adding Al on the growth surface morphology have already been reported by Mitani [12].

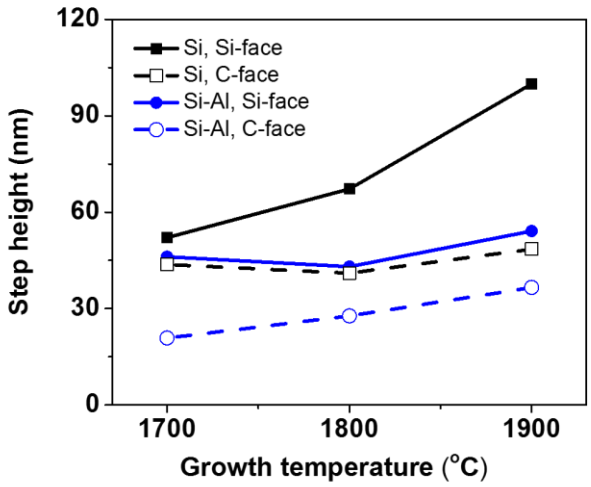


Figure 4.8. Evolution of the nanometer scale step heights (average) as a function of temperature for 4°off-axis samples, after 10 minutes of growth both in pure Si and in Al-Si solvents. The data have been measured by AFM and are restricted here to step heights varying from nm up to 100 nm.

### 4.3.3. Technical approach for transient 2D nucleation of 3C-SiC

At first glance, it is rather difficult to extract clear trends from the different results and to draw some conclusions. Even worse, some of the apparent conclusions could be in contradiction with

the existing literature. The most puzzling point is the formation of 3C-SiC in pure Si solvent even at temperatures higher than 1800°C and whatever the surface polarity. 3C-SiC polytype is usually referred to as a metastable "low temperature" polytype [13] and it is much unlikely to occur at such high temperature and in a process, which is supposed to be close to the thermodynamic equilibrium. This is actually the first report of 3C-SiC epilayers on 4H-SiC substrates under such conditions using solution growth. With the same idea, why there is no visible 3C-SiC at 1700°C on both Si- and C-faces in Al-Si solvent (Figure 4.5a and d) over the entire grown surface? Conversely, how 3C-SiC domains are formed at higher temperature (Figure 4.5b and c)? Expected to be formed for low temperature process, the coverage of 3C-SiC and the quantitative assessment of polytype distribution over the entire surfaces should be decreased, while increasing the process temperature. The nucleation of 3C-SiC has been extensively studied; it is always attributed to 2D nucleation [14-16]. There is here an apparent random-like behavior for the formation of 3C-SiC on the nominal 4H-SiC surfaces. For the vicinal surfaces, it is also clear that Figure 4.6b, which comes from the case grown at 1800°C do not look like intermediate case on an expected continuous evolution from 1700°C to 1900°C. Once again, the results seem to partially exhibit an erratic behavior.

To explain these results, technical issues related to the TSSG process must be considered. Usually the seed crystal is kept far above the solvent (about 70 mm higher than the solvent surface) before contact, so as to avoid some parasitic condensation of particles on the seed surface, coming from the vaporization of the solvent. Then the seed crystal is moved down to the solvent surface up to the contact establishment. To assess the temperature variations with time close to the seed surface after touching the solvent surface, we performed some numerical simulations using finite element method on a two dimensional axisymmetric geometry. All the calculation details for the

stationary case have been given previously [17, 18], and have been straightforwardly extended to the time dependent case. Thus, we will only present for the purpose of this study, the temperature evolution with time on several locations, which is the bottom and the surface of the solvent (both before and after contacting) and the seed surface (before contacting only). This is presented in Figure 4.9. The growth temperature of the solvent for the simulation was chosen to be around 1730°C, considering the temperature difference between the solvent surface and top of the furnace in real system (described in chapter 2.1.1). We proceeded in two different stages. In the first stage, describing the temperature before contact (BC) when the seed crystal is kept far from the solvent surface, computations are performed at the steady state. The calculated temperature difference between the top and bottom of the solvent is very small ($\Delta T \sim 1°C$) as seen in Figure 4.9. Meanwhile, the seed crystal temperature of around 1480°C is much smaller than the solvent surface. To help understanding this situation, the temperature distributions are represented in Figure 4.10. In the figure 4.10a, the coldest zone (left side) is the center of the solvent, and the hottest zone (right side) is located at the crucible wall. This temperature profile is then taken as the initial condition (t=0) for running the time dependent temperature evolution after contacting (AC) the seed crystal to the solvent surface. Strictly speaking, this approach is not suitable to give an accurate description of the evolution of the temperature distribution because the temperature of seed crystal should start to raise while entering into the crucible and moving down to the solvent surface. The transition speed of seed holder is usually 0.2 mm/sec and the normal distance between the seed crystal and solvent surface is about 5~7 mm. However, we consider that our calculations would draw an extreme case that would be adapted for describing the phenomenon. From the contact time (t=0), all the temperatures undergo a sudden and strong variation. The temperature at the solvent surface strongly drops down while the temperature of the seed crystal strongly

increases. From this moment, these two temperatures are equal for the sake of continuity of temperature at the interface. As a consequence, a large temperature difference (ΔT ~135°C) appears between the surface and the bottom of the solvent. As can be seen in Figure 4.10b, big thermal fluctuations are created at the solvent center area, which is directly in contact with the seed crystal. Such thermal gradient is significantly reduced in the following 100 sec as shown in Figure 4.10c. Reaching the thermal equilibrium thus requires a two-step process. During the first 100 seconds, strong heat fluxes from the solvent to the crystal help rapidly reducing such large temperature difference. Then a much slower process progressively equilibrates the temperature distribution. After 30 minutes, the thermal equilibrium is still not totally reached and almost 1 hour would be necessary to get a stationary state by extrapolating the curve of Figure 4.9. At higher growth temperature, such effect should be more pronounced where the temperature difference between seed and solvent surface before contact is larger than the lower temperature case.

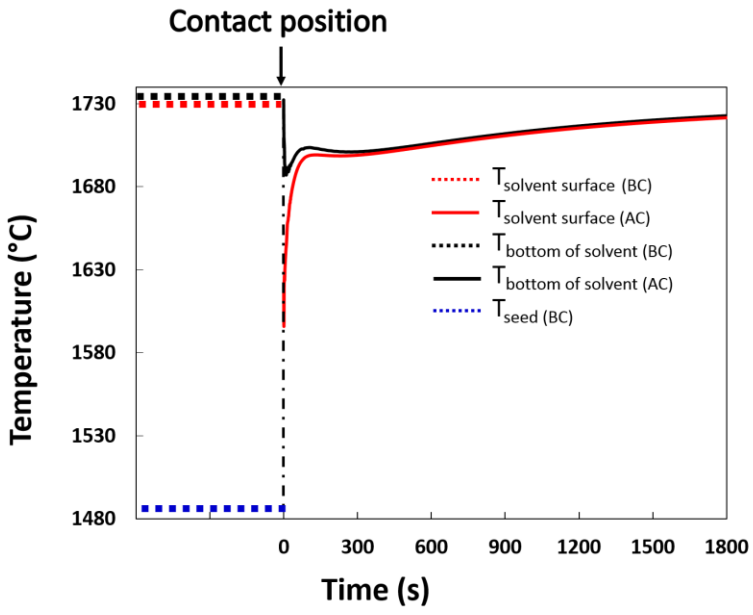


Figure 4.9. The time evolution of seed crystal and solvent (bottom and top parts) temperatures before and after contact.

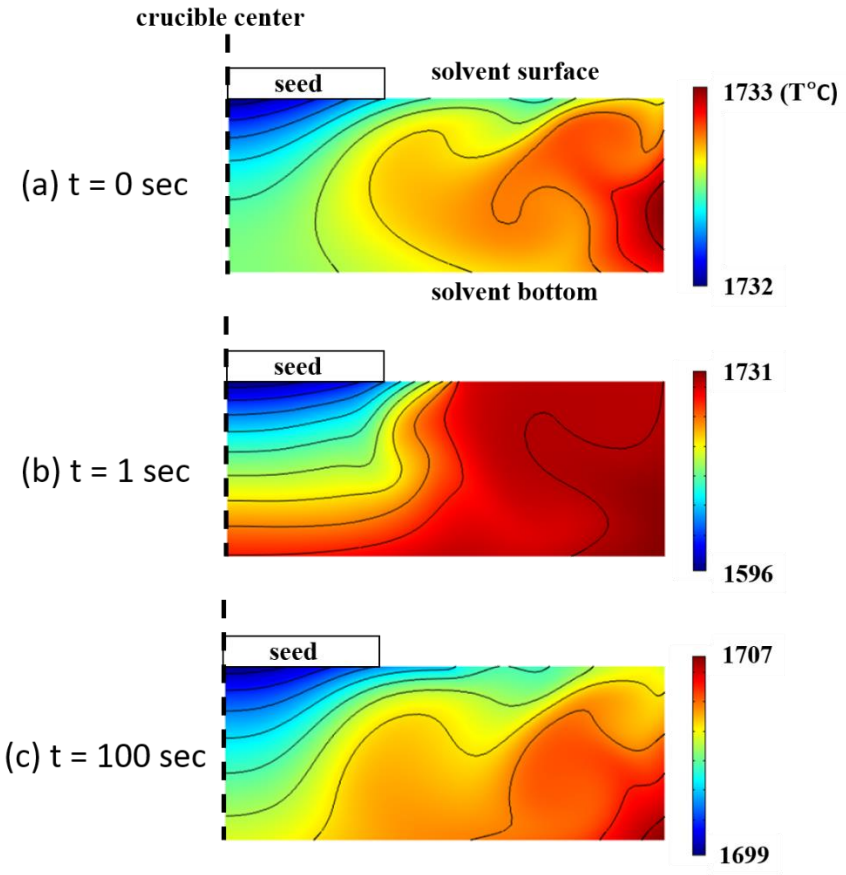


Figure 4.10. Temperature profiles of (a) before contact, (b) after contact, and (c) after first 100 sec.

### 4.3.4. Relation between the growth mode and carbon concentration distribution

In general, carbon solubility in the SiC equilibrated liquid increases with temperature [19]. Assuming that the carbon distribution follows roughly a similar behavior as the temperature distribution in the vicinity of the seed crystal, it may be speculated that the crystal surface experiences a very high supersaturation during the seeding stage $t$=1~100 sec. Such environmental changes could affect the growth mode and the growth rate. It is thus not surprising that the metastable polytype (3C-SiC) nucleates under such strong deviation from thermodynamic equilibrium, even at high temperature. After the seeding stage, the carbon supersaturation

decreases resulting in the decreasing of the 2D nucleation frequency together with the activation of 4H-SiC spiral growth centers induced by screw dislocations. The previously formed 3C-SiC can thus be progressively overlapped by the growing layer propagated from the spirals. That is the reason why some 3C-SiC residues are still observed at the down step of big spiral centers (Figure 4.5b, c, e, and f).

The occurrence of 3C-SiC is also drastically decreased by using an Al-Si solvent. Adding 10at% of Al to the Si solvent, the carbon solubility should not be dramatically changed compared with pure Si solvent. For a given temperature distribution, such solvent composition should thus not affect the supersaturation distribution while changing the solvent compositions from pure Si to Al-Si. Two hypotheses can be proposed to explain this phenomenon.

- First, the presence of Al helps reducing the 2D nucleation frequency of 3C-SiC. The experimental results on on-axis substrate are rather obvious, although its exact role is still unclear. Indeed, similar phenomenon has already been demonstrated by Soueidan et al., using the VLS method [20]. They have shown that SiC homoepitaxial layer could be obtained on both 6H- and 4H-SiC substrates without 3C-SiC inclusion under Al-rich solvent condition. Without Al, the epilayers consisted mainly of the 3C polytype. In those cases, the grown surfaces were covered by spirals related hillock, very similar to our results at much higher temperature. Assuming that the surface offers terraces large enough to allow 2D nucleation (i.e. nucleation sites are available), this first hypothesis considers that Al acts on the 2D nucleation energy of 3C.
- Second, the high density of steps associated with 4° off-angle naturally reduces (and even supresses) the probability of 2D nucleation, at the origin of 3C-SiC formation. Assuming that the 2D nucleation energy of 3C can be reached, this second hypothesis considers that Al acts

on the step and terrace structure. Differently said, by reducing the terrace widths, Al reduces the nucleation sites density as well. However, this concept needs growth rate fast enough for step bunching.

### 4.3.5. Suppression of parasitic 3C-SiC nucleation

Using numerical simulation, it has been shown that the former experimental procedure of approaching the seed crystal until contacting it to the solvent surface was a source of strong and rapid temperature fluctuation during the seeding stage, which in turn induced transient nucleation of parasitic 3C-SiC on the 4H-SiC substrates. To reduce this temperature drop during seeding stage, we implemented the pre-heating stage of the seed crystal by keeping it 1 mm above the solvent surface during 30 minutes (see the series 3 in Table 1). This experiment was performed at 1800°C while other growth conditions were similar to series 1. The surface morphologies grown on the nominal surfaces were rather different from Figure 4.2b and 4.2e, respectively, but similar with Figure 4.6b and 4.6e (see Figure 4.11). From the optical microscopy observation, it is clear that no evidence of domain-like structure was observed on both on- and off-axis surfaces. Furthermore, the surface morphologies grown on the off-axis surfaces were very close to the cases of Figure 4.7b and 4.7e as shown in Figure 4.11.

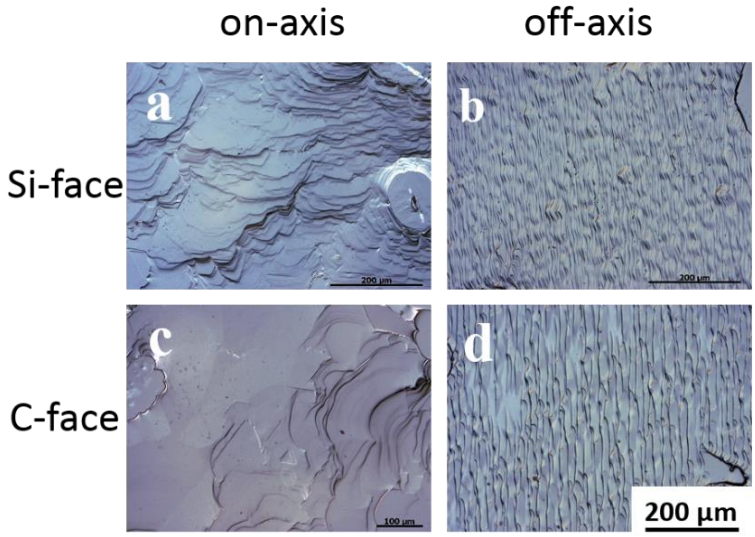


Figure 4.11. NDIC optical microscopy images of grown surface after preheating procedure (series 3 condition).

The corresponding EBSD maps of this additional experiment are gathered in Figure 4.12. The grown layers on the on-axis surfaces consisted of mainly 4H-SiC and 3C-SiC polytype is scattered only near the solvent inclusions or other macroscopic defects. On the off-axis samples, especially Si-face, 4H-SiC was observed over the entire surface, because of the absence of the defects and homogeneous step structure. These results were confirmed by Raman spectroscopy and no evidence of other hexagonal polytypes on the grown layers of series 3 was observed.

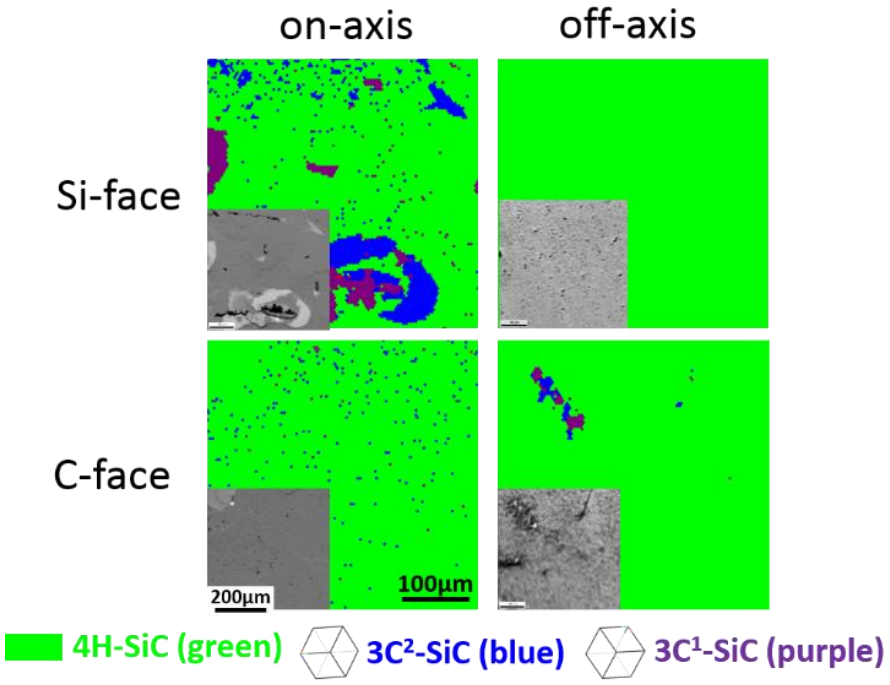


Figure 4.12. EBSD maps for the on- and off-axis samples of the series 3 (Si- and C-faces; 10at%Al-Si solvent, 1800°C, growth time of 10 min). Inserts are the SEM images at the same location as EBSD maps. The mapping scale is squares of 500 x 500 $\mu m^2$, and the step size is 5µm.

### 4.3.6. Polytype identification by Raman spectroscopy

The polytype of the grown layers have been identified by Raman spectroscopy in order to support the EBSD data. Using EBSD analysis, it is easy to distinguish cubic (3C-SiC) and hexagonal-SiC structures because the symmetry axis (c-axis) are different in both cases. However, if the crystal consists of two similar structures (here same symmetry axis) but different stacking sequences, such as 4H-SiC (hexagonal) and 6H-SiC (hexagonal), the differences are so small that the EBSD polytype identification is not accurate and thus not reliable. In such a case, Raman spectroscopy is the best tool to identify doubtlessly the nature of the hexagonal polytype. The 3C-

SiC spectra from such analysis should also be carefully distinguished because it has the same peak positions as 4H-SiC and 6H-SiC polytypes (796-797$cm^{-1}$).

As with EBSD results, 3C-SiC polytype formed on 4H-SiC polytype has been confirmed on the on-axis surface of series 1 (see Figure 4.13). On the other hand, 4H-SiC polytype has mainly been observed but 6H-SiC polytype has also been occasionally identified in the grown layers of series 2 and 3 (see Figure 4.13). From the results, it is possible that the measured spots include 3C-SiC polytype very slightly because the intensity of 3C-SiC is obviously small compared with other polytypes. However, in the off-axis samples, which are not convenient for EBSD analysis, the grown layers are exclusively of 4H-SiC polytype without any 3C-SiC or 6H-SiC polytypes in the grown layers of series 2 and 3 (see Figure 4.14). On the contrary, the peaks of 6H-SiC polytype formed on 4H-SiC polytype has been observed in the grown layer of series 1. We consider that it may be due to unstable growth condition caused by technical issue condition during the seeding stage.

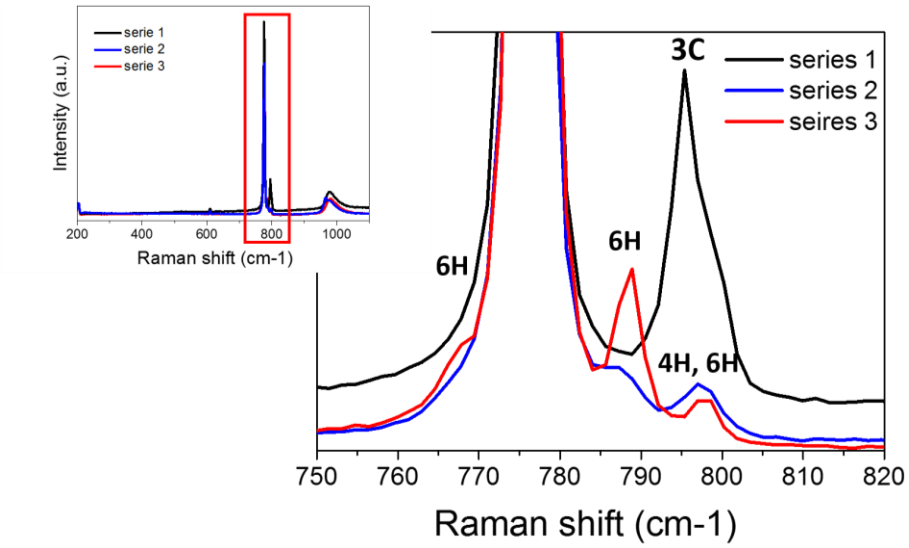


Figure 4.13. Raman spectra on the grown layers of series 1-3 (on-axis, Si-face at 1800°C). This analysis has been performed at five different positions on each sample and confirmed the same tendency for each sample. The same tendencies have also been observed on the C-faces.

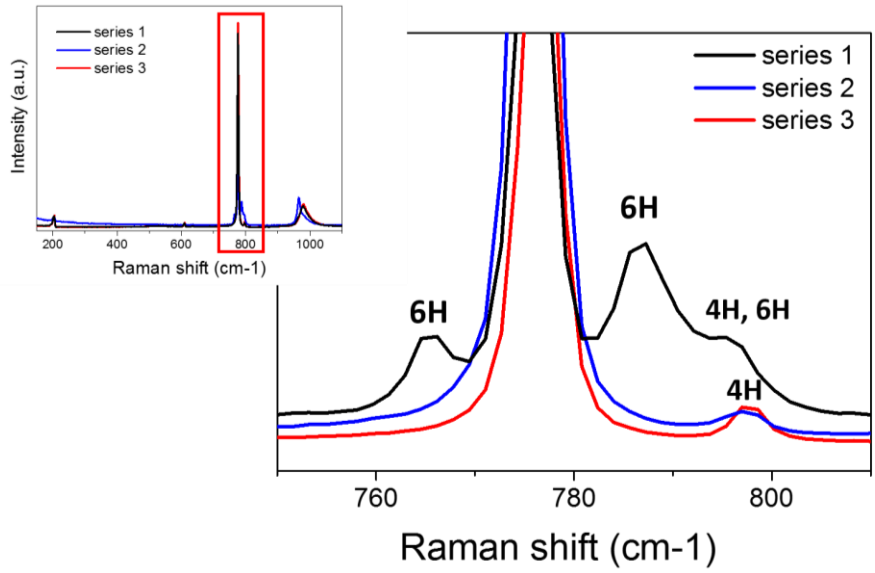


Figure 4.14. Raman spectra on the grown layers of series 1-3 (off-axis, Si-face at 1800°C). This analysis has been performed at five different positions on each sample and confirmed the same tendency for each sample. The same tendencies have been observed on the C-faces.

## 4.4. Conclusions of chapter 4

In this chapter, we addressed the "seeding stage" of the SiC top seeded solution growth process under various conditions. For that, we have systematically observed the initial growth layers, 10 minutes after contacting the liquid surface, for different solvents (pure Si and 10at%Al-Si), different temperatures (1700, 1800 and 1900°C) and different 4H-SiC substrate termination (nominal and vicinal Si-/C-faces). The experimental results show that 3C-SiC polytype can form by 2D nucleation on the nominal surfaces in pure Si solvent, even at high temperature (1900°C), i.e. conditions for which it is very unlikely to occur.

We have demonstrated using numerical simulation that a fast approaching of the seed to the solvent surface induced strong and rapid temperature fluctuations in the crucible. This fluctuation was characterized by a strong temperature drop during the first 100 seconds and a relaxation time of about 60 minutes before reaching the thermal equilibrium of the system. During this first stage, the liquid at the seed surface experiences a very strong supersaturation, at the origin of transient nucleation of 3C-SiC.

Additional experiments were performed in order to reduce the effect of thermal fluctuations that occur at the seeding stage. By pre-heating the seed before contacting the liquid surface, we could almost totally suppress the formation of 3C-SiC. Adding Al to the Si solvent was also effective to decrease the 3C-SiC formation, probably by decreasing its nucleation frequency. In addition, we observed that the roughness of grown surface on C-face is smaller than that Si-face in Al-Si solvent. The understanding of the real interaction between Al and the crystal surface would require further investigations.

## 4.5. References


[1] C. R. Eddy and D.K. Gaskill, Science, 324(5933): p. 1398-1400, 2009.

[2] Y. Yamamoto et al., Appl. Phys. Express, 5(11): p. 115501, 2012.

[3] Y. Yamamoto et al., Appl. Phys. Express, 7(6): p. 065501. 2014.

[4] B. Pelissier et al., Mat. Sci. Forum 338-342, p. 47-50, 2000.

[5] R. V. Drachev et al., J. Cryst. Growth, 233(3): p. 541-547. 2001.

[6] C. Ohshige, et al., J. Cryst. Growth, 408: p. 1-6. 2014.

[7] K. Ariyawong et al., Mat. Sci. Forum, 778−780, p. 71-74, 2014.

[8] D. Chaussende et al. Mat. Sci. Forum, 457-460, p. 387-390, 2004.

[9] M. Soueidan and G. Ferro, Adv. Funct. Mater. 16(7): p. 975-979. 2006.

[10] A. F. Gourgues-Lorenzon, Int. Mater. Rev., 52(2): p. 65-128. 2007.

[11] L. Latu-Romain et al., Crys. Growth & Design, 6(12): p. 2788-2794. 2006.

[12] T. Mitani et al., J. Cryst. Growth, 423: p. 45-49. 2015.

[13] G. C. Trigunayat, Solid State Ionics, 48(1–2): p. 3-70. 1991.

[14] K. Seki et al., J. Cryst. Growth, 335(1): p. 94-99. 2011.

[15] M. Soueidan et al., Acta Materialia, 55(20): p. 6873-6880. 2007.

[16] R. Vasiliauskas et al., Crys. Growth & Design, 12(1): p. 197-204. 2012.

[17] J. Lefebure et al., Crys. Growth & Design, 12(2): p. 909-913. 2012.

[18] F. Mercier et al., J. Cryst. Growth, 312(2): p. 155-163. 2010.

[19] F. Durand and J.C. Duby, J. Phase Equilib., 20(1): p. 61-63. 1999.

[20] M. Soueidan et al., J. Cryst. Growth, 293(2): p. 433-437. 2006.

[21] C. Qiu and R. Metselaar, J. Alloys & Compounds, 216, p. 55-60. 1994.

# Chapter 5. Investigation of the macro-step formation during 4H-SiC TSSG process

After having investigated the equilibrium liquid-SiC interaction and the nucleation of the epitaxial layer on the substrate, this chapter addresses one aspect of surface instability while trying to increase the growth rate by increasing forced convection.

## 5.1. Introduction

Although TSSG process is seen as a suitable method for obtaining high quality SiC single crystal, the growth surface stability and more precisely the development of morphological instabilities is one of the key issue for long lasting growth runs because it can easily give rise to foreign polytype and/or solvent inclusions in the growing crystal [1, 16-17]. During solution growth, vicinal surfaces, such as the standard 4° off-axis 4H-SiC one towards the <11-20> direction, usually exhibit huge step bunching. Macroscopically, the step bunching is viewed as a rearrangement of the surface to a hill and valley structure which lowers the total interfacial energy [2]. At a nanoscopic scale, the step bunching phenomenon also indicates that an additional energy barrier exists at the step edge, reducing the diffusion of adatoms toward the down-step [3]. During SiC growth, macro-step formation has already been observed and shown different consequences. On the one hand, the generation and movement of macro-steps contribute to improve the crystal quality as under specific conditions, a defect conversion mechanism can occur. If the macro-steps propagate in the basal plane from the center toward the edge of the crystal, the dislocation lines can be bent and pushed outside the crystal while the growth front moves [4, 5]. On the other hand,

the macro-steps can dramatically decrease the crystalline quality, as they can be at the origin of solvent inclusions, polytype inclusions and for the worse case a total and definitive transition from single to polycrystal. The combination of phenomena affecting the surface stability is extremely complex and is the subject of many investigations in the crystal growth community. In order to obtain the high crystalline quality, it is necessary to understand and control such surface instabilities for both formation and evolution of the macro-steps.

Recently, Zhu et al. suggested that large macro-steps could be observed if the fluid flow and the step flow had the same direction (parallel flow condition) while they can be suppressed under antiparallel flow condition [6]. They observed this trend locally and the question arising is the following: what would be the interaction between a vicinal surface and the fluid flow during rotation of the crystal? This is of the first importance for the further development of the process, especially for further upscaling. In this chapter, and based on the mechanism proposed by Zhu, the surface stability is investigated as a function of the rotation rate of the crystal by a systematic observation of the macro-step formation. The results show that the rotation of crystal introduces an intrinsic source of inhomogeneity on the growing surface when coupled to off-axis crystal orientation. In addition, the mechanism of interaction between step flow and fluid flow combining the experimental and the numerical simulation results will be discussed.

## 5.2. Experimental details

TSSG experiments have been implemented using the SiC growth setup introduced in chapter 2. High purity silicon (99.999%) was used as the solvent. Both Si- and C-faces with 4° off-cut towards <11-20> directions 4H-SiC crystals were used as seed crystals with typical seed diameter

of ~16 mm. The process was carried out at the temperature of 1700°C under a confining argon pressure of 1.05 bar. For all experiments, we applied a counterclockwise rotation to the seed crystal (as observed at the seed-solvent interface from below) with a rotation speed varying between 0 and 200 rpm. The growth morphologies were also compared with experiments conducted without rotation. A meniscus of ~1.5 mm in height has been used systematically to avoid polycrystal formation at the periphery of the growing crystals. All experimental parameters are summarized in Table 5.1. The growth duration was 2 hrs. After experiments, the residual solvent solidified on the crystals was removed by acidic etching in HF + $HNO_3$ (1:1) solution if necessary.

Table 5.1. The experimental details of 4H-SiC solution growth

| No. | Seed crystal | Solvent | T (°C) | $\Omega_{seed}$ (rpm) | $h_{meniscus}$ (mm) |
|---|---|---|---|---|---|
| Hulk032 | 4H-SiC, 4°-off, Si-face | Si 100% | 1700 | 0 | 1.2 ~ 1.5 |
| Hulk029 | | | | 100 | |
| Hulk034 | 4H-SiC, 4°-off, C-face | | | 0 | |
| Hulk033 | | | | 100 | |
| Hulk035 | | | | 200 | |

Polytype of the crystals was identified by Raman spectroscopy with an incident laser beam operating at a wavelength of 532 nm. Surface morphologies were systematically observed using NDIC optical microscopy. The heights and widths of the steps on the grown surfaces were measured by AFM.

## 5.3.Experimental results

### 5.3.1. The formation of the steps

In the solution growth method, surface instabilities are usually related to the interaction between the local distribution of supersaturation on the crystal surface and the growth kinetics along the surface, as suggested by Chernov [7, 8]. Such surface instabilities are usually evidenced by morphological features, such as huge step bunching involving solvent inclusions (see chapter 2.2.4). SiC single crystal growth from the liquid phase on a vicinal surface is expected to grow by the so called step flow mechanism, i.e. by the lateral motion of a train of parallel steps, as described in the standard theory of crystal growth by Burton, Cabrera, and Frank (BCF) [9]. Quite often, atomicsteps can interact between them, forming different size of step heights and terraces widths. This is associated to non-equivalent individual step velocities and is known as the step bunching mechanism. For SiC liquid phase growth, its occurrence has been associated to a minimization of the surface energy [10]. Growth surfaces can thus exhibit a large variety of step heights, which could have different origin and different behavior. For the sake of clarity, the steps will be classified into three different categories in this study.

- Atomic steps or nano-steps. In SiC, they consist of a Si-C bilayer (0.25 nm) or a multiple of bilayers, typically one or half of the structure unit cell height along the c-direction. This kind of step is usually encountered and well controlled during epitaxial growth by CVD [11].
- Micro-steps. They are issued from the bunching of nano-steps and are typically up to 100 nm height.

- Macro-steps. They come from the bunching of the two previous categories of steps, and consist of a large number of stacked micro-steps. They form huge steps that can reach the micrometer scale in height.

### 5.3.2. The surface morphology without rotation of the seed crystal

The typical growth morphologies of non-rotating seed on the Si-face (Hulk032) and on the C-face (Hulk034) are shown in the Figure 5.1 and Figure 5.2, respectively. In both cases, the micro-steps are oriented systematically toward [11-20] direction (from the left to the right side) according to the off-cut direction of the SiC crystal. These micro-steps are starting to bunch and organize each other. On the Si-face, they form a few zigzag-like pattern with well-defined crystallographic orientation (Figure 5.3). On the C-face, bunching of micro-steps gives rise to a "cloudy-like" morphology without defined crystallographic orientation. In both cases, no solvent inclusion or no visible structural defects are evidenced. Moreover, the morphology is homogeneous over the whole seed surface.

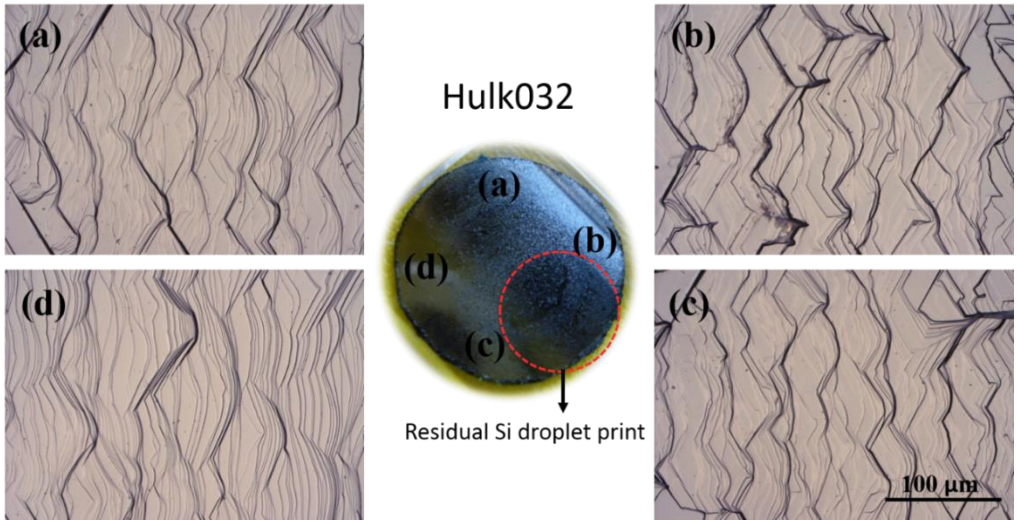


Figure 5.1. NDIC optical microscopy images of the growth surface morphologies on the Si-face. These pictures were taken from different locations as marked in the picture of the Hulk032 sample.

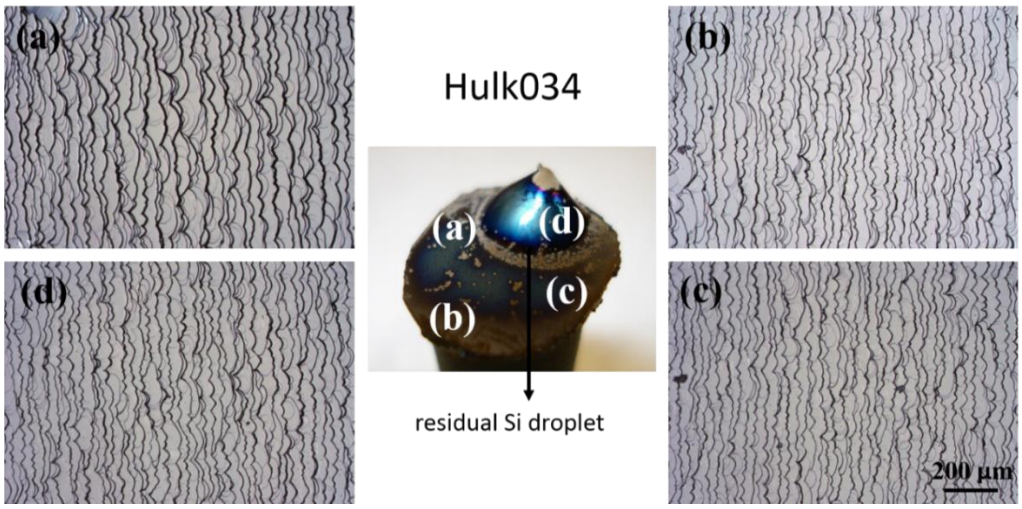


Figure 5.2. NDIC optical microscopy of the grown surface morphologies on the C-face. These pictures were taken from different locations as marked in the picture of the Hulk034 sample.

### 5.3.3. The surface morphology with rotation of the seed crystal

For comparison, we applied a rotation to the seed crystal to both Si-face (Hulk029) and C-face (Hulk033) with a high rotation speed, varying from 100 to 200 rpm. Other growth conditions are similar to the case without rotation. On the Si-face with a seed rotation of 100 rpm, the surface morphology can be separated into three categories:

(i) a train of regular zig-zag micro-steps, similar to no-rotation case (see Figure 5.3(a)),

(ii) a set of black wavy lines present over the micro-steps (see Figure 5.3(b, d)), and

(iii) big zigzag-like black lines forming above the micro-steps (see Figure 5.3(c)).

Interestingly, the black wavy lines of the second category are clearly caused by the bunched step edges (facetted). These black lines are what we defined as "macro-steps". They are formed by the bunching of the step edges along the two equivalent <1-100> directions adjacent to the <11-20> direction, according to the crystallographic symmetry of SiC crystal. For example, the macro-steps observed in Figure 5.3(b) and (d) are close to the [01-10] and [10-10] directions, respectively. The macro-steps are observed to be also distorted along the elongated direction. In the case of the third category, the zigzag shaped macro-steps correspond to the both [10-10] and [01-10] directions.

The height of the micro-steps where there is no macro-step is about 100 nm. The average terrace width is, in such a case, evaluated to be 5 μm. However, in the mixed areas of micro- and macro-steps, the height of micro-step is increased beyond 300 nm while the height of the macro-steps are varied from a few hundreds of nm to a few μm. Also, the average terrace width was about 6~7 μm. In other words, the micro-step bunching is more pronounced by the presence of the macro-steps.

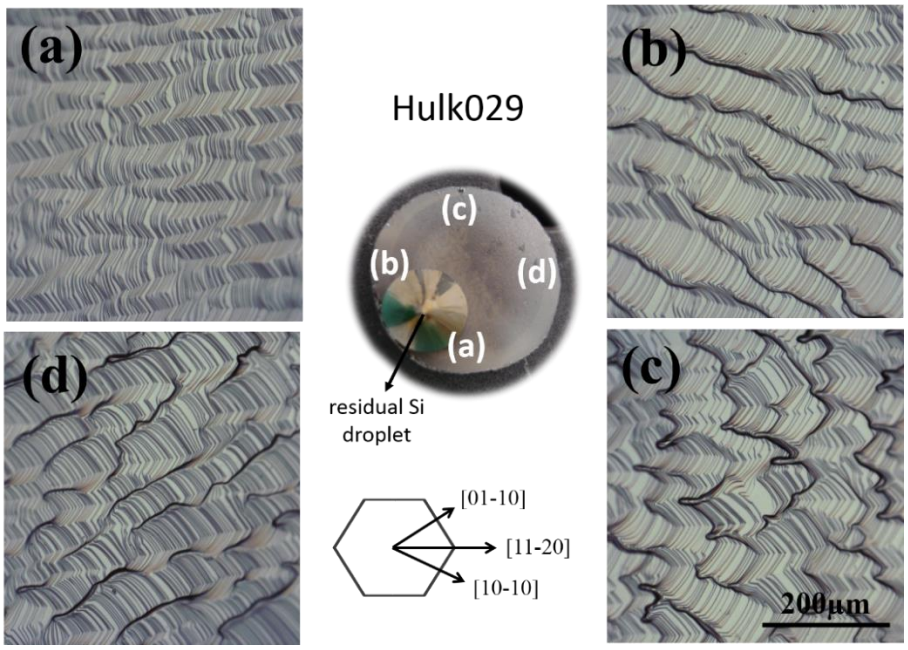


Figure 5.3. NDIC optical microscopy of the grown surface morphologies on the Si-face with a seed rotation of 100 rpm. These pictures were taken from different areas as marked in the picture of the Hulk029 sample (middle).

Figure 5.4 shows that there is no evidence of the macro-step formation on the C-face with the rotation speed of 100 rpm. The morphology of micro-steps in Hulk033 sample exhibits a similar tendency as the case without rotation (Hulk034) while the width of micro-steps is increased. The average width value of Figure 5.4(b-d) areas was over 20 μm while more dense micro-steps (about 16 μm) are observed in the areas of Figure 5.4(a). Such micro-step evolution seems to be dependent on the location on the crystal surface, similarly to the case of Si-face (Hulk029).

The formation of macro-steps is observed on the C-face when the seed rotation is increased to 200 rpm, as shown in Figure 5.5. The directionality of the macro-steps depends on the crystal location but not as obvious as on the Si-face. The macro-steps are specifically formed close to the [01-10] and/or [10-10] directions as shown in Figure 5.5(b, d), respectively. Such tendency of

macro-steps formation is well matched with Si-face. The structure of micro-steps in this sample was not homogeneous. Thus the width of the terraces was not evenly distributed compared to the other cases. We tried nevertheless to extract some representative values. The terrace widths in Figure 5.5(a) area was observed to be ~15 μm. In the mixed areas of micro- and macro-steps, the micro-steps are less densely packed, giving slightly higher terrace widths, about 17~19 μm in (see Figure 5.5(b-d). Thus, it is worth noting that the micro-steps are usually denser with a seed rotation speed of 100 rpm on the Si-face. Additionally, this value is very dependent on the presence or absence of macro-steps on the C-face. For instance on the C-face, the difference of terrace widths in each area was rather high at 100 rpm. All the average values of the micro-terrace width as a function of the seed rotation speed are plotted in Figure 5.6.

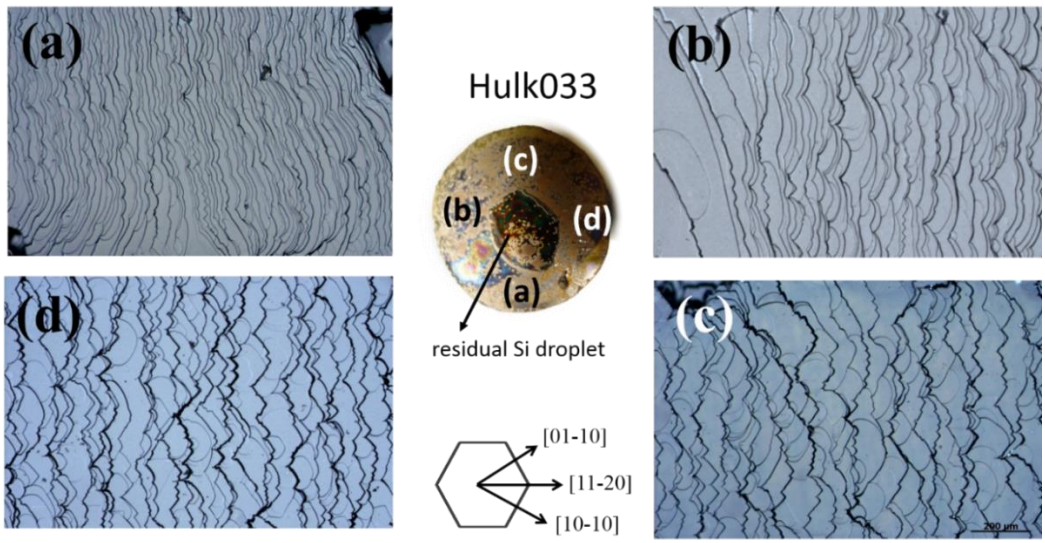


Figure 5.4. NDIC optical microscopy of the grown surface morphologies on the C-face with the seed crystal rotation of 100 rpm. These pictures were taken from different areas as marked in the picture of the Hulk033 sample (middle).

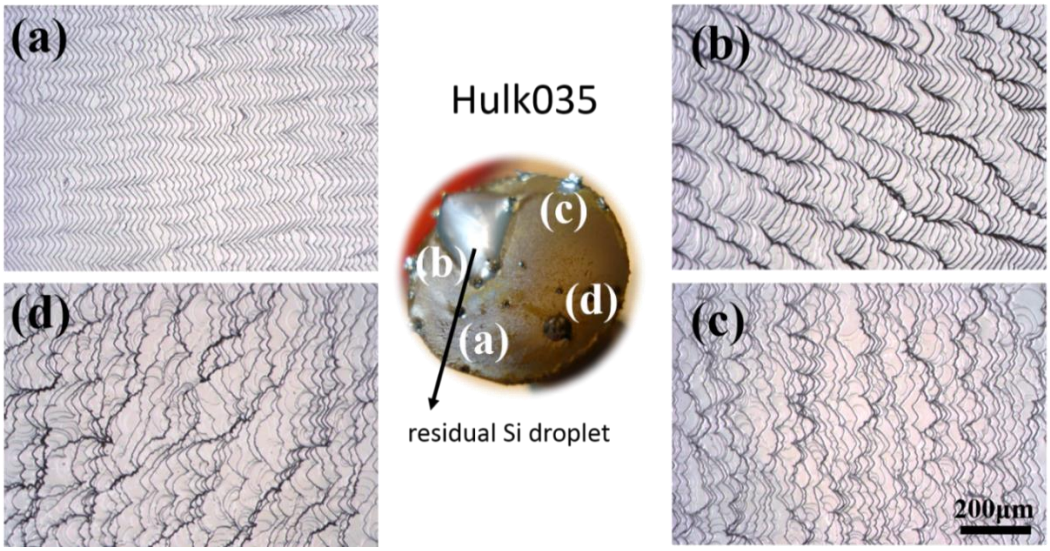


Figure 5.5. NDIC optical microscopy of the grown surface morphologies on the C-face with a seed crystal rotation of 200 rpm. These pictures were taken from different areas as marked in the picture of the Hulk035 sample (middle).

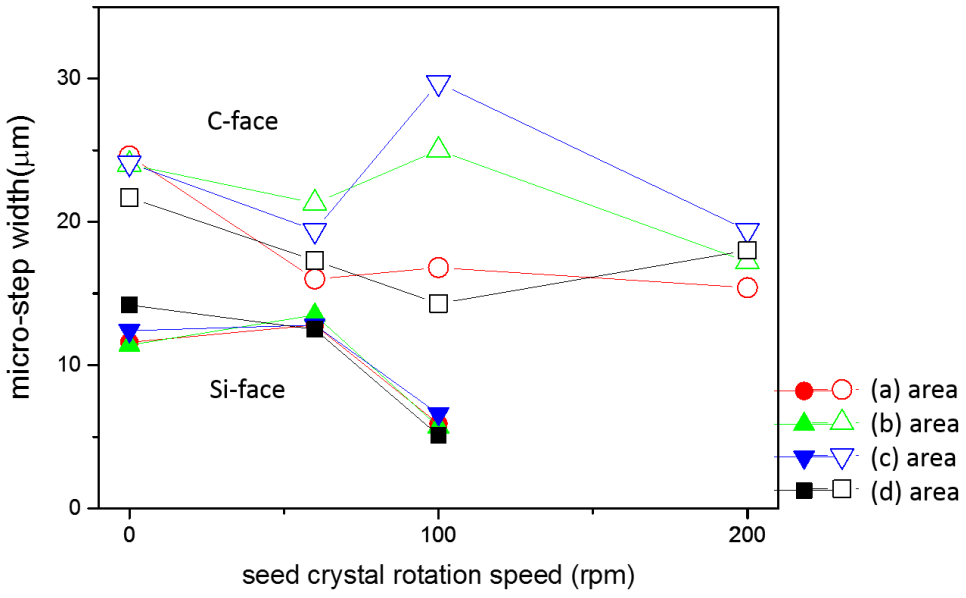


Figure 5.6. Variation of the average micro-step distances as function of seed crystal rotation speed on the Si- and C-faces.

## 5.4. Discussions

From the experimental results, the macro-steps are observed in specific conditions, and come from a reorganization of the train of parallel micro-steps. As the macro-steps seem to be linked with the rotation speed of the seed, it is reasonable to think that the mechanism of macro-step formation is related to the interaction between the step flow on the crystal surface and the fluid flow close to the crystal surface. Zhu et al. suggested [6] that when the fluid flow and the [11-20] step flow have the same directions (case named 'parallel flow'), step bunching is favored according to the solute (carbon) distribution along the surface [12]. We extended this basic idea to the zigzag-like morphology, as illustrated in Figure 5.7. To better describe the different situations, it is necessary to describe the fluid flow behavior when a rotation is applied to the seed and also to compare the step flow direction with the fluid flow direction for the different areas on the crystal surface. Then, if the fluid flow has the same orientation than the [01-10] propagating micro-steps, macro-steps perpendicular to the [01-10] direction can form (Figure 5.7(a)). Their height will be maximum. If the fluid flow direction is exactly the opposite of the [01-10] propagating micro-steps, the micro-steps will be stable and no macro-steps will develop. The same description can be done for the equivalent [10-10] direction, as shown in Figure 5.7(b). Now, if the fluid flow is oriented towards the [11-20] direction, which direction is a combination of [01-10] and [10-10], macro-steps can also form along these two directions, producing zigzag-like macro-steps. Conversely, when the fluid flow and step flow move to the opposite directions, named 'antiparallel flow', the distribution of carbon concentration would be changed as if the solute concentration was swept toward the step edge. As a results, the step velocity increases which stabilizes the step flow growth and reduces the step bunching phenomenon.

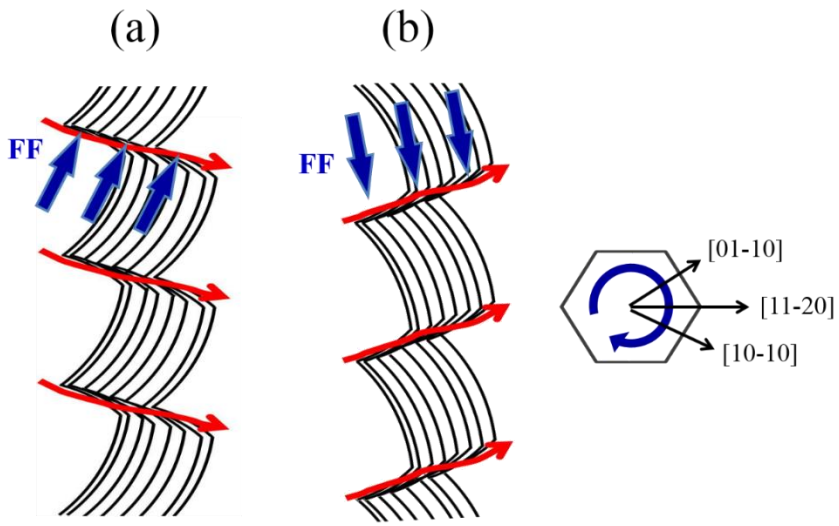


Figure 5.7. The schematic of macro-steps development (depicted by the red lines) and the direction of step flows (SFs) in [11-20] direction and fluid flows (FF; blue arrows), respectively. The cases of (a) and (b) correspond to the location in Figure 5.3(b) and (d), respectively.

- **Qualitative analysis of macro-step formation**

We proposed an analytical model for analyzing the interaction between fluid flow and step flow directions [13, 14]. To describe the fluid flow in the TSSG process, let consider two components of the fluid velocity, which are azimuthal component ($v_\phi$) and radial component ($v_r$). By considering the seed at rest the relative fluid velocity in both directions can be written as the relative velocity $\Delta v_\phi$ and $\Delta v_r$, which are the fluid velocities relative to the seed crystal. The characteristics of these components are visualized in Figure 5.8(a) and (b). For a matter of simplicity, these two components of $\phi$ and $r$ will be taken as positive. This means that a counterclockwise direction is applied to the crystal (azimuthal) and that the fluid flows from the center of the seed to the periphery. All the configurations are thoroughly described in Ref. [13, 14]. If the fluid flow involves only azimuthal component, the flow pattern below the seed can be depicted as in Figure 5.8(a). Considering the interaction between step in [11-20] direction and a

pure azimuthal component of the fluid flow, the parallel flow are defined (theoretically) in the half of the crystal, as marked by red tips, and thus the other half area is defined as the antiparallel flow, as marked by blue tips. For a pure radial component, as shown in Figure 5.8(b), the dotted line separating the parallel and antiparallel flows is shifted by 90° compared to the first case. In reality, the combination of both components gives rise to a deviation angle, as shown in Figure 5.8(c). In such case, the boundary line separating the parallel and antiparallel flow areas deviates of ξ degrees from the original, reference position ($l_{original}$). The angle of deviation can be derived from single trigonometry consideration suggested by Ariyawong,

$$\xi(r) = \tan^{-1}\left(\Delta V_r / \Delta V_\phi\right)$$

where $r$ is the radius of the position considered on the seed crystal. For $\Delta V_r$=0, the deviation ξ is 0° ($\Delta V_\phi$>0), or ξ=180° ($\Delta V_\phi$<0). For $\Delta V_\phi$=0, the deviation is ξ=90° ($\Delta V_r$>0) or ξ=-90° ($\Delta V_r$<0). The relative fluid velocities below seed crystal were extracted from the numerical modeling of coupled induction heating and fluid dynamics (see chapter 2). Their profiles along the crystal radius are plotted in Figure 5.9 [14]. It can be seen that the azimuthal component of fluid velocity near the seed crystal is larger than the radial component due to the crystal rotation.

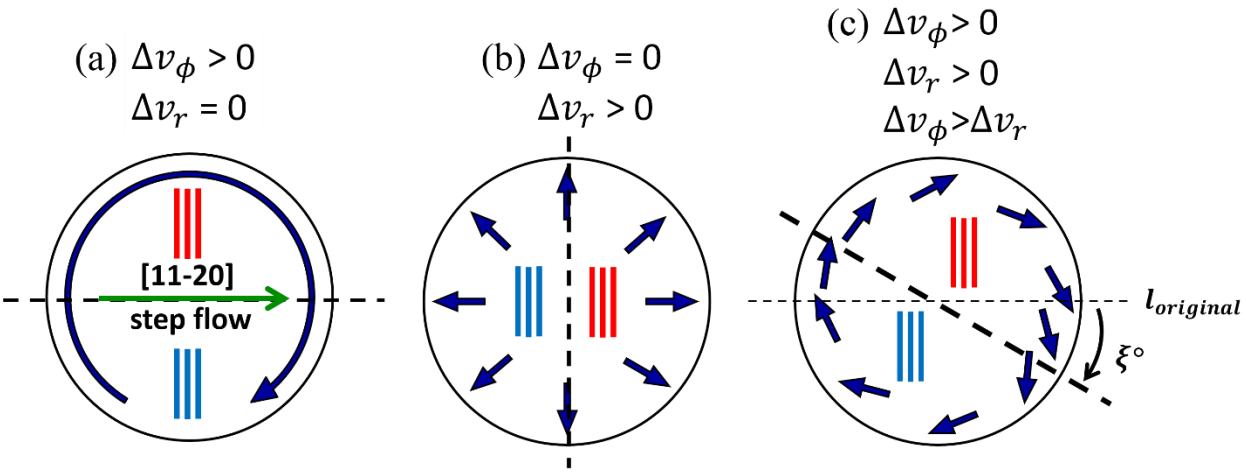


Figure 5.8. Illustration of the fluid and step flows with (a) the azimuthal and (b) radial components of the fluid velocity on the crystal [13, 14]. The blue arrows represent the fluid flow direction tangential to the crystal surface, and the black dashed lines in the middle of the circles separates the parallel (red bars) and antiparallel (blue bars) flows areas.

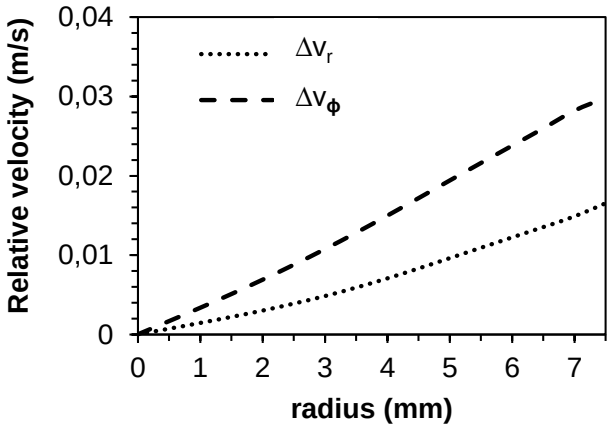


Figure 5.9. The profile of the calculated relative fluid velocity as a function of the seed crystal radius for both azimuthal and radial components [14]. The rotation speed of seed crystal is set at 100 rpm in the counterclockwise direction.

In reality, the situation is more complicated because of the six-fold symmetry axis of the SiC hexagonal system. On the vicinal surface, the growth rate of SiC single crystal is larger on the {11-20} plane than on the {1-100} plane for similar growth conditions close to thermodynamic equilibrium [15]. This is the reason why the initial parallel steps evolve to develop the zigzag-type morphology with (10-10) and (0-110) facets. Based on such step formation, the interaction between step flow and fluid flow due to both the azimuthal and radial components can be defined as shown in Figure 5.10(a), where two dashed lines can be drawn to separate the four different domains. These two dashed lines are also used as the reference lines in their original positions. The deviation of those lines from the original positions can be considered in the same way as in the simplified case described earlier. From Figure 5.9, the deviation angle $\xi$ from the original boundary lines is calculated to be 28° via the equation above, when the radius of seed crystal is about 6 mm. The fluid flow pattern below the seed computed from the numerical simulation using the same set of experimental conditions is shown in Figure 5.10(b). By combining the experimental results with numerical modeling results, it is noted that the parallel flow (marked by red tips) and antiparallel flow (marked by blue tips) areas in Figure 5.10 are exactly matched with our experimental results as shown in Figure 5.3 and Figure 5.5.

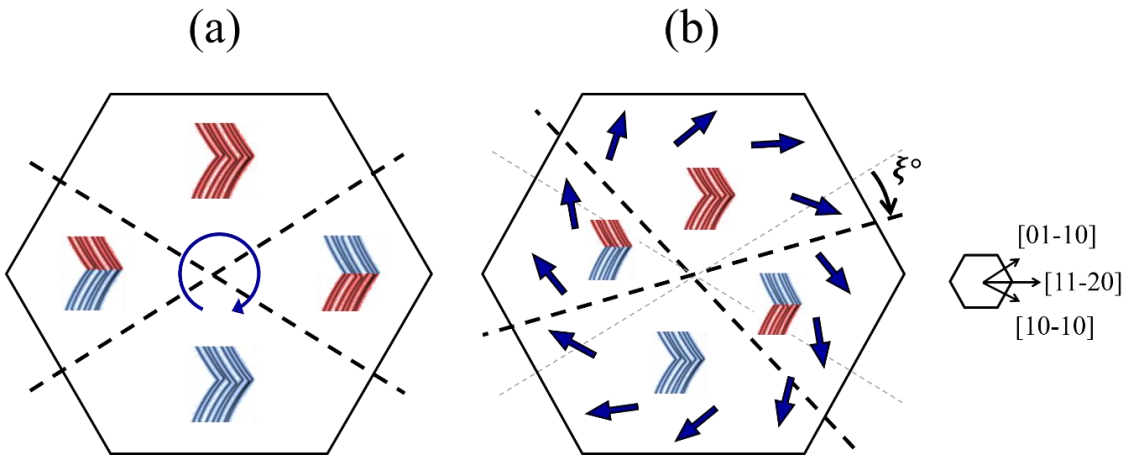


Figure 5.10. Illustration of the interaction between the step (as marked by tips) and fluid (as marked by arrows) flows in the hexagonal system of SiC crystal.

In order to describe the formation of a macro-step, the scenario is presented in Figure 5.11. These optical microscopy images were taken at four different locations on the same as grown crystal surface. From them, we can suggest four steps of macro-step formation in the [01-10] direction, which can be generalized to the other directions as well:

i) When the fluid flow moves in the same direction with the step flow, small steps are subject to bunching in the [01-10] direction.

ii) The formed macro-step, though of small height forms a small protuberance that will affect locally the fluid flow pattern (see Figure 5.11(b))

iii) Due to a higher supersaturation at the protuberance tip, the top of the macro-step will develop (see Figure 5.11(c)),

iv) This process can only extend forming big and long macro-steps (see Figure 5.11(d)).

v) The last stage, not represented here is that the top of the macro-step can move faster than the bottom of the macro-step creating a hole with solvent trapping. In this latter case, the growth front can be considered as destabilized.

Thanks to the evolution of the fluid velocity along the seed surface, especially due to the azimuthal and radial components, there is a kind of macro-step size and density gradient along the radius, for a given azimuth.

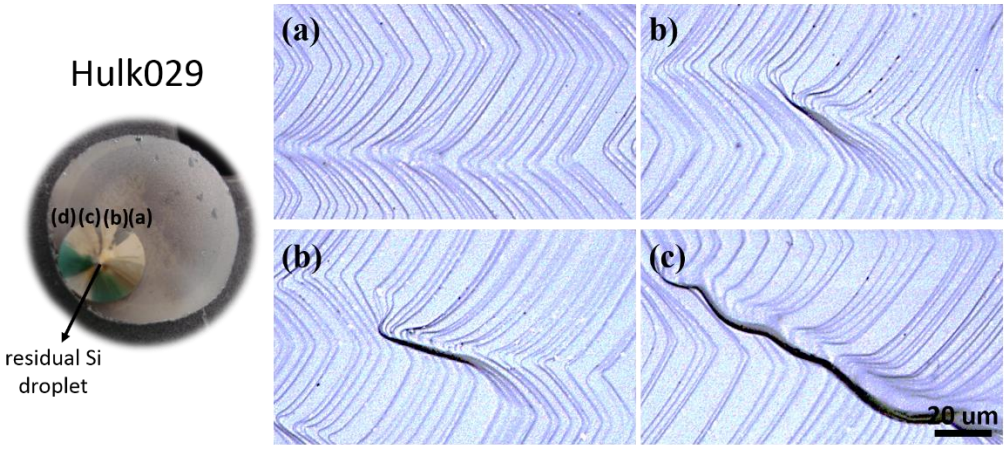


Figure 5.11. NDIC images of the macro-step formation under the condition of parallel flow, which were observed from the middle of crystal (a) toward the edge of crystal (d). The left picture is as grown crystal before acidic etching.

## 5.5. Conclusions of chapter 5

In this chapter, new insights about the macro-step formation during the top seeded solution growth process has been discussed. Increasing the rotation rate is a good way to increase the growth rate of the crystal, as demonstrated in Chapter 2. However, there exists a critical rotation

speed above which the interaction between the step flow on the crystal surface and the fluid flow pattern can interact to create surface instabilities, which in turn can give rise to solvent inclusion. This can be qualitatively described by considering first the step flow direction (after "hexagonalization" of the original train of parallel steps) and second the fluid flow direction which must be split into two azimuthal and radial components.

## 5.6. References


[1] D. H. Hofmann and M. H. Müller, Mater. Sci. Eng., B, **61–62**. pp. 29–39, 1999.

[2] T. Kimoto et al., Appl. Phys. Lett. **66**, 3645, 1995.

[3] R. L. Schwoebel and E. J. Shipsey, J. Appl. Phys. **37**(10), pp. 3682-3686, 1966.

[4] Y. Yamamoto et al., Mat. Sci. Forum **717-720**, pp. 53-56, 2012.

[5] T. Ujihara et al., Mat. Sci. Forum **717-720**, pp. 351-354, 2012.

[6] C. Zhu et al., Cryst. Growth Des. **13**, pp. 3691−3696, 2013.

[7] A. A. Chernov, J. Cryst. Growth, 24-25, pp. 11-31, 1974.

[8] A. A. Chernov and H.J. Scheel, 149, pp. 187-195, 1995.

[9] W. K. Burton et al., Philos. Trans. R. Soc. London, Ser. A **243**, pp. 299-358, 1951.

[10] M. Syväjärvi et al., J. Electrochem. Soc. **146**(4), pp.1565-1569, 1999.

[11] T. Kimoto et al., J. Appl. Phys. **81**(8), pp. 3494-3500, 1997.

[12] A. A. Chernov et al., J. Cryst. Growth **275**, pp. 1–18, 2005.

[13] K. Ariyawong PhD thesis, Université Grenoble Alpes, 2015.

[14] K. Ariyawong et al., Cryst. Growth Des. **16**(6), pp 3231–3236, 2016.

[15] M. Syväjärvi et al., J. Cryst. Growth **236**, pp. 297–304, 2002.

[16] T. Ujihara et al., Mat. Sci. Forum, **717-720**, pp. 351, 2012.

[17] K. Kusunoki et al., J. Crys. Growth, **395**, pp. 68, 2014.

# Chapter 6. Doping concentration in n- and p-type 4H-SiC

## 6.1. Introduction

So far, we discussed the growth of SiC single crystals using the TSSG method with a focus on the different aspects related to the growth interface. Through the optimization of the growth conditions, we have achieved solution grown 4H-SiC crystals. To apply those crystals in power electronic applications, highly conducting n-type and/or p-type 4H-SiC crystals are required. In general, nitrogen (N) is widely used as an n-type dopant and aluminum (Al) as a p-type dopant. Several studies have already been experimentally conducted by PVT method and n-type resistivity lower than 10mΩcm has been obtained [1]. The recent improvements of the TSSG process made it very attractive for the growth heavily doped substrates of both n- and p-type 4H-SiC. In this chapter, carrier concentration and atomic concentrations in the grown crystal will be evaluated respectively.

## 6.2. Experimental details

4H-SiC crystals were grown by the TSSG process using the puller described in chapter 2.1. Since 4H-SiC grow is favorable on C-face due to its lower surface energy than Si-face [14], on-axis and off-axis 4H-SiC seeds of (000-1) C-face were used in this study. Pure Si and $Al_x$-$Cr_y$-$Si_{1-x-y}$ solvents were used to grow n- and p-type samples. The fixed amounts of Cr (19~20 at%) were used in order to have similar growth rate in each experiment. The growth was carried out at the temperature of 1700°C with pure Si solvent and 1850°C in the Al-Cr-Si alloys. For all experiments, the rotation rate of the seed was set at 30 rpm. A meniscus height of 1 mm was applied. After the

growth, the residual solvent solidified on the crystals was removed by acidic etching in HF + HNO3 (1:1) solution and slightly polished for getting a flat surface when it was necessary. All experimental parameters are summarized in Table 6.1.

Table 6.1. The experimental details of n- and p-type 4H-SiC solution growth

| No. | Seed crystal | T (°C) | Solvent | $R_g$ (um/h) |
|---|---|---|---|---|
| Hulk027 | 4H-SiC, 4°off, C-face | 1700 | Si | ~15 |
| Hulk051 | 4H-SiC, 0°off, C-face | 1850 | 1at%Al-19at%Cr-Si | 150~180 |
| Hulk068 | | | 5at%Al-20at%Cr-Si | |
| Hulk053 | | | 10at%Al-20at%Cr-Si | |

Polytype of the crystals was identified by Raman spectroscopy (Jobin Yvon/Horiba LabRam) at room temperature in a backscattering geometry. A green laser excitation ($\lambda$ = 514.5 nm, ~1 $\mu m^2$ diameter spot size) was used. Raman spectra were calibrated using silicon at room temperature. From the Raman spectra, we approximatively assessed the crystal quality from the TO-mode peak, and carrier concentration with the LOPC peak. The grown crystals were also characterized by secondary ion mass spectroscopy (SIMS) to evaluate $^{14}N$ and $^{21}Al$ atoms concentrations [2, 3]. The primary beam high voltage was 15 kV while the impact energy was reduced to 10.5 kV (15 – 4.5 kV) since the secondary beam high voltage was 4.5 kV. The mass resolution was fixed at M/ΔM = 1500. The concentration profiles measured by SIMS were calibrated using RSFs (Relative Sensitivity Factors) from reference samples in which the concentration profiles were well known (see Table 6.2). In this work $^{12}C_2$ isotope signal has been used as reference matrix.

Table 6.2. RSF values used in $O_2^+$ configuration

| | $^{14}N^+ / {}^{12}C_2$ | $^{27}Al^+ / {}^{12}C_2$ |
|---|---|---|
| RSF | $1.5\times10^{21}$ | $1\times10^{18}$ |

## 6.3. Results and discussion

### 6.3.1. Raman spectroscopy

Raman spectroscopy is a convenient technique to identify 1) a polytype from the peak positions [4], 2) a substitutional impurity from the localized vibrational mode [5], and 3) structural defect and the anisotropy by breaking of the translational symmetry of the crystal [6, 7]. Firstly, we identified the polytype of grown crystals with pure Si and Al-Cr-Si solvents with varying the amount of Al from 1 to 10 at%. In all spectra gathered in Figure 6.1, typical 4H-SiC Raman peaks can be observed. They are typically the folded longitudinal acoustic mode (FLA; 610 $cm^{-1}$) and two $E_1$ and $E_2$ folded transverse optic modes (FTO; 775 and 796 $cm^{-1}$). The two FTO modes correspond to the different vibration behavior between Si and C atoms (Figure 6.2), and such vibrations are strongly affected by the crystal quality [7]. It clearly appears that the $E_2$-FTO mode (796 $cm^{-1}$) becomes broader while increasing the amount of Al in the solvent. For example, the full width at half-maximum (FWHM) of $E_2$-FTO peak in Hulk027 was found to be 7 $cm^{-1}$. When increasing the amount of Al, FWHM is also increased from 8 to 13 $cm^{-1}$. In general, FTO peak shifts with the stress. In other words, the bonding forces are changed by the stress owing to the defect generation during the growth process. However, there is no peak shift of FTO modes compared to the seed crystal case, we thus think that there is no measurable stress in our TSSG grown crystals, meaning that our growth conditions are well optimized for 4H-SiC crystal growth without serious defect generation.

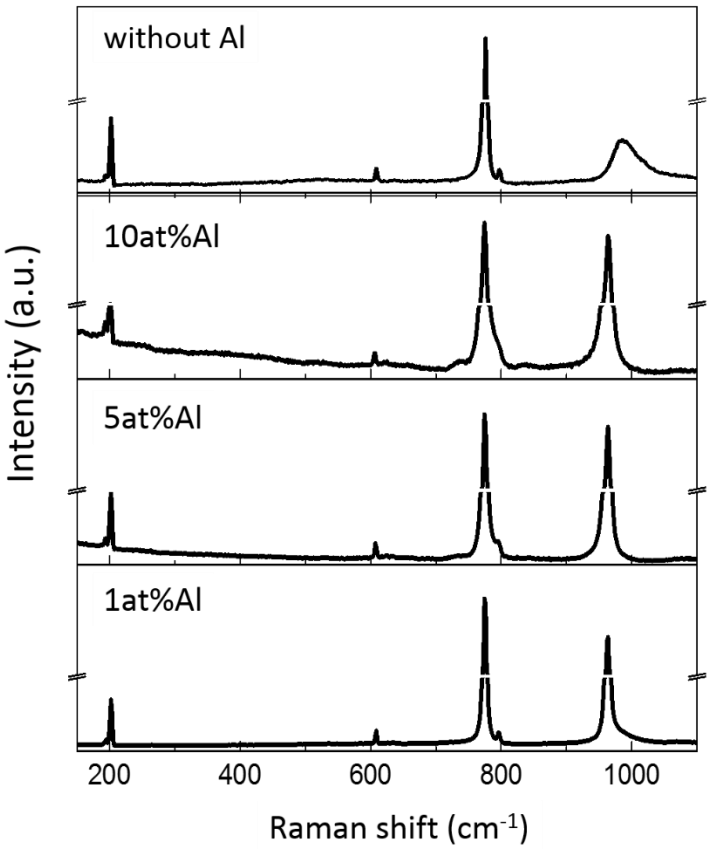


Figure 6.1. Raman spectra of grown crystals correspond to the list in Table 1.

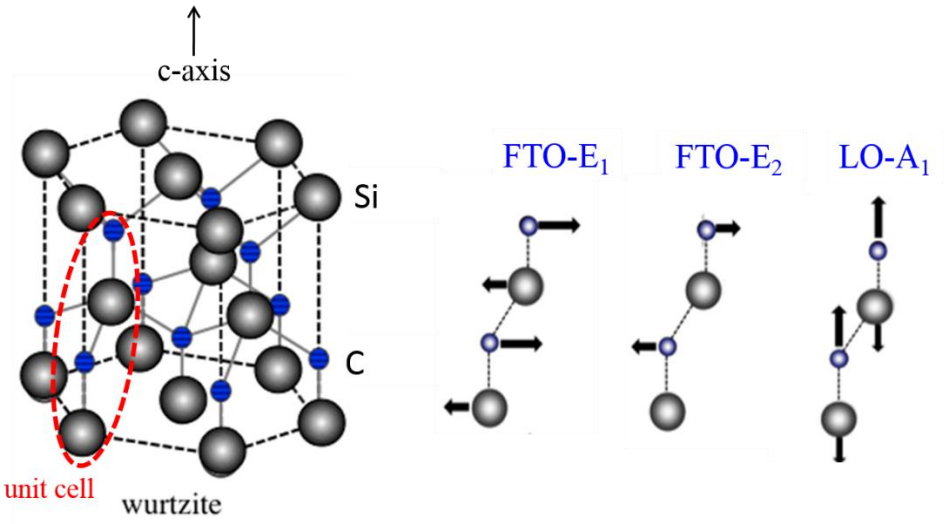


Figure 6.2. Different optical phonon modes in SiC measured by Raman spectroscopy.

In n-type semiconductor materials, LO phonon mode is coupled with plasmon (the so-called LOPC mode), resulting in a drastic change in peak-shape with the free carriers concentration. Within a given range, we can thus evaluate the electric transport parameters such as free carrier density and mobility by analyzing the peak frequency and shape. Nakashima and Harima [4] described the theoretical equation of the Raman band profile of LOPC mode for cubic crystals,

$$I(\omega) = SA(\omega)Im[-\frac{1}{\epsilon(\omega)}]$$

Where $\omega$ is the Raman shift, S is a proportionality constant and $\epsilon(\omega)$ is the dielectric function written as

$$\epsilon(\omega) = \epsilon_\infty \left(1 + \frac{\omega_L^2 - \omega_T^2}{\omega_T^2 - \omega^2 - i\omega\Gamma} - \frac{\omega_P^2}{\omega(\omega + i\gamma)}\right)$$

$A(\omega)$ is given by

$$A(\omega) = 1 + 2C\omega_T^2[\omega_P^2\gamma(\omega_T^2 - \omega^2) - \omega^2\Gamma(\omega^2 + \gamma^2 - \omega_P^2)]/\Delta$$

$$+ (C\omega_T^4/\Delta)\{\omega_P^2[\gamma(\omega_L^2 - \omega_T^2) + \Gamma(\omega_P^2 - \omega^2)] + \omega^2\Gamma(\omega^2 + \gamma^2)\}/(\omega_L^2 - \omega_T^2)$$

Here, $\omega_T$ and $\omega_L$ are TO and LO phonon frequencies, respectively. $\gamma$ is the plasmon damping constant written as $\gamma = e/(m_{\text{effective mass}}\epsilon_\infty)$, $\Gamma$ is the phonon damping constant. Details of $\omega_p$ and $\Delta$ are described in Ref. [4]. *C* is the Faust-Henry coefficient which is related to the Raman intensity ratio of LO and TO modes in an undoped crystal given by

$$\frac{I_{LO}}{I_{TO}} = \left(\frac{\omega_1 - \omega_L}{\omega_1 - \omega_T}\right)^4 \frac{\omega_T}{\omega_L}\left(1 + \frac{\omega_T^2 - \omega_L^2}{C\omega_T^2}\right)^2$$

where $\omega_1$ is the incident photon frequency. C is a coefficient related to wurtzite semiconductors such as SiC; it is usually about 0.4 [8]. The LOPC mode consists of upper and lower frequency

branches (named L+ and L-). With increasing the nitrogen density, the L+ mode shifts to higher frequency and becomes broader, while the L- mode sharpens and approaches to TO-mode frequency ($\Gamma = \gamma = 0$). However we do not considered L- mode because this mode was not observed as shown in Figure 6.1.

Theoretical line-shape fitting to LOPC mode is conducted by $I(\omega)$. Particular attention has been paid in the line-fitting to reproducing: 1) The peak intensity, treating S as a proportionality constant which is independent on the carrier density, 2) The peak shift from the uncoupled LO-phonon frequency, and 3) The asymmetric peak shape. The fitting of peak intensity is quite important for the unique determination of the parameters. We used the important basic parameters from the Ref. [4, 8] such as pure LO-phonon ($\omega_L^{\parallel}$ =964.2 $cm^{-1}$) and TO-phonon (783 $cm^{-1}$) frequencies corresponding to the lowest carrier density ($5\times10^{16}$ $cm^{-3}$) of n-type 4H-SiC (intrinsic). If the carrier density becomes higher, LOPC is red shifted to higher frequency. This phenomenon has been observed by Feldman et al., and confirmed by Harima et al [8, 9]. Figure 6.3 shows the fitted line of LOPC peak in Hulk027 sample. In this case, calculated free carrier density at the LOPC mode frequency of 985.79 $cm^{-1}$ was about $4.5\times10^{18}$ $cm^{-3}$. On the other hand, LOPC mode does not exhibit significant shift in p-type SiC because of weak coupling between LO-phonon and plasmon. Such a weak coupling is explained by low mobility of hole [2, 4, 10, 11]. Especially, our samples grown in Al-Cr-Si solvent exhibited very low frequencies (962~963 $cm^{-1}$) which is not available for LO-mode fitting and the fano-parameters (FTA peaks) were not clear enough to be analyzed.

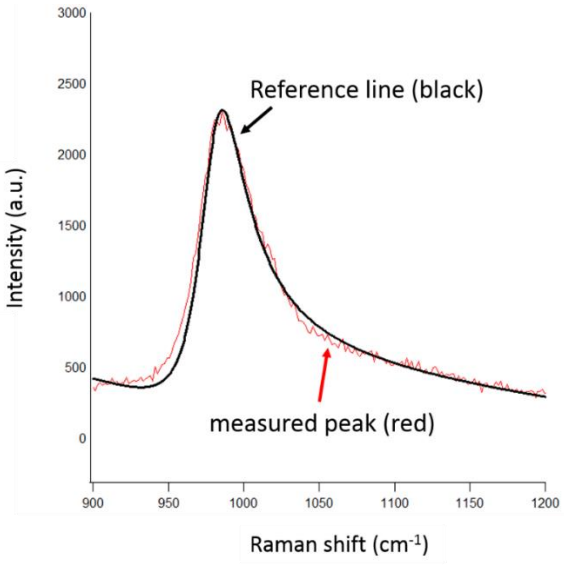


Figure 6.3. Profile of LOPC mode observed on Hulk027 sample grown in pure Si solvent. The black line is a reference line according to the parameters in Ref. [4, 8]. The red line is a data of Hulk027. The calculated carrier density was about $4.5\times10^{18}$ $cm^{-3}$.

### 6.3.2 SIMS analysis

Since Raman spectrum gives the free carrier concentration in the crystal, SIMS determines the total dopant concentration in the lattice which is the total amount of the incorporated atoms in the crystal. Therefore, Raman and SIMS are often studied because of their complementarity.

The N and Al concentrations have been analyzed. The results of all samples are shown in Figure 6.4. SIMS analysis have been performed in the two different locations on each sample, to evaluate both $^{14}N$ and $^{27}Al$ concentrations.

In case of pure Si (Figure 6.4(a)), N concentration is very high, about $4.5\times10^{19}$ $cm^{-3}$ while Al concentration was close to the detection limit (~$5\times10^{15}$ $cm^{-3}$). In this case, the depth profile corresponding to both N and Al shows concentration values at a rather stable level after 1.5 µm.

In case of 1 at% of Al (Figure 6.4(b)), the concentration of both N and Al were quite similar to 5 at% and 10 at% cases (Figure 6.4(d)). Due to the rough grown surface in 10 at% of Al case, Al concentration at point B (blue color, triangle dots) was unexpectedly higher than point A. This can be attributed to Al aggregates formed at the surface of the crystal. The concentrations of N and Al for all cases are summarized in Table 6.3. It is interesting to note that the concentration of both N and Al are higher than ~$10^{19}$ $cm^{-3}$ in all samples. In addition, N concentration increases with increasing the Al concentration. In other words, increasing the amount of Al in the solvent leads to the increase of both N and Al incorporation.

Comparing the results between Raman and SIMS, crystal quality is affected by N and Al incorporations. For example, when the concentrations of both Al and N atoms are increased up to ~$10^{19}$ $cm^{-3}$, the FWHM of $E_2$-FTO peaks are also increased from 8 to 13 $cm^{-1}$. This phenomenon is possibly related to the generation of stacking faults under the high doping concentration [12]. However, there is almost one order of magnitude difference between carrier concentration measured by Raman and dopant concentration by SIMS on Hulk027 sample. In this high concentration range, the activation yield of dopants is normally lower. That is the reason why the free carrier concentration is different from the atomic concentration, measured by Raman and SIMS respectively.

Table 6.3. Doping concentration of nitrogen and aluminum measured by SIMS

| No. | carrier concentration ($cm^{-3}$) | [$^{12}$N] ($cm^{-3}$) | [$^{27}$Al] ($cm^{-3}$) |
|---|---|---|---|
| Hulk027 | $4.5\times10^{18}$ $cm^{-3}$ | ~$4\times10^{19}$ | ~$3\times10^{15}$ |
| Hulk051 | - | ~$2\times10^{19}$ | ~$1.6\times10^{19}$ |
| Hulk068 | - | ~$1.5\times10^{20}$ | ~$4.5\times10^{20}$ |
| Hulk053 | - | ~$2.8\times10^{20}$ | ~$5\times10^{20}$ |

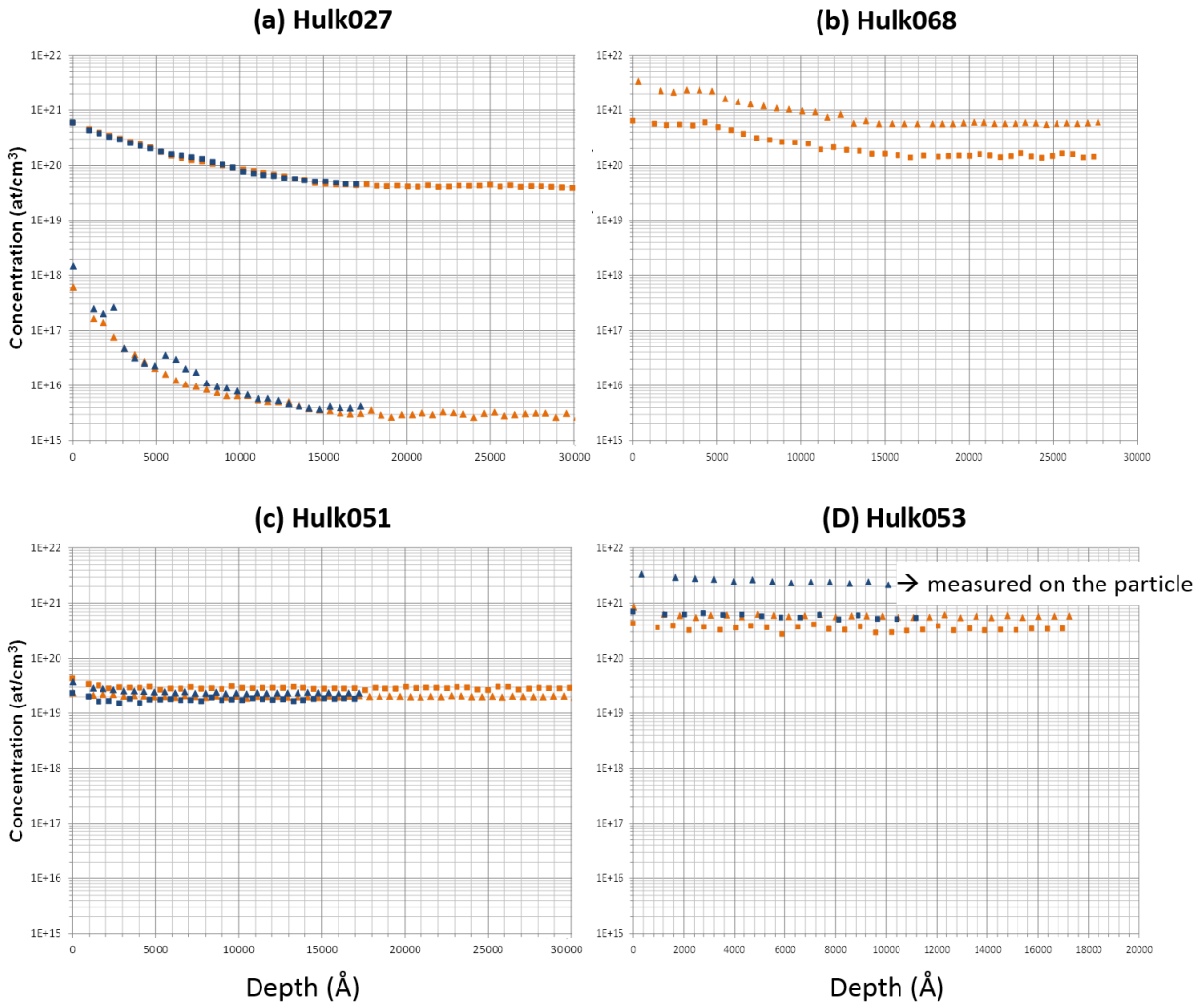


Figure 6.4. SIMS profiles of nitrogen and aluminum collected on the samples in Table 1. The orange and blue colors correspond to measured two different locations on the each sample and square and triangles correspond to the $^{12}N$ and $^{27}Al$, respectively. In case of $^{27}Al$ concentration on Hulk053 are measured on the particle, which may be the Al alloy.

## 6.4 Conclusions of chapter 6

The free carrier concentration and total dopant concentration in selected 4H-SiC crystals grown by the TSSG process were estimated by Raman spectroscopy and SIMS, respectively. We have shown that:

i) The nitrogen background level is extremely high in our TSSG set-up, about $4\times10^{19}$ at/cm$^{-3}$ at 1700°C in pure Si. As crystals were grown on the C-face, which is known to incorporate more nitrogen, we could easily reduce this level by using the Si-face. Nevertheless, this level is very high and constitutes a good basis for low resistivity n+ substrates, without doing any effort.

ii) Using Al in the solvent easily incorporate Al in the crystals. With only 1 at% of Al in the solvent, the Al content in the crystal directly increases of roughly 4 orders of magnitude. Then, it asymptotically increases with increasing the Al content of the solvent.

iii) The maximum Al concentration reached $5\times10^{20}$ at/cm$^{-3}$ with 10 at% of Al in the liquid. This very high value is also very promising for low resistivity p+ substrates.

iv) The nitrogen concentration in the crystal increases correlatively with the increasing Al content.

Though very promising, further work is necessary for understanding and controlling the dopant incorporation during TSSG. In particular, it will be necessary to reduce the nitrogen background in order to get more flexibility in the n-type and p-type doping ranges.

## 6.5 References


[1] N. Ohtani et al., J. Cryst. Growth, **311**, pp.1475-1481, 2009.

[2] P. Kwasnicki PhD thesis, Université de Montpellier, 2014.

[3] S. Contreras et al., Mater. Sci. Forum, **858**, pp. 249-252, 2016.

[4] S. Nakashima and H. Harima, phys. stat. sol.(a), **162**, pp. 39-64, 1997.

[5] R. Nemanich, Mater. Res. Soc. Symp. Proc. **69**, pp. 23-37, 1986.

[6] G. Burns et al., Solid State Commun. **62**, pp. 449-454, 1987.

[7] J. G. Kim PhD thesis, Kyoto Institute of Technology, 2012.

[8] H. Harima et al, J. Appl. Phys. **78**, pp. 1996-2005, 1995.

[9] D. W. Feldman et al., Phys. Rev. **173**, 1968.

[10] H. Harima et al., Mater. Sci. Forum **338-342**, pp. 607-610, 2000.

[11] T. Mitani et al., Mater. Sci. Fourm **778-780**, p. 475-478, 2014.

[12] Y. Yang et al., Mater. Sci. Forum **858**, pp. 105-108, 2016.

[13] N. Dilawar et al., J. Phys. Chem. Solids **61**, pp. 1927-1933, 2000.

[14] K. Kojima et al., J, Crys. Growth **269**, pp.367–376, 2004.

# Chapter 7. General Conclusion

Silicon Carbide is a wide band gap semiconductor which has recently imposed as a key material for modern power electronics. Despite its industrial maturity, there are still some issues on SiC material that are worth investigating. This is the case for instance for highly conductive 4H-SiC substrates, and more specifically of p-type. The standard seeded sublimation process is not really adapted for such material, especially for keeping a constant aluminum (Al; p-type dopant) concentration all along the crystal length. The high temperature solution growth is currently being revisited due to its potential for achieving outstanding structural quality. It should be also more adapted for p+ doped substrate growth. This work aimed at developing further the TSSG process, with a special focus on heavily p-type doped 4H-SiC crystals by using Al based solvent. Different elementary steps of the growth process have been studied and optimized to control the growth front stability with suitable growth rate and a good crystal quality. For each steps, the effect of Al has been investigated.

In a first part, we investigated and developed the three elementary steps of the process, which are i) dissolution of carbon, ii) transport of carbon from the source to the seed and iii) crystallization of SiC on the seed. We mainly explored different strategies to improve the process. For example, in order to increase the growth rate, we tried to use transition metal additives to the solvent (Cr, Fe) to increase the carbon solubility. The carbon transport has been improved by studying forced convection in the liquid, imposed by the rotation of the crystal. Parasitic crystallization of polycrystal around the seed has been controlled by a proper implementation of the meniscus technique. Combining all those improvements, we have successfully grown a 4H-

SiC crystal, at a growth rate of over 300 µm/h and enlarged the diameter by about 40% compared to the original seed size.

In a second stage of the work, we studied more specifically the growth interface behavior without and with Al addition to the solvent. We have shown the following important points:

- To reach equilibrium (no growth condition), a Si-face 4H-SiC surface in contact with a liquid (Si or Al-Si) evolves with three consecutive stages: i) a fast creation of steps due to an initial slight dissolution of the substrate surface, ii) step-bunching leading to parallel macro-steps (which seems to be a metastable state) and iii) a slower step leading to equilibrium morphology, composed of (0001), (10-1n) and (01-1n) facets. Al strongly increases the kinetics of step movements on the surface.
- The "seeding stage", i.e. the early stage of growth when the SiC contacts the liquid surface is critical. 3C-SiC transient nucleation can occur at this even at the high temperature (1900°C), i.e. conditions for which it is very unlikely to appear. Using numerical simulation, we have shown that this is due to a strong and rapid temperature fluctuations close to the crystal surface, characterized by a strong temperature drop during the first 100 seconds and a relaxation time of about 60 minutes before reaching the thermal equilibrium of the system. By pre-heating the seed before contacting the liquid surface and/or adding Al to the solvent, we could almost totally suppress the formation of 3C-SiC. Al would thus affect the 3C-SiC nucleation probability.
- Increasing the rotation rate of the seed crystal is a good way to increase the growth rate. However, there exists a critical rotation speed above which the interaction between the step flow on the crystal surface and the fluid flow pattern can interact to create surface instabilities, which in turn can give rise to solvent inclusion. This can be qualitatively

described by considering first the step flow direction (after “hexagonalization” of the original train of parallel steps) and second the fluid flow direction which must be split into two azimuthal and radial components.

In a last part of the work, we evaluated the dopant concentration (both nitrogen as donor and aluminum as acceptor) from a few selected 4H-SiC samples. In order to evaluate dopant concentration in a good quality crystal, growth was carried out by optimized conditions (see table 6.1) for 4H-SiC single crystal on the C-face. As a consequence, the nitrogen background level is extremely high in our TSSG set-up, about 4E19 at/cm$^{-3}$ at 1700°C in pure Si. By adding 10 at% of Al in the liquid, we could reach an Al concentration of 5E20 at/cm$^{-3}$ in the crystal.

These very high values of N and Al concentrations are extremely promising for the development of heavily doped n-type and p-type 4H-SiC substrates, respectively. Without doing “specific efforts”, TSSG seems to be suitable for heavily doping. Without Al in the liquid, the Al level in the crystal is rather low, below the detection limit of SIMS. Al level can be easily tuned by the Al content in the liquid. Nitrogen is more problematic because the residual level of our TSSG puller is quite high. For the development of p+ substrates, this level should be reduced. As crystals were grown on the C-face, which is known to incorporate more nitrogen, we could easily reduce this level by using the Si-face. Some efforts would be also necessary to get a “cleaner” growth atmosphere in the TSSG puller.

From our different results, we could draw a better picture of the effect of aluminum at the growth front. It is for instance shown that Al modifies the growth kinetics, and reduces the transient 3C-SiC nucleation during the early stage of growth. But the exact nature of its interactions with the crystal at the growth interface would require further works.

# List of table

# List of figures

## *8Résumé de la thèse en français*

## A. Introduction

Dans la tendance récente des économies d'énergie et réduction des émissions de $CO_2$ pour assister à réduire le réchauffement climatique, l'un des objectives les plus importants est améliorer l'efficacité dans l'utilisation de l'énergie électrique. Avec cet objectif en vue, les dispositifs modernes de l'électronique de puissance doivent être adaptés pour une réduction drastique des pertes d'énergie. Comme les matériaux électroniques les plus populaires, le silicium (Si) s'est établi comme le matériau principal pour fabriquer les appareils électroniques de puissance depuis les années 1950. Cependant, les dispositifs électroniques à base de Si ne sont pas satisfaisants dans les environnements difficiles à cause de la limitation de leurs propriétés physiques. Pour cette raison, les matériaux semi-conducteurs à large bande électronique (WBG), tels que le carbure de silicium (SiC), le nitrure de gallium (GaN), Diamant, sont reconnus comme étant les matériaux les plus prometteurs. Parmi eux, les dispositifs à base de SiC promettent de meilleures performances pour les applications de l'électronique de puissance.

### A.1 Objet et principale contribution de la thèse.

Le présent travail se concentre sur la croissance des cristaux de SiC par la méthode TSSG. Deux aspects principaux seront discutés: premièrement, le développement du procédé TSSG pour le cristal SiC de haute qualité, et deuxièmement, l'étude de l'effet de l'aluminium (Al) sur le procédé et son incorporation dans les cristaux. Dans ce travail, la croissance du polytype 4H-SiC est considéré. Dans les chapitres suivants, les différents éléments du processus de Top Seeded Solution Growth (TSSG) seront discutés afin d'optimiser les conditions pour contrôler la stabilité du front de croissance avec une vitesse de croissance raisonnable et une bonne qualité de cristalline. En outre, la stabilité morphologique à la surface du cristal sera étudiée systématiquement dans l'état d'équilibre sans croissance et également pendant la phase initiale du processus. À la fin de cette thèse, nous évaluerons les concentrations d'azote et d'Al dans les cristaux développés et montrerons que le TSSG serait une méthode appropriée pour le fort dopage d'Al.

## 1. Cristallographie de SiC

### 1.1. Polytypisme de SiC

SiC est un composé semi-conducteur composé de Si et C. L'unité de maille dans les couches de SiC se compose d'un atome de C (Si) entouré par trois atomes de Si (C) dans la bicouche et ayant une liaison simple liée à un atome de Si en dessus. Ils ont formé une structure tétraédrique comme représenté sur la Figure 1 (a). Ces tétraèdres sont disposés de telle sorte que tous les atomes peuvent être décrits comme formant un plan compact hexagonal (qui est le plan basal dite {0001}). La Figure 1 (b) montre la structure simplifiée de la couche de SiC dans le plan (0001). En utilisant un modèle de balle simple, la première bicouche est représentée par A. La bicouche suivante a alors la possibilité de positionner en "B" ou "C". Ce faisant, la séquence d'empilement des trois types de bicouches (A, B ou C) détermine les polytypes.

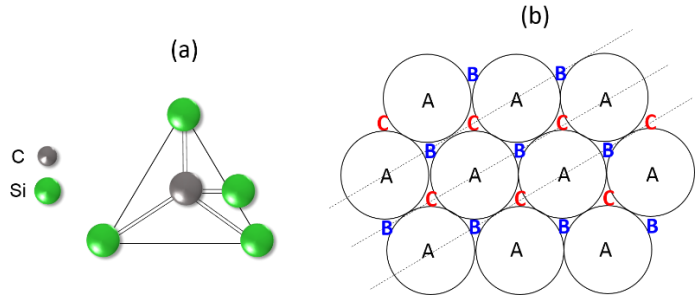


Figure 1. Illustration of (a) the SiC unit tetrahedra and (b) projection of the three different positions of the bilayers (hexagonal compact planes).

Les cristaux de SiC existent en quelques dizaines de structures cristallines polymorphes rapportées [1], appelées polytypes. Ces différents polytypes sont habituellement caractérisés par les séquences d'empilement de bicouches SiC. Les polytypes sont exprimés par le nombre (2, 3, 4 ...) de bicouches SiC dans la cellule unitaire, s'ajoute une lettre faisant référence au type de réseau (C: cubique, H: hexagonal et R: rhomboédrique). Une projection des séquences d'empilement des polytypes principaux est représentée sur la Figure 2. Si toutes les couches bi-atomiques sont de même orientation, la structure cubique appelée 3C-SiC (β-SiC) est obtenue. En revanche, si les couches bi-atomiques sont alternées le long de l'axe c, on obtiendra des structures hexagonales ou rhomboédriques, appelées 2H, 4H ou 6H-SiC, (α-SiC). Chaque polytype de SiC a son propre propriétés électriques. Parmi eux, uniquement 4H-SiC est actuellement utilisée commercialement.

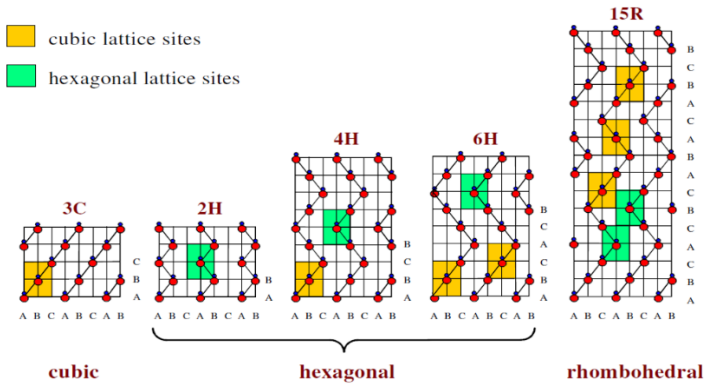


Figure 9. The stacking sequences for different SiC polytypes in the [11-20] plane. The cubic lattice site (yellow color box) has the stacking sequence of ABCABC while the stacking sequence of hexagonal lattice sites (green color box) is ABA.

**1. 2. Croissance du monocristal SiC de la phase liquide**

Récemment, la technique de croissance du SiC de la phase vapeur a été significativement avancée. Cependant, un monocristal SiC de haute qualité avec un grand diamètre, comparable à la technologie de Si, demeure un défi. La raison principale est le nombre de défauts cristallographiques restant dans le cristal SiC, tels que les dislocations et les défauts d'empilage. Cependant, il est bien connu que la croissance des cristaux de SiC de la phase liquide conduit à une densité de dislocation plus faible que les autres méthodes de croissance [2].

Selon le diagramme de phase présenté à la Figure 3, il n'existe pas de phase stoechiométrique SiC liquide [3]. Ainsi, la croissance de la solution de SiC doit utiliser des solutions non stœchiométriques contenant à la fois Si et C [4]. La solubilité de C dans le Si liquide est plutôt faible, environ 0,03% à 1400 ° C et 15% à 2600 ° C. Cependant, la solubilité C peut être augmentée par l'addition d'éléments de transition (Sc, Fe, Cr, Ti, etc.) au Si liquide.

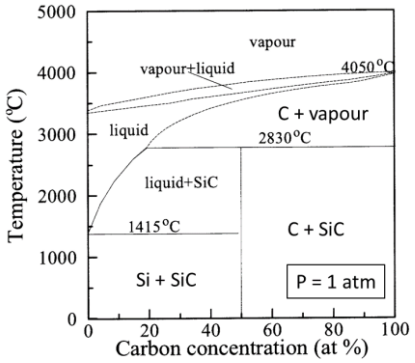


Figure 3. Phase diagram of Si-C system.

Plusieurs techniques de croissance des cristaux de SiC et de croissance épitaxie à partir de la phase liquide ont été démontrées, telles que la méthode de déplacement des solvants [4-7]. Parmi ceux-ci, la méthode de croissance de solution TSSG, basée sur le concept du procédé de Czochralski, est probablement la méthode la plus réussi pour la croissance monocristalline de SiC de la phase liquide jusqu'à présent.

## 2. L'installation de l'exacteur TSSG et le développement de processus

Un extracteur Czochralski (Cz) modifié, nommé "HULK", a été configuré pour le procédé TSSG. Cet extracteur se compose de trois parties principales: (1) l'unité de supervision et de commande, (2) l'unité de chauffage et (3) le réacteur (Figure 4).

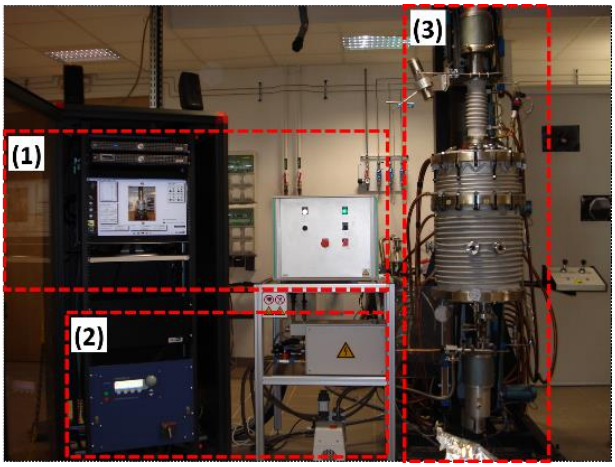


Figure 4. Picture of the TSSG puller implemented at LMGP for the growth of SiC, with the three functional units. (1) The supervision and control/command unit. (2) The heating unit. (3) The reactor.

La Figure 5 montre les détails de la géométrie du réacteur. Dans le procédé TSSG, le cristal germe est monté sur une tige de graphite insérée dans la source de Si fondue. En règle générale et dans tout ce travail, un gradient de température est appliqué entre la surface du liquide (qui est en contact avec le cristal germe pendant le processus) et le fond du creuset. La température est plus élevée au fond du petit creuset (zone de dissolution) et plus basse à la surface du liquide, où le germe est en contact avec le solvant (zone de cristallisation).

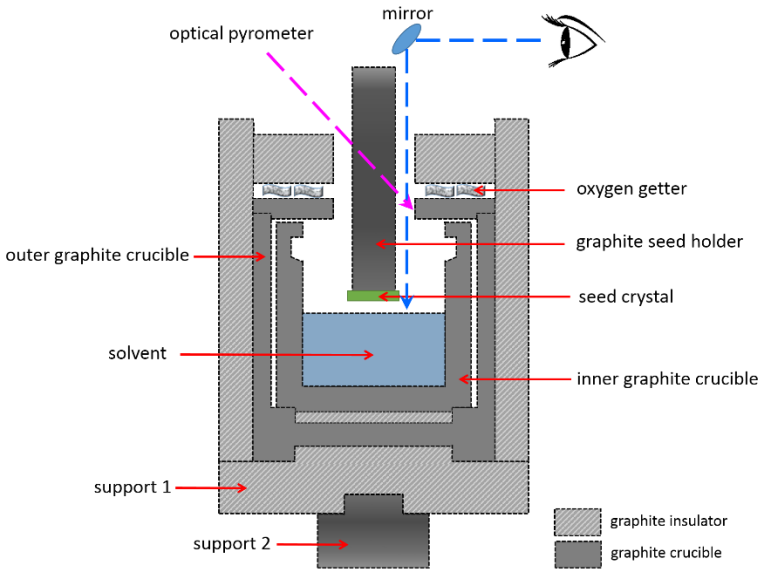


Figure 5. Drawing of the TSSG furnace geometry.

Dans le procédé TSSG, il y a trois étapes élémentaires de processus (i) la dissolution du carbone, (ii) le transport du carbone de la source au germe et (iii) la cristallisation du SiC sur le germe. Ces étapes sont strictement liées à des paramètres techniques, tels que les compositions de solvants, la rotation du germe / creuset et du ménisque, etc., afin d'améliorer le processus de croissance. Après l'optimisation des paramètres de croissance, la vitesse de croissance typique avec une qualité homogène du cristal obtenue a été choisie de ~120µm/h. En combinant toutes ces améliorations, nous avons réussi à faire croître un cristal 4H-SiC, à une vitesse de croissance de plus de 300µm/h et agrandi le diamètre d'environ 41% par rapport à la taille origine du germe.

## 3. Le comportement de l'interface de croissance dans des conditions d'équilibre

### 3.1. Introduction

Un des principaux objectifs de cette thèse est de obtenir un dopage élevé en Al (de type p +) de cristaux 4H-SiC. Ainsi, il est important d'étudier l'effet de l'addition d'Al au liquide sur le front de croissance. Récemment, quelques pourcents Al ajoutés au solvant (généralement un alliage à base de Si) ont été rapportés pour stabiliser le front de croissance, en réduisant le développement des macro-marches sur la face C (0001) [8]. Bien que démontré, son rôle exact n'est toujours pas clair en raison de la complexité des phénomènes qui se produisent dans le processus de croissance. [9]. Toutes les études précédentes ont tenté de lier la morphologie de la surface avec les paramètres du processus [10], i.e. dans des conditions de croissance, mais aucun d'entre eux n'a pu apporter des données fondamentales sur les propriétés intrinsèques de l'interface liquide-SiC sans croissance. Cette partie a pour but de décrire davantage la nature de l'effet de l'Al sur l'interface de croissance.

### 3.2. Détails expérimentaux

Une méthode de chute sessile a été réalisée dans des conditions parfaitement isothermes pour étudier la reconstruction de la surface d'une face Si, 4° off-axis (0001)Si 4H-SiC en contact avec du silicium pur ou des alliages Al-Si à haute température. La séquence des opérations est la suivante: (1) mettre un morceau de Si (Al) sur la face (0001)Si des substrats 4H-SiC et les placer dans un creuset en graphite.Avant l'expérience, les substrats SiC et des pièces en alliage sont d'abord désoxydé dans une solution de HF. (2) Le creuset est tout d'abord chauffé à 1100°C sous vide pour dégazer les différentes pièces de graphite. À 1100°C, la chambre est remplie de 0,9 bar d'argon de haute pureté. Les échantillons sont ensuite chauffés à 16 °C/min et gardés pour differentes periodes de temps, températures et compositions d'alliages Al-Si. (3) A la fin du plateau de température, le liquide est absorbé (avec du feutre de graphite ou un morceau de Ta ou Nb, qui est parfaitement mouillé par du silicium liquide). L'absorption du liquide est très rapide, inférieur à 1 seconde. Cela garantit qu'aucune modification de la morphologie de surface ne peut se produire en raison de la cristallisation parasite lors du refroidissement de la goutte saturée. (4) Le creuset est alors naturellement refroidi et ouvert.

Après l'expérience, les statistiques des largeurs de marche sont évaluées à partir d'un échantillon de 300 à 400 marches collectées à partir de plusieurs images par Nomarski contraste d'interférence différentiel (NDIC) représentatives des différents échantillons. Afin d'obtenir la description quantitative des surfaces, nous avons effectué quelques statistiques des images NDIC.

### 3.3. Résultats et discussion

A partir des expériences, les résultats sont classés en fonction de l'effet du temps, de la température et de la nature du solvant. Dans le silicium pur et à 1600 °C, la surface évolue avec trois étapes consécutives (voir Figure 6): (i) une création rapide des marches en raison d'une légère dissolution initiale de la surface du substrat, (ii) step-bunching menant à desmacro-marches parallèles (ce qui semble être un état métastable) et (iii) une étape plus lente qui conduit à l'équilibre de morphologie, composé de facettes (0001), (10-1n) et (01-1n).

En augmentant la durée mais les mêmes conditions En augmentant le temps dans les mêmes conditions, nous avons observé que les étapes de reconstruction de surface n'étaient pas modifiées et que les macro-marches se rassemblent deux par deux. L'augmentation de la température à 1800 °C ou l'addition de quelques pourcents d'Al améliorent de manière drastique la deuxième étape (stade métastable), mais apparemment réduit la troisième (étape d'équilibre). À partir de l'observation de la première étape, il est clair que l’Al augmente la cinétique de mouvements des marches sur la surface.

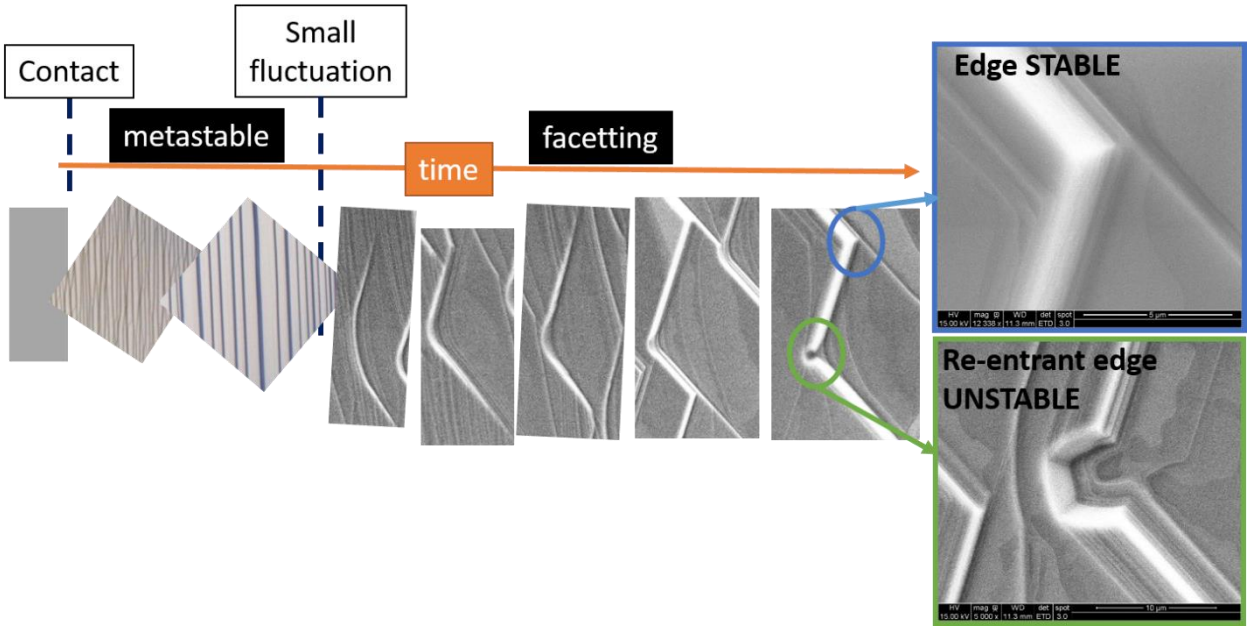


Figure 6. Description of the surface evolution scenario when the 4H-SiC surface is put in contact with liquid silicon at 1600°C.

D'autres investigations sont nécessaires pour identifier le mécanisme exact des tendances observées. Les mesures d'angle de mouillage seraient très bénéfiques pour étudier l'effet de la température et des additifs sur l'énergie interfaciale du liquide-SiC.

## 4. Phénomènes transitoires au cours de 'seeding stage' du processus TSSG

### 4.1. Introduction

Le "seeding stage" du processus, qui regroupe habituellement la préparation in-situ de surface et des premiers stades de la croissance, est d'une importance primordiale puisqu'il affecte toute la croissance ultérieure. Cependant, considérée comme une problème technologique, le seeding stage du processus TSSG n'est pas étudiée en profondeur malgré son importance critique. Dans ce travail, nous abordons le seeding stage de la croissance de la solution de 4H-SiC avec ou sans ajout d'Al au solvant. En particulier, nous avons systématiquement observé les morphologies de surface obtenues sur différentes terminaisons du substrat de germination. Nous avons également imposé une contrainte supplémentaire à ce travail: nous voulons éviter la gravure in-situ (dissolution) du

germe cristallin au début, afin d'être en mesure de commencer la croissance, même à partir d'une couche épitaxiale très mince.

### 4.2. Les détails expérimentaux

Un procédé SiC TSSG standard a été mis en œuvre, en utilisant un creuset en graphite chauffé par induction, isolé avec des feutres de graphite. Le principe général et une description complète de la conception du creuset a déjà été expliqué dans le chapitre 2 dans cette thèse. Dans chaque expérience, à la fois les faces Si(0001) et C(000-1) et avec les deux directions sur l'axe et 4° off-axis vers la direction <11-20> des substrats 4H-SiC ont été utilisés comme germes cristallins. Ces quatre cristaux ont été montés sur le même support de germe en graphite en utilisant de la colle graphite et maintenus en contact avec le solvant pendant 10 minutes. La température du procédé a été varié de 1700°C à 1900°C. Avant le contact, le solvant a été maintenu à la température du procédé pendant 30 minutes pour obtenir une saturation en carbone. Cela a été mis en œuvre pour réduire, ou idéalement éviter la fonte du germe pendant les premières étapes après contact avec la surface liquide. Dans l'expérience supplémentaire, nous préchauffons les germes cristallins dans le but de réduire l'effet des fluctuations thermiques qui se produisent au début de l'étape de trempage.

A la fin des expériences, le solvant résiduel solidifié sur les cristaux a été éliminé par attaque acide dans solution HF + $HNO_3$ (1: 1). Les morphologies de surface de croissance ont été systématiquement observées par NDIC microscopie optique, microscopie électronique à balayage (MEB) et microscopie à force atomique (AFM). Les polytypes dans les couches ont été systématiquement identifiés par Raman spectroscopie. Ensuite, l'analyse de diffraction d'électrons rétrodiffusés (EBSD) a été appliquée pour cartographier quantitativement la distribution des polytypes sur les surfaces.

### 4.3 Résultats et discussion

Figure 7 montres les images NDIC des morphologies sur les surfaces nominales dans le solvant Si pur. Sur les faces Si/C et à toutes les températures, la morphologie de surface est caractérisée

par une structure de domaine, ce qui est assez différent par rapport à la surface de croissance habituelle dans le solvant Si pur après des expériences de longue durée. De plus, les cartes EBSD correspondantes (voir Figure 8) montrent que 3C-SiC peut se former par nucléation 2D, même à haute température (1900 °C), i.e. cela ne favorise pas la formation de 3C-SiC.

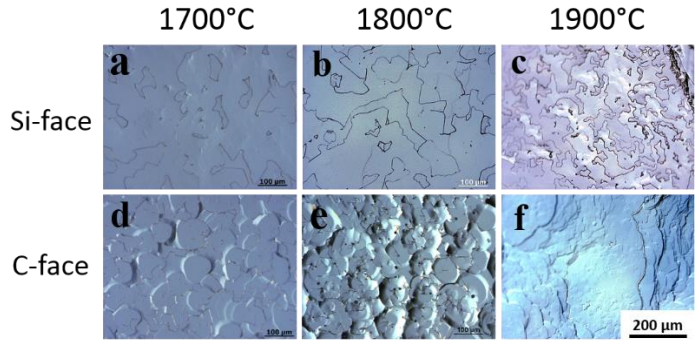


Figure 7. As grown surface morphologies observed by NDIC optical microscopy, for the on-axis samples (Si- and C-faces; pure Si solvent, three different temperatures, 1700, 1800, 1900°C; growth time of 10 min).

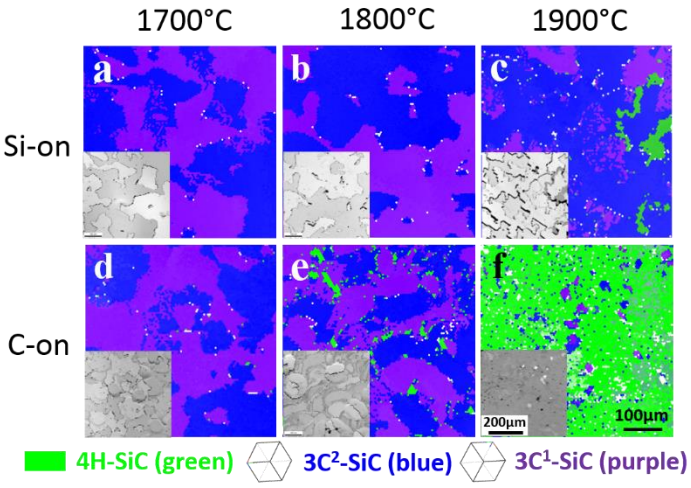


Figure 8. The corresponding EBSD maps of Figure 7. Blue and purple areas correspond to two different orientations of 3C-SiC. Green areas correspond to 4H-SiC polytype. Inserts are the SEM images at the same location as EBSD maps (mapping scale: squares of 500 x 500 µm$^2$)

Cependant, il n'y a pas de limite de macle qui puisse être observée dans un solvant à base de Si avec une teneur en Al de 10at%, comme le montre Figure 9. Ces morphologies partagent une caractéristique commune avec Figure 7f: la surface est composée des marches de hauteurs différentes avec des grandes terrasses. Toutes les marches se propagent dans une seule direction et la densité des marches est très élevée, comme on peut le voir sur les Figures 9a, d et e. Ces morphologies sont donc issues d'une énorme source unique de marches. Sur les Figures 9b, c et f,

plusieurs directions de propagation de marche peuvent être mises en évidence. Ces morphologies proviennent de la contribution de différentes sources de marches, spatialement séparées. Ces sources de marches ont été identifiées comme des spirales pour la plupart des cas. Les cartes EBSD correspondantes sont montrées dans Figure 10. Pour faciliter la visualisation, nous indiquons l'emplacement des centres de croissance en spirale sur les encadrés inserts SEM de Figure 10, lorsqu'ils sont clairement identifiables. La corrélation est simple; il n'y a pas de polytype 3C-SiC où l'on peut mettre en évidence des centres de croissance en spirale. A partir de la spectroscopie Raman, on a observé principalement polytype 4H-SiC, mais on a également identifié occasionnellement polytype 6H-SiC dans la couche. Dans le cas de substrats vicinaux, seul le polytype 4H-SiC a été observé avec la morphologie de marche.

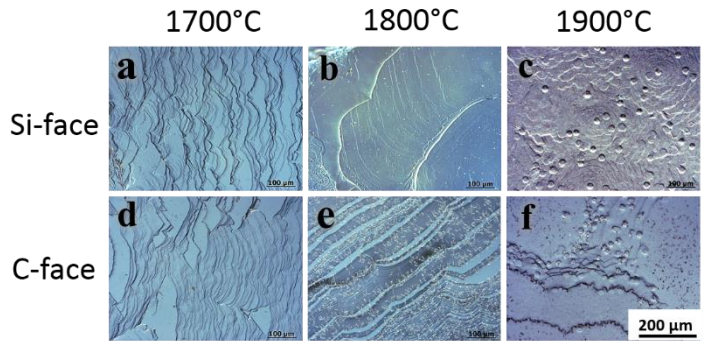


Figure 9. As grown surface morphologies observed by NDIC optical microscopy for the on-axis samples (Si- and C-faces; Si-10%Al solvent, three different temperatures, 1700, 1800, 1900°C; growth time of 10 min).

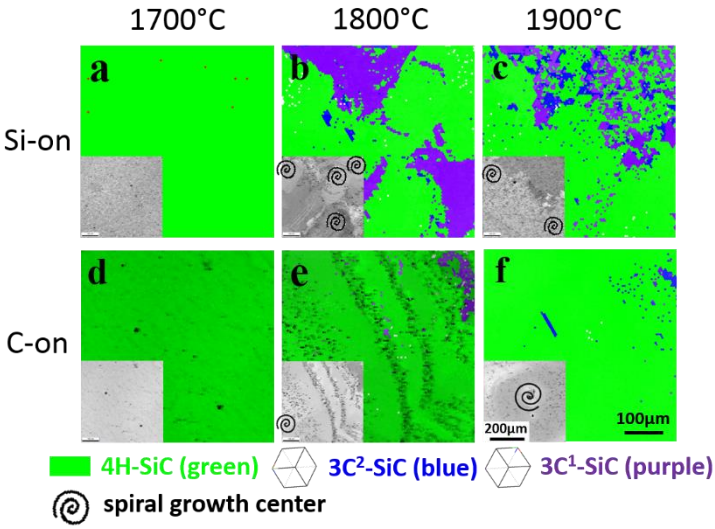


Figure 10. The corresponding EBSD maps of Figure 9. Blue and purple areas correspond to two different orientations of 3C-SiC. Green areas correspond to 4H-SiC polytype. Inserts are the SEM images at the same location as EBSD maps (mapping scale: squares of 500 x 500 $\mu m^2$)

Afin de comprendre le mécanisme de nucléation 3C, nous avons démontré la fluctuation de la température dans le solvant par simulation numérique. Les résultats de la simulation montrent qu'une approche rapide du germe vers la surface du solvant induit des fluctuations de température fortes et rapides dans le solvant. Cette fluctuation a été caractérisée par une forte chute de température pendant les 100 premières secondes et un temps de relaxation d'environ 60 minutes avant d'atteindre l'équilibre thermique du système. Au cours de cette première étape, le liquide à la surface du germe connaît une sursaturation très élevée pendant l'étape de germination t = 1~100 sec, à l'origine de nucléation transitoire de 3C-SiC. Une telle fluctuation thermique entraînera une évolution drastique de la répartition de la sursaturation C dans le solvant.

Cependant, l'occurrence de 3C-SiC est également considérablement réduite en utilisant un solvant Al-Si. En ajoutant 10%at d'Al au solvant de Si, la solubilité du carbone ne devrait pas être considérablement modifiée par rapport au solvant Si pur. Pour une distribution de température donnée, une telle composition de solvant ne devrait donc pas affecter la distribution de sursaturation tout en changeant les compositions de solvant de Si pur à Al-Si. Deux hypothèses peuvent être proposées pour expliquer ce phénomène: (1) la présence d'Al aide à réduire la fréquence de nucléation 2D de 3C-SiC. Les résultats expérimentaux sur le substrat sur l'axe sont plutôt évidents, bien que son rôle exact reste incertain. En effet, le phénomène similaire a déjà été démontré par Soueidan et al., en utilisant la méthode VLS [11]. (2) La densité élevée des marches associées à 4° off-axis réduit naturellement (et même suprime) la probabilité de nucléation 2D, à l'origine de la formation de 3C-SiC. En supposant que l'énergie de nucléation 2D de 3C-SiC peut être atteint, cette seconde hypothèse considère que Al agit sur la structure de marche et de terrasse.

En utilisant la simulation numérique, il a été démontré que l'ancienne procédure expérimentale de l'approche du germe cristallin jusqu'à la mise en contact à la surface du solvant est une source de fluctuation de température forte et rapide au cours de l'étape de germination, qui à son tour induit la nucléation transitoire parasite 3C-SiC sur les substrats 4H-SiC. Pour réduire cette chute de température pendant l'étape de germination, nous avons mis en oeuvre l'étape de préchauffage du germe cristallin en le gardant 1 mm au-dessus de la surface du solvant pendant 30 minutes. En préchauffant le germe avant la mise en contact avec la surface liquide, nous pourrions presque totalement supprimer on pourrait presque totalement supprimer la formation de 3C-SiC confirmée

par des cartes EBSD (voir Figure 11). La compréhension de l'interaction réelle entre Al et la surface du cristal nécessiterait d'autres investigations.

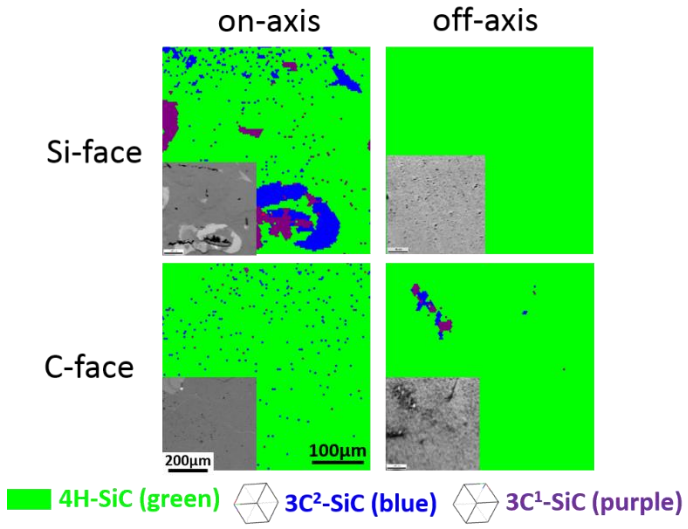


Figure 11. EBSD maps for the on- and off-axis of pre-heating seeds (Si- and C-faces; 10at%Al-Si solvent, 1800°C, growth time of 10 min). Inserts are the SEM images at the same location as EBSD maps. The mapping scale is squares of 500 x 500 $\mu m^2$, and the step size is 5µm

## 5. Etude de la formation de macro-marche pendant le processus de TSSG

### 5.1. Introduction

Récemment, Zhu et al. ont suggéré que des grandes macro-marches pourraient être observées si l'écoulement du fluide et l'écoulement de la marche avaient la même direction (condition d'écoulement parallèle) alors qu'ils peuvent être supprimés dans des conditions d'écoulement antiparallèle [12]. Ils ont observé cette tendance localement et la question qui se pose est la suivante: quelle serait l'interaction entre une surface vicinale et l'écoulement du fluide pendant la rotation du cristal? Ceci est d'une importance primordiale pour le développement ultérieur du processus, en particulier pour une mise à niveau plus poussée. Dans cette partie, et sur la base du mécanisme proposé par Zhu, la stabilité de surface est étudiée en fonction de la vitesse de rotation du cristal par une observation systématique de la formation des macro-marches.

### 5.2. Les détails expérimentaux

Pour les expériences, nous avons appliqué une rotation dans le sens inverse des aiguilles d'une montre au germe (comme observé à l'interface germe-solvant d'en bas). Ces morphologies de croissance ont été comparées aux expériences menées sans rotation. Tous les paramètres expérimentaux sont résumés dans le Tableau 1. A la fin des expériences, le solvant résiduel solidifié sur les cristaux a été éliminé par attaque acide dans la solution de HF + $HNO_3$ (1: 1). Le polytype des cristaux a été identifié par spectroscopie Raman avec un faisceau laser incident fonctionnant à une longueur d'onde de 532 nm. Les morphologies de surface ont été systématiquement observées en utilisant le NDIC.

Table 2. The experimental details of 4H-SiC solution growth

| No. | Seed crystal | Solvent | T (°C) | $\Omega_{seed}$ (rpm) | $h_{meniscus}$ (mm) |
|---|---|---|---|---|---|
| Hulk032 | 4H-SiC, 4°-off, Si-face | Si 100% | 1700 | 0 | 1.2 ~ 1.5 |
| Hulk029 | | | | 100 | |
| Hulk034 | 4H-SiC, 4°-off, C-face | | | 0 | |
| Hulk033 | | | | 100 | |
| Hulk035 | | | | 200 | |

### 5.3. Résultats et discussion

#### 5.3.1. La morphologie de surface sans rotation du germe cristallin

Dans les cas de Hulk032 et Hulk034, les micro-marches sont orientées systématiquement vers la direction [11-20] selon le sens de coupe du SiC. Ces micro-marches commencent à se grouper et à s'organiser. Dans tous les cas, aucune inclusion de solvant ou aucun défaut de structure visible n'est mis en évidence. De plus, la morphologie est homogène sur toute la surface de la graine.

#### 5.3.2. La morphologie de surface avec la rotation du cristal germe

Sur la face Si avec une rotation de germe de 100 rpm (Hulk029), la morphologie de surface peut être séparée en trois catégories:

(i) un train de micro-marches en zigzag régulier, semblable à un cas de non-rotation (voir Figure 12 (a)),

(ii) un ensemble de lignes ondulées noires (macro-marches) présentes sur les micro-marches le long des deux directions équivalentes <1-100> adjacentes à la direction <11-20> (voir Figure 12 (b, d)), et

(iii) grandes lignes noires en forme de zigzag se formant au-dessus des micro-marches correspondent aux deux directions [10-10] et [01-10] (voir Figure 12 (c)).

La Figure 13 montre qu'il n'y a aucune preuve de la formation de macro-marches sur la face C avec la vitesse de rotation de 100 rpm. Cependant, avec une vitesse de rotation de 200 rpm, les macro-marches sont formées comme représenté sur la Figure 14. La directionnalité des macro-marches dépend de la position du cristal mais pas aussi évidente que sur la face en Si.

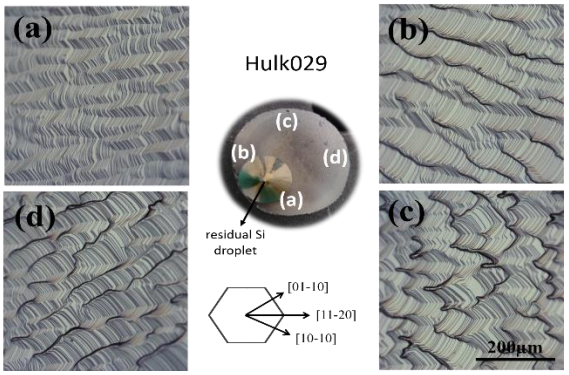


Figure 12. NDIC optical microscopy of the grown surface morphologies on the Si-face with a seed rotation of 100 rpm.

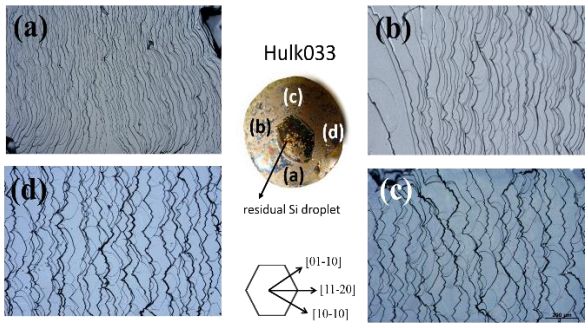


Figure 13. NDIC optical microscopy of the grown surface morphologies on the C-face with the seed crystal rotation of 100 rpm.

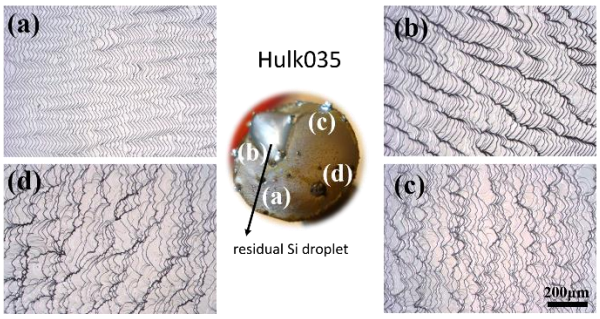


Figure 14. NDIC optical microscopy of the grown surface morphologies on the C-face with a seed crystal rotation of 200 rpm.

Le taux de rotation du cristal germe existe une vitesse de rotation critique au-dessus de laquelle l'interaction entre l'écoulement de marches sur la surface cristal et la configuration d'écoulement de fluide peut interagir pour créer des instabilités de surface, qui peuvent à leur tour donner lieu à l'inclusion de solvant. Ceci peut être décrit qualitativement en considérant tout d'abord le sens d'écoulement de marche (après "hexagonisation" du train original de marche parallèles) et, deuxièmement, le sens d'écoulement du fluide qui doit être divisé en deux composantes azimutales et radiales.

## 6. Concentration dopage dans le n- et p-type 4H-SiC

### 6.1. Introduction

Jusqu'à présent, nous avons discuté la croissance de monocristaux de SiC en utilisant la méthode TSSG avec un mettant l'accent sur différents aspects liés à l'interface de croissance. Pour utiliser ces cristaux dans les applications électroniques de puissance, des cristaux hautement conducteurs de type n- et/ou p- 4H-SiC sont nécessaires. Dans cette partie, la concentration du porteur et les concentrations atomiques dans le cristal seront évaluées.

### 6.2. Les détails expérimentaux

Pour l'évaluation du niveau de dopage, tous les échantillons ont été préparés avec les paramètres expérimentaux résumés dans le Tableau 2.

Table 2. The experimental details of n- and p-type 4H-SiC solution growth

| No. | Seed crystal | T (°C) | Solvent | $R_g$ (um/h) |
|---|---|---|---|---|
| Hulk027 | 4H-SiC, 4°off, C-face | 1700 | Si | ~15 |
| Hulk051 | 4H-SiC, 0°off, C-face | 1850 | 1at%Al-19at%Cr-Si | 150~180 |
| Hulk068 | | | 5at%Al-20at%Cr-Si | |
| Hulk053 | | | 10at%Al-20at%Cr-Si | |

Le polytype des cristaux a été identifié par spectroscopie Raman (Jobin Yvon/Horiba LabRam). À partir des spectres Raman, nous avons approximativement évalué la qualité du cristal à partir du pic du mode TO, et la concentration du porteur avec le pic LOPC. Les cristaux ont également été caractérisés par spectrométrie de masse à ionisation secondaire (SIMS) pour évaluer les concentrations d'atomes $^{14}N$ et $^{21}Al$ [13, 14]. La tension élevée du faisceau primaire était de 15 kV tandis que l'énergie d'impact était réduite à 10,5 kV (15 – 4.5 kV) puisque le haute tension du faisceau secondaire est de 4,5 kV. La résolution de masse a été fixée à $M/\Delta M = 1500$. Les profils de concentration mesurés par SIMS ont été étalonnés en utilisant des RSFs (Relative Sensitivity Factors) provenant d'échantillons de référence dans lesquels les profils de concentration étaient bien connus (voir Tableau 3). Dans ce travail, le signal isotopique $^{12}C_2$ a été utilisé comme matrice de référence.

Table 3. RSF values used in $O_2^+$ configuration

| | $^{14}N^+ / {}^{12}C_2$ | $^{27}Al^+ / {}^{12}C_2$ |
|---|---|---|
| RSF | $1.5\times10^{21}$ | $1\times10^{18}$ |

### 6.3. Les résultats et la discussion

Tout d'abord, nous avons identifié le polytype des cristaux avec des solvants purs de Si et d'Al-Cr-Si avec une variation de la quantité d'Al de 1 à 10%. A partir des spectres Raman, on peut observer des pics Raman 4H-SiC typiques. Il apparaît clairement que le mode E2-FTO (796 $cm^{-1}$) devient plus large tout en augmentant la quantité d'Al dans le solvant. Par exemple, lorsqu'on

augmente la quantité d'Al de 0 à 10 at%, le FWHM est également augmenté de 8 à 13 $cm^{-1}$. En général, le pic FTO se déplace avec le stress. Cependant, il n'y a pas de décalage de pics des modes FTO par rapport aux celles du cristal germe. Nous pensons donc que nos conditions de croissance sont bien optimisées pour la croissance de 4H-SiC sans génération de défauts graves. Dans les matériaux semiconducteurs de type n, le mode phonon LO est couplé au plasmon (mode dite LOPC), ce qui entraîne un changement radical de la forme des pics avec la concentration des porteurs libres. Nous pouvons ainsi évaluer les paramètres de transport électrique tels que la densité de porteurs libres et la mobilité en analysant la fréquence et la forme des pics [15]. Dans l'échantillon avec du Si pur, la densité de support libre calculée à la fréquence du mode LOPC de 985.79 $cm^{-1}$ était d'environ $4.5\times10^{18}$ $cm^{-3}$. D'autre part, le mode LOPC ne présente pas de changement significatif dans le p-type SiC en raison d'un faible couplage entre le LO-phonon et le plasmon. Un tel couplage faible s'explique par la faible mobilité du trou [13, 15-17]. En particulier, nos échantillons elaborés dans du solvant Al-Cr-Si présentent des fréquences très basses (962~963 $cm^{-1}$) qui ne sont pas disponibles pour l'ajustement du mode LO et les fano-paramètres (pics FTA) ne sont pas suffisamment clairs pour être analysés.

SIMS détermine la concentration totale en dopant dans le réseau, qui est la quantité totale des atomes incorporés dans le cristal. Les concentrations de N et d'Al ont été analysées. Les concentrations de N et d'Al pour tous les cas sont résumées dans le Tableau 4. Dans le cas du Si pure, la concentration en N est très élevée, environ $4.5\times10^{19}$ $cm^{-3}$ alors que la concentration en Al était proche de la limite de détection (~$5\times10^{15}$ $cm^{-3}$).

Dans le cas de 1 at% d'Al, la concentration de N et d'Al était assez similaire à 5 at% et 10 at% de cas. Il est intéressant de noter que la concentration de N et d'Al est supérieure à ~$10^{19}$ $cm^{-3}$ dans tous les échantillons. Cette valeur très élevée est également très prometteuse pour les substrats p + à faible résistivité. En outre, la concentration de N augmente avec l'augmentation de la concentration d'Al. Autrement dit, l'augmentation de la quantité d'Al dans le solvant conduit à l'augmentation de l'incorporation de N et d'Al.

Table 4. Doping concentration of nitrogen and aluminum measured by SIMS

| No. | carrier concentration ($cm^{-3}$) | $[^{12}N]$ ($cm^{-3}$) | $[^{27}Al]$ ($cm^{-3}$) |
|---|---|---|---|
| Hulk027 | $4.5\times10^{18}$ $cm^{-3}$ | $\sim4\times10^{19}$ | $\sim3\times10^{15}$ |
| Hulk051 | - | $\sim2\times10^{19}$ | $\sim1.6\times10^{19}$ |
| Hulk068 | - | $\sim1.5\times10^{20}$ | $\sim4.5\times10^{20}$ |
| Hulk053 | - | $\sim2.8\times10^{20}$ | $\sim5\times10^{20}$ |

## 7. Conclusions générales

Ce travail a pour but de développer davantage le procédé TSSG, en mettant particulièrement l'accent sur les cristaux fortement dopés de type 4H-SiC à l'aide de solvant à base d'Al.

Dans une première partie, nous avons étudié et développé les trois étapes élémentaires du processus. En conséquence, nous avons elaboréé avec succès un cristal 4H-SiC, à une vitesse de croissance de plus de 300μm/h et augmenté le diamètre d'environ 40% par rapport à la taille du germe d'origine. Dans une deuxième phase du travail, nous avons étudié plus spécifiquement le comportement de l'interface de croissance sans et avec addition d'Al au solvant. Nous avons montré les points importants suivants:

- Pour atteindre l'équilibre (absence de condition de croissance), une surface Si-face 4H-SiC en contact avec un liquide (Si ou Al-Si) évolue avec trois étapes consécutives: i) une création rapide des marches dues à une légère dissolution initiale de la surface substrat, ii) le regroupement de marche conduisant à des macro-marches parallèles (qui semble être un état métastable) et iii) une marche plus lente conduisant à la morphologie d'équilibre, composée de (0001), (10-1n) et (01-1n) facettes. Al augmente fortement la cinétique des mouvements de marche sur la surface.
- Le seeding stage, c'est-à-dire le stade précoce de croissance lorsque le SiC entre en contact avec la surface du liquide est critique. La nucléation transitoire 3C-SiC peut se produire à cette même température élevée (1900°C), c'est-à-dire des conditions pour lesquelles il est très peu probable qu'elle apparaisse. En utilisant la simulation numérique, nous avons montré que cela est dû à des fluctuations de température fortes et rapides proches de la surface du cristal,

caractérisées par une forte chute de température pendant les 100 secondes premières. En préchauffant le germe avant de mettre la surface du liquide en contact et/ou en ajoutant de l'Al au solvant, on pourrait presque totalement supprimer la formation de 3C-SiC. Al affecterait ainsi la probabilité de nucléation 3C-SiC.

- L'augmentation du taux de rotation du cristal germe est un bon moyen d'augmenter le taux de croissance. Cependant, il existe une vitesse de rotation critique au-dessus de laquelle l'interaction entre l'ecoulement de marche sur la surface de cristal et la configuration de l'ecoulement du fluide peut interagir pour créer des instabilités de surface, qui peuvent à leur tour donner lieu à l'inclusion du solvant. Ceci peut être décrit qualitativement en considérant tout d'abord le sens de l'ecoulement de marche (après "hexagonisation" du train original de marches parallèles) et deuxièment le sens de l'ecoulement du fluide qui doit être divisé en deux composantes azimutales et radiales.

Dans une dernière partie du travail, nous avons évalué la concentration du dopant. En conséquence, le niveau de fond d'azote est extrêmement élevé dans notre configuration TSSG, environ 4E19 at/cm$^{-3}$ à 1700°C en le solvant Si. En ajoutant 10 at% Al dans le liquide, on pourrait atteindre une concentration d'Al de 5E20 at/cm$^{-3}$ dans le cristal. Ces valeurs très élevées de concentrations de N et d'Al sont extrêmement prometteuses pour le développement de substrats fortement dopés de type n et p 4H-SiC, respectivement.

D'après nos différents résultats, nous pourrions mieux appréhender l'effet de l'Al sur le front de la croissance. Il est par exemple montré que l'Al modifie la cinétique de croissance et réduit la nucléation transitoire de 3C-SiC au cours de la phase de croissance. Mais la nature exacte de ses interactions avec le cristal à l'interface de croissance nécessiterait d'autres travaux.

## 8. Références

[1] A.P. Mirgorodsky, Physical Review B, 52(6), p. 3993, 1995.

[2] D. Elwell and H. J. Scheel, Crystal Growth from High-Temperature Solutions, Academic Press, 2011.

[3] Tairov et al., Electrotechnical Materials, Eds. Koritskii, Yu.V., V.V. Pasynkov, B.M. Tareev. 3, pp. 446, 1988.

[4] D. H. Hofmann and M. H. Müller, Mater. Sci. Eng., B, 61–62. pp. 29–39, 1999.

[5] M. Syväjärvi et al., J. Cryst. Growth, 197, pp. 147-154. 1999.

[6] M. Soueidan et al., J. Cryst. Growth, 293(2): p. 433-437. 2006.

[7] D. Rytz and H. J. Scheel, J. Cryst. Growth 59, pp. 468, 1982.

[8] T. Mitani et al., J. Cryst. Growth, 2014. 401: p. 681-685.

[9] F. Mercier et al., J. Cryst. Growth, 2010. 312(2): p. 155-163.

[10] C. Zhu et al., J. Cryst. Des., 2013. 13(8): p. 3691-3696.

[11] M. Soueidan et al., J. Cryst. Growth, 293(2): p. 433-437. 2006.

[12] C. Zhu et al., Cryst. Growth Des. 13, pp. 3691−3696, 2013.

[13] P. Kwasnicki PhD thesis, Université de Montpellier, 2014.

[14] S. Contreras et al., Mater. Sci. Forum, 858, pp. 249-252, 2016.

[15] S. Nakashima and H. Harima, phys. stat. sol.(a), 162, pp. 39-64, 1997.

[16] H. Harima et al., Mater. Sci. Forum 338-342, pp. 607-610, 2000.

[17] T. Mitani et al., Mater. Sci. Fourm 778-780, p. 475-478, 2014.

## Summary of the thesis

Silicon Carbide is a wide band gap semiconductor which has recently imposed as a key material for modern power electronics. The high temperature solution growth is currently being revisited due to its potential for achieving outstanding structural quality. This work aims at developing further the TSSG process, with a special focus on heavily p-type doped 4H-SiC crystals by using Al based solvent. Different elementary steps of the growth process are studied and optimized to control the growth front stability with suitable growth rate and a good crystal quality. For each step, the effect of Al is investigated. It is for instance shown that Al modify the growth kinetics, and reduces the transient 3C-SiC nucleation during the early stage of growth. Finally, Al incorporation as high as 5E+20 at/cm$^3$ has been achieved at 1850°C. This value is very promising for the future development of p+ 4H-SiC substrates.

## Résumé de la thesis en français

Le carbure de silicium est un semi-conducteur à grand gap qui s'est récemment imposé comme un matériau clé pour l'électronique de puissance. Le procédé de croissance en solution à haute température est actuellement revisité en raison de sa capacité à atteindre des qualités cristallines exceptionnelles. Ce travail est une contribution au développement du procédé de croissance en solution à partir d'un germe, avec comme objectif principal l'accès à des cristaux de 4H-SiC fortement dopés de type p. L'effet de l'ajout d'aluminium dans le solvant (dopant de type p) sur les différentes étapes élémentaires du procédé a été étudié. Par exemple, il a été montré que Al modifie la cinétique de croissance et réduit la probabilité de former transitoirement le 3C-SiC pendant les premiers stades de croissance. Une concentration en Al aussi élevée que 5E+20 at/cm3 a pu être obtenue à 1850°C. Cette valeur est très prometteuse pour le futur développement de substrats de 4H-SiC de type p+.